WiMAX System Level Evaluation Methodology

Draft V0.0.4

July 10, 2006

Table of Contents

1. Introduction

Mobile WiMAX is a broadband wireless solution that enables convergence of mobile and fixed broadband networks through a common wide area broadband radio access technology and flexible network architecture. Mobile WiMAX has made major strides over the past year and is rapidly proving itself as a leading solution for broadband wireless services.

The Mobile WiMAX Air Interface is based on the IEEE 802.16-2004 [i] Air Interface Standard and the IEEE 802.16e Mobile Amendment [ii] to the standard. Mobile WiMAX Air Interface adopts Orthogonal Frequency Division Multiple Access (OFDMA) for improved multi-path performance in non-line-of-sight environments. Scalable OFDMA (SOFDMA)[iii] is introduced in the IEEE 802.16e Amendment [II] to support scalable channel bandwidths operation from 1.25 to 20 MHz. The Mobile Technical Group (MTG) in WiMAX Forum is working on the Mobile WiMAX profiles. The Mobile WiMAX System Profile defines the mandatory and optional features of the IEEE standard that are necessary to build a Mobile WiMAX-compliant air interface that can be certified by the WiMAX Forum. The Mobile WiMAX System Profile enables mobile systems to be configured based on a common base feature set. The Mobile WiMAX system profiles are designed to ensure baseline functionality on terminals and base stations that are fully interoperable. Some elements of the base station profiles are specified as optional to provide additional flexibility for deployment based on specific deployment scenarios that may require different configurations that are either capacity-optimized or coverage-optimized. Initial Mobile WiMAX profiles will cover 5, 7, 8.75, and 10 MHz channel bandwidths for licensed worldwide spectrum allocations in the 2.3 GHz, 2.5 GHz, and 3.5 GHz frequency bands.

Figure 1: Mobile WiMAX System Profile

In the mean time, the WiMAX Forum Network Working Group (NWG) defines the higher-level networking specifications [iv] for Mobile WiMAX systems beyond what is defined in the IEEE 802.16 standard. The combined effort of IEEE 802.16 and the WiMAX Forum help define the end-to-end system solution for Mobile WiMAX.

Mobile WiMAX systems offer scalability in both radio access technology and network architecture, thus providing a great deal of flexibility in network deployment options and service offerings. Some of the salient features supported by Mobile WiMAX are:

- **High Data Rates:** The inclusion of MIMO antenna techniques along with flexible sub-channelization schemes,

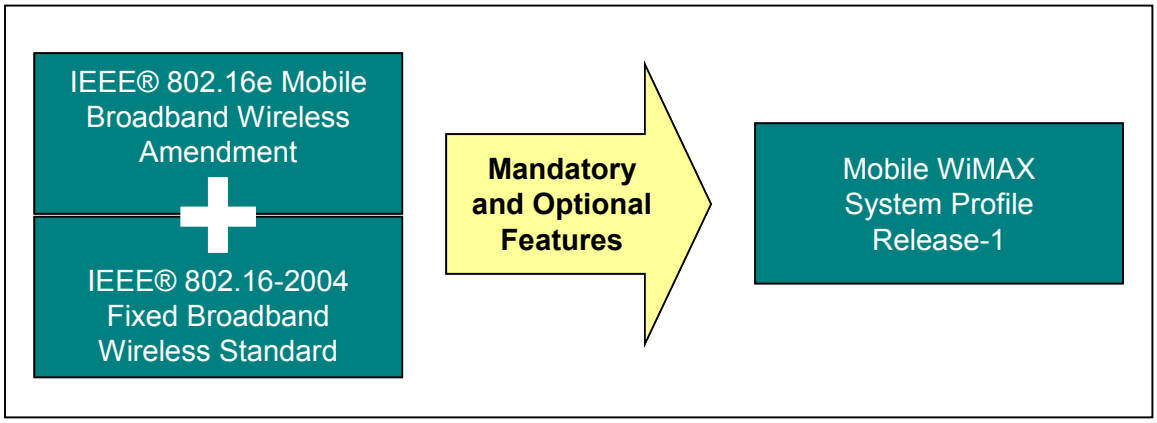

  Advanced Coding and Modulation all enable the Mobile WiMAX technology to support peak DL data rates up to 63 Mbps and peak UL data rates up to 28 Mbps in a 10 MHz channel.

- **Quality of Service (QoS):** The fundamental premise of the IEEE 802.16 MAC architecture is QoS. It defines Service Flows which can map to DiffServ code points or MPLS flow labels that enable end-to-end IP based QoS. Additionally, sub-channelization and MAP-based signaling schemes provide a flexible mechanism for optimal scheduling based on space, frequency and time-based packet access slots on the air interface that can be scheduled differently for each frame. This flexibility assures robustness is maintained along with adaptive modulation coding techniques.

- **Scalability**: Despite an increasingly globalized economy, spectrum resources for wireless broadband worldwide are still quite disparate in its allocations. Mobile WiMAX technology therefore, is designed to be able to scale to work in different channelizations from 1.25 to 20 MHz to comply with varied worldwide requirements as efforts proceed to achieve spectrum harmonization longer term. This also allows diverse economies to realize the multi-faceted benefits of the Mobile WiMAX technology for their specific geographic needs such as providing affordable internet access in rural settings versus enhancing the capacity of mobile broadband access in metro and suburban areas.

- **Security:** The features provided for Mobile WiMAX security aspects are best in class with EAP-based authentication, AES-CCM-based authenticated encryption, and CMAC and HMAC based control message protection schemes. Support for a diverse set of user credentials exists including; SIM/USIM cards, Smart Cards, Digital Certificates, and Username/Password schemes based on the relevant EAP methods for the credential type.
- **Mobility:** Mobile WiMAX supports optimized handover schemes with latencies less than 50 milliseconds to ensure real-time applications such as VoIP perform without service degradation. Flexible key management schemes assure that security is maintained during handover.

The 802.16e amendment was ratified by the IEEE in December, 2005. With the IEEE approval completed, the WiMAX Forum are now defining system performance and certification profiles based on the 802.16e amendment and network architecture to be completed in 2006. Initial profiles will be completed in the Release-1 profiles to be completed in early 2006. While the standards activity has been progressing, equipment suppliers have been aggressively developing equipment that will be WiMAX/802.16e compliant. With commercial availability of Mobile WiMAX[1]-compliant equipment anticipated in the very near future and the launch of WiBro services (also based on 802.16e) this year in Korea, it begs the question as to how the WiMAX/802.16e technology relates to and impacts concurrent advances in 3G cellular technology. To address this question it is necessary to gain an understanding of the underlying technology for Mobile WiMAX as well as the planned 3G enhancements.

The white paper is comprised of two parts. Part I is focused on Mobile WiMAX. It provides a detailed discussion of the Mobile WiMAX technology based on the planned WiMAX Forum Certification profiles. The section also includes a detailed analysis of Mobile WiMAX performance in a mobile environment. This OFDM/OFDMA-based technology enables the deployment of cost-effective wireless networks to provide broadband fixed and mobile services. Part II [v] of the white paper offers a comparative analysis of Mobile WiMAX relative to alternative cellular technologies.

1.2 Physical Layer Description

1.2.1 OFDMA Basics

Orthogonal Frequency Division Multiplexing (OFDM) [vi,vii] is a multiplexing technique that subdivides the bandwidth into multiple frequency sub-carriers as shown in Figure 2. In an OFDM system, the input data stream is divided into several parallel sub-streams of reduced data rate (thus increased symbol duration) and each sub-stream is modulated and transmitted on a separate orthogonal sub-carrier. The increased symbol duration improves the robustness of OFDM to delay spread. Furthermore, the introduction of the cyclic prefix (CP) can completely eliminate Inter-Symbol Interference (ISI) as long as the CP duration is longer than the channel delay spread. The CP is typically a repetition of the last samples of data portion of the block that is appended to the beginning of the data payload as shown in Figure 3. The CP prevents inter-block interference and makes the channel appear circular and permits low-complexity frequency domain equalization. A perceived drawback of CP is that it introduces overhead, which effectively reduces bandwidth efficiency. While the CP does reduce bandwidth efficiency somewhat, the impact of the CP is similar to the "roll-off factor" in raised-cosine filtered single-carrier systems. Since OFDM has a very sharp, almost "brick-wall" spectrum, a large fraction of the allocated channel bandwidth can be utilized for data transmission, which helps to moderate the loss in efficiency due to the cyclic prefix.

[1] The term WiMAX has been used generically to describe wireless systems based on the WiMAX certification profiles based on the IEEE 802.16-2004 Air Interface Standard. With profiles pending based on the IEEE 802.16e amendment, it is necessary to differentiate between the two systems. "Fixed" WiMAX is used to describe 802.16-2004 based systems and "Mobile" WiMAX is used to describe 802.16e-based systems.

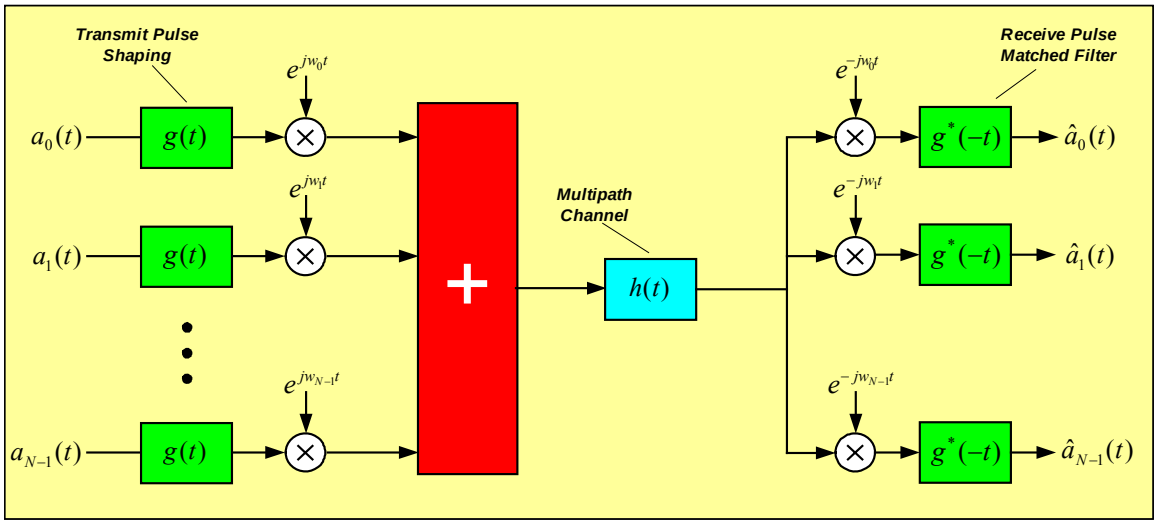

Figure 2: Basic Architecture of an OFDM System

OFDM exploits the frequency diversity of the multipath channel by coding and interleaving the information across the sub-carriers prior to transmissions. OFDM modulation can be realized with efficient Inverse Fast Fourier Transform (IFFT), which enables a large number of sub-carriers (up to 2048) with low complexity. In an OFDM system, resources are available in the time domain by means of OFDM symbols and in the frequency domain by means of sub-carriers. The time and frequency resources can be organized into sub-channels for allocation to individual users. Orthogonal Frequency Division Multiple Access (OFDMA) is a multiple-access/multiplexing scheme that provides multiplexing operation of data streams from multiple users onto the downlink sub-channels and uplink multiple access by means of uplink sub-channels.

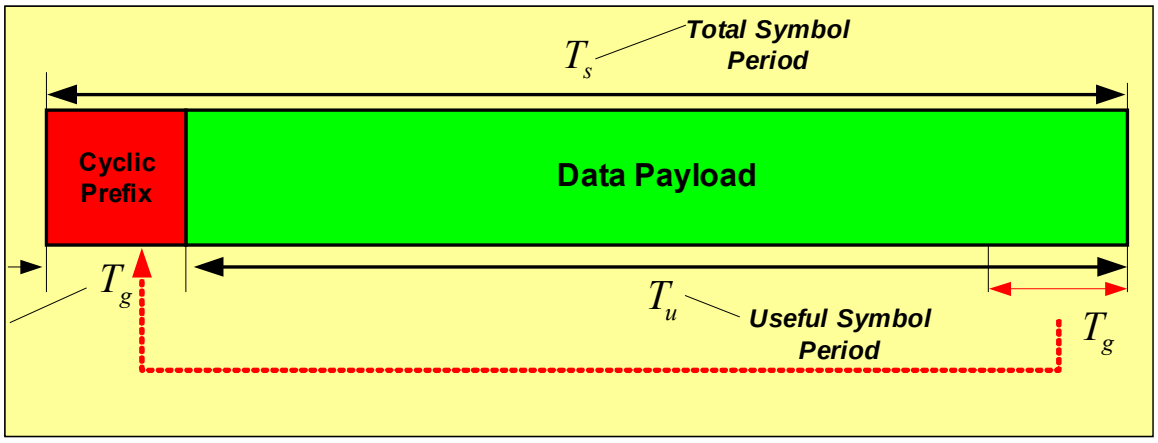

Figure 3: Insertion of Cyclic Prefix (CP)

1.2.2 OFDMA Symbol Structure and Sub-Channelization

The OFDMA symbol structure consists of three types of sub-carriers as shown in Figure 4:

- Data sub-carriers for data transmission
- Pilot sub-carriers for estimation and synchronization purposes
- Null sub-carriers for no transmission; used for guard bands and DC carriers

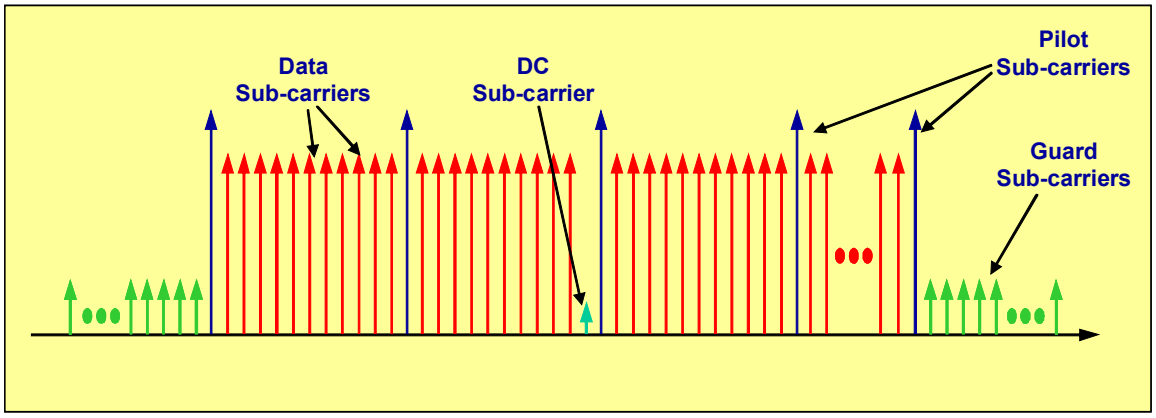

Figure 4: OFDMA Sub-Carrier Structure

Active (data and pilot) sub-carriers are grouped into subsets of sub-carriers called sub-channels. The WiMAX OFDMA PHY [3] supports sub-channelization in both DL and UL. The minimum frequency-time resource unit of sub-channelization is one slot, which is equal to 48 data tones (sub-carriers).

There are two types of sub-carrier permutations for sub-channelization; *diversity* and *contiguous*. The diversity permutation draws sub-carriers pseudo-randomly to form a sub-channel. It provides frequency diversity and inter-cell interference averaging. The diversity permutations include DL FUSC (Fully Used Sub-Carrier), DL PUSC (Partially Used Sub-Carrier) and UL PUSC and additional optional permutations. With DL PUSC, for each pair of OFDM symbols, the available or usable sub-carriers are grouped into *clusters* containing 14 contiguous sub-carriers per symbol, with pilot and data allocations in each cluster in the even and odd symbols as shown in Figure 5.

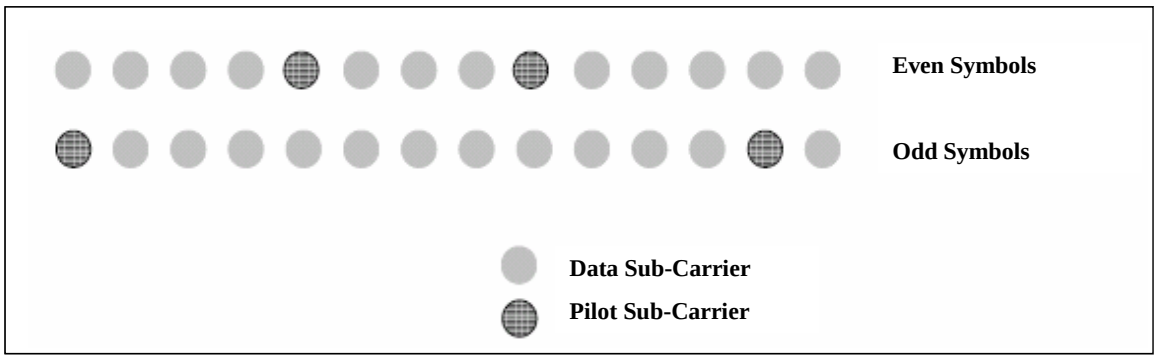

Figure 5: DL Frequency Diverse Sub-Channel

A re-arranging scheme is used to form *groups* of clusters such that each group is made up of clusters that are distributed throughout the sub-carrier space. A sub-channel in a group contains two (2) clusters and is comprised of 48 data sub-carriers and eight (8) pilot sub-carriers.

Analogous to the cluster structure for DL, a *tile* structure is defined for the UL PUSC whose format is shown in Figure 6.

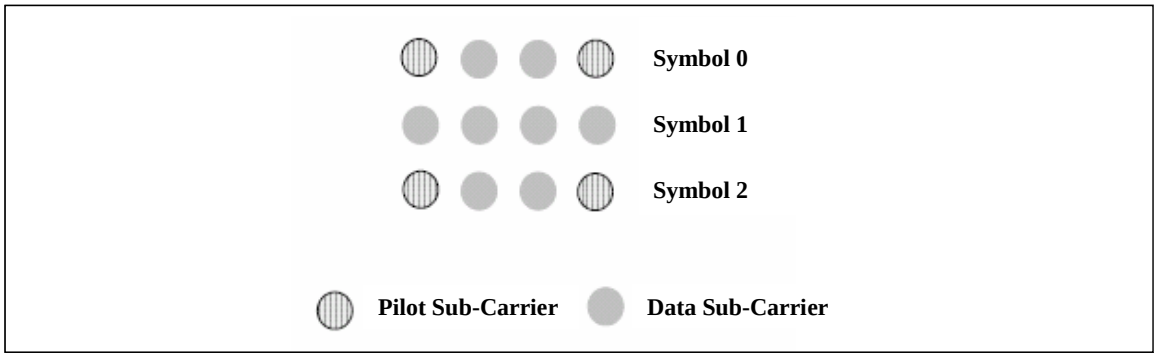

Figure 6: Tile Structure for UL PUSC

The available sub-carrier space is split into tiles and six (6) tiles, chosen from across the entire spectrum by means of a re-arranging/permutation scheme, are grouped together to form a *slot*. *The slot is comprised of 48 data sub-carriers and 24 pilot sub-carriers in 3 OFDM symbols.*

The contiguous permutation groups a block of contiguous sub-carriers to form a sub-channel. The contiguous permutations include DL AMC and UL AMC, and have the same structure. A bin consists of 9 contiguous sub-carriers in a symbol, with 8 assigned for data and one assigned for a pilot. A *slot* in AMC is defined as a collection of bins of the type (N x M = 6), where N is the number of contiguous bins and M is the number of contiguous symbols. Thus the allowed combinations are [(6 bins, 1 symbol), (3 bins, 2 symbols), (2 bins, 3 symbols), (1 bin, 6 symbols)]. AMC permutation enables multi-user diversity by choosing the sub-channel with the best frequency response.

In general, diversity sub-carrier permutations perform well in mobile applications while contiguous sub-carrier permutations are well suited for fixed, portable, or low mobility environments. These options enable the system designer to trade-off mobility for throughput.

1.2.3 Scalable OFDMA

The IEEE 802.16e Wireless MAN OFDMA mode is based on the concept of scalable OFDMA (S-OFDMA). S-OFDMA supports a wide range of bandwidths to flexibly address the need for various spectrum allocation and usage model requirements. The scalability is supported by adjusting the FFT size while fixing the sub-carrier frequency spacing at 10.94 kHz. Since the resource unit sub-carrier bandwidth and symbol duration is fixed, the impact to higher layers is minimal when scaling the bandwidth. The S-OFDMA parameters are listed in Table 1. The system bandwidths for the initial planned profiles being developed by the WiMAX Forum Technical Working Group for Release-1 are 5 and 10 MHz (highlighted in the table).

Parameters	Values			
System Channel Bandwidth (MHz)	1.25	5	10	20
Sampling Frequency (F_p in MHz)	1.4	5.6	11.2	22.4
FFT Size (N_{FFT})	128	512	1024	2048
Number of Sub-Channels	2	8	16	32
Sub-Carrier Frequency Spacing	10.94 kHz			
Useful Symbol Time ($T_b = 1/f$)	91.4 microseconds			
Guard Time ($T_g = T_b/8$)	11.4 microseconds			
OFDMA Symbol Duration ($T_s = T_b + T_g$)	102.9 microseconds			
Number of OFDMA Symbols (5 ms Frame)	48			

Table 1: OFDMA Scalability Parameters

1.2.4 TDD Frame Structure

The 802.16e PHY [3] supports TDD, FDD, and Half-Duplex FDD operation, however the initial release of Mobile WiMAX certification profiles will only include TDD. With ongoing releases, FDD profiles will be considered by the WiMAX Forum to address specific market opportunities where local spectrum regulatory requirements either prohibit TDD or are more suitable for FDD deployments. To counter interference issues, TDD does require system-wide synchronization; nevertheless, TDD is the preferred duplexing mode for the following reasons:

- TDD enables adjustment of the downlink/uplink ratio to efficiently support asymmetric downlink/uplink traffic, while with FDD, downlink and uplink always have fixed and generally, equal DL and UL bandwidths.
- TDD assures channel reciprocity for better support of link adaptation, MIMO and other closed loop advanced antenna technologies.
- Unlike FDD, which requires a pair of channels, TDD only requires a single channel for both downlink and uplink providing greater flexibility for adaptation to varied global spectrum allocations.
- Transceiver designs for TDD implementations are less complex and therefore less expensive.

Figure 7 illustrates the OFDM frame structure for a Time Division Duplex (TDD) implementation. Each frame is divided into DL and UL sub-frames separated by Transmit/Receive and Receive/Transmit Transition Gaps (TTG and RTG, respectively) to prevent DL and UL transmission collisions. In a frame, the following control information is used to ensure optimal system operation:

- **Preamble:** The preamble, used for synchronization, is the first OFDM symbol of the frame.
- **Frame Control Head (FCH):** The FCH follows the preamble. It provides the frame configuration information such as MAP message length and coding scheme and usable sub-channels.
- **DL-MAP and UL-MAP:** The DL-MAP and UL-MAP provide sub-channel allocation and other control information for the DL and UL sub-frames respectively.
- **UL Ranging:** The UL ranging sub-channel is allocated for mobile stations (MS) to perform closed-loop time, frequency, and power adjustment as well as bandwidth requests.
- **UL CQICH:** The UL CQICH channel is allocated for the MS to feedback channel-state information.
- **UL ACK:** The UL ACK is allocated for the MS to feedback DL HARQ acknowledgement.

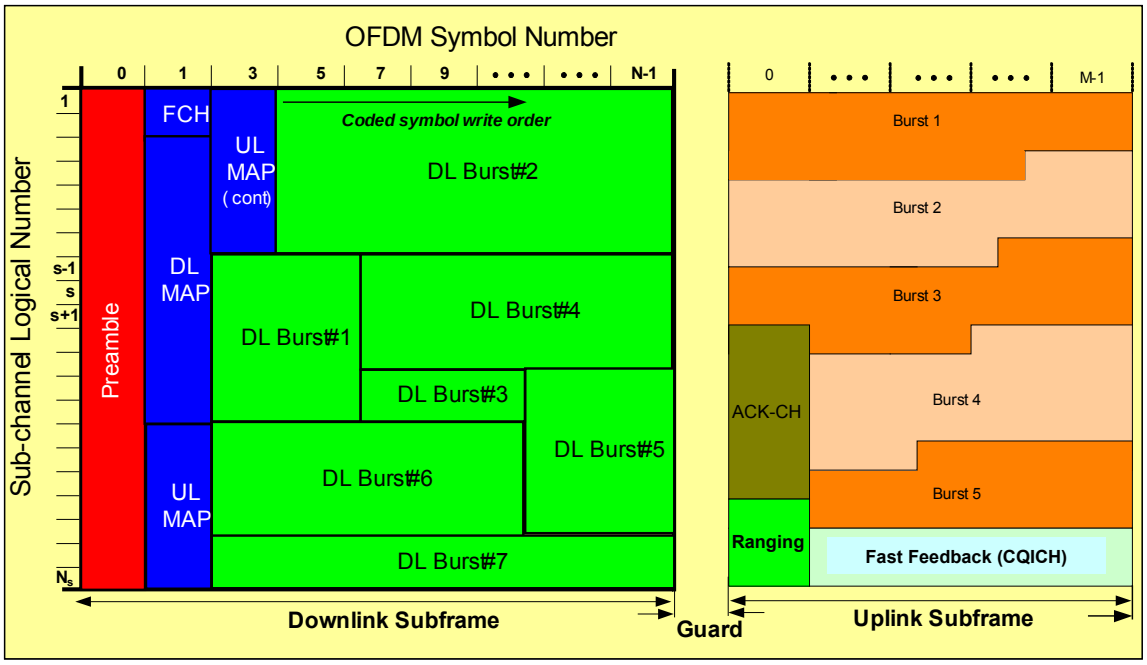

Figure 7: WiMAX OFDMA Frame Structure

1.2.5 Other Advanced PHY Layer Features

Adaptive modulation and coding (AMC), Hybrid Automatic Repeat Request (HARQ) and Fast Channel Feedback (CQICH) were introduced with Mobile WiMAX to enhance coverage and capacity for WiMAX in mobile applications.

Support for QPSK, 16QAM and 64QAM are mandatory in the DL with Mobile WiMAX. In the UL, 64QAM is optional. Both Convolutional Code (CC) and Convolutional Turbo Code (CTC) with variable code rate and repetition coding are supported. Block Turbo Code and Low Density Parity Check Code (LDPC) are supported as optional features. Table 2 summarizes the coding and modulation schemes supported in the Mobile WiMAX profile the optional UL codes and modulation are shown in italics.

		DL	UL
Modulation		QPSK, 16QAM, 64QAM	QPSK,16QAM, *64QAM*
Code Rate	CC	1/2, 2/3, 3/4, 5/6	1/2, 2/3, *5/6*
	CTC	1/2, 2/3, 3/4, 5/6	1/2, 2/3, *5/6*
	Repetition	x2, x4, x6	x2, x4, x6

Table 2: Supported Code and Modulations

The combinations of various modulations and code rates provide a fine resolution of data rates as shown in Table 3 which shows the data rates for 5 and 10 MHz channels with PUSC sub-channels. The frame duration is 5 ms. Each frame has 48 OFDM symbols, with 44 OFDM symbols available for data transmission. The highlighted values indicate data rates for optional 64QAM in the UL.

Parameter	Downlink	Uplink	Downlink	Uplink
System Bandwidth	5 MHz		10 MHz	
FFT Size	512		1024	
Null Sub-Carriers	92	104	184	184

Pilot Sub-Carriers	60	136	120	280
Data Sub-Carriers	360	272	720	560
Sub-Channels	15	17	30	35
Symbol Period, T_S	102.9 microseconds			
Frame Duration	5 milliseconds			
OFDM Symbols/Frame	48			
Data OFDM Symbols	44			

Mod.	Code Rate	5 MHz Channel		10 MHz Channel	
		Downlink Rate, Mbps	Uplink Rate, Mbps	Downlink Rate, Mbps	Uplink Rate, Mbps
QPSK	1/2 CTC, 6x	0.53	0.38	1.06	0.78
	1/2 CTC, 4x	0.79	0.57	1.58	1.18
	1/2 CTC, 2x	1.58	1.14	3.17	2.35
	1/2 CTC, 1x	3.17	2.28	6.34	4.70
	3/4 CTC	4.75	3.43	9.50	7.06
16QAM	1/2 CTC	6.34	4.57	12.07	9.41
	3/4 CTC	9.50	6.85	19.01	14.11
64QAM	1/2 CTC	9.50	*6.85*	19.01	*14.11*
	2/3 CTC	12.67	*9.14*	26.34	*18.82*
	3/4 CTC	14.26	*10.28*	28.51	*21.17*
	5/6 CTC	15.84	*11.42*	31.68	*23.52*

Table 3: Mobile WiMAX PHY Data Rates with PUSC Sub-Channel[2]

The base station scheduler determines the appropriate data rate (or burst profile) for each burst allocation based on the buffer size, channel propagation conditions at the receiver, etc. A Channel Quality Indicator (CQI) channel is utilized to provide channel-state information from the user terminals to the base station scheduler. Relevant channel-state information can be fed back by the CQICH including: Physical CINR, effective CINR, MIMO mode selection and frequency selective sub-channel selection. With TDD implementations, link adaptation can also take advantage of channel reciprocity to provide a more accurate measure of the channel condition (such as sounding).

Hybrid Auto Repeat Request (HARQ) is supported by Mobile WiMAX. HARQ is enabled using *N* channel "Stop and Wait" protocol which provides fast response to packet errors and improves cell edge coverage. Chase Combining and optionally, Incremental Redundancy are supported to further improve the reliability of the retransmission. A dedicated ACK channel is also provided in the uplink for HARQ ACK/NACK signaling. Multi-channel HARQ operation is supported. Multi-channel stop-and-wait ARQ with a small number of channels is an efficient, simple protocol that minimizes the memory required for HARQ and stalling [viii]. WiMAX provides signaling to allow fully asynchronous operation. The asynchronous operation allows variable delay between retransmissions which gives more flexibility to the scheduler at the cost of additional overhead for each retransmission allocation. HARQ combined together with CQICH and AMC provides robust link adaptation in mobile environments at vehicular speeds in excess of 120 km/hr.

[2] PHY Data Rate=(Data sub-carriers/Symbol period)*(information bits per symbol)

1.3. MAC Layer Description

The 802.16 standard was developed from the outset for the delivery of broadband services including voice, data, and video. The MAC layer is based on the time-proven DOCSIS standard and can support bursty data traffic with high peak rate demand [ix] while simultaneously supporting streaming video and latency-sensitive voice traffic over the same channel. The resource allocated to one terminal by the MAC scheduler can vary from a single time slot to the entire frame, thus providing a very large dynamic range of throughput to a specific user terminal at any given time. Furthermore, since the resource allocation information is conveyed in the MAP messages at the beginning of each frame, the scheduler can effectively change the resource allocation on a frame-by-frame basis to adapt to the bursty nature of the traffic.

1.3.1 Quality of Service (QoS) Support

With fast air link, symmetric downlink/uplink capacity, fine resource granularity and a flexible resource allocation mechanism, Mobile WiMAX can meet QoS requirements for a wide range of data services and applications.

In the Mobile WiMAX MAC layer, QoS is provided via service flows as illustrated in Figure 8. This is a unidirectional flow of packets that is provided with a particular set of QoS parameters. Before providing a certain type of data service, the base station and user-terminal first establish a unidirectional logical link between the peer MACs called a connection. The outbound MAC then associates packets traversing the MAC interface into a service flow to be delivered over the connection. The QoS parameters associated with the service flow define the transmission ordering and scheduling on the air interface. The connection-oriented QoS therefore, can provide accurate control over the air interface. Since the air interface is usually the bottleneck, the connection-oriented QoS can effectively enable the end-to-end QoS control. The service flow parameters can be dynamically managed through MAC messages to accommodate the dynamic service demand. The service flow based QoS mechanism applies to both DL and UL to provide improved QoS in both directions. Mobile WiMAX supports a wide range of data services and applications with varied QoS requirements. These are summarized in Table 4.

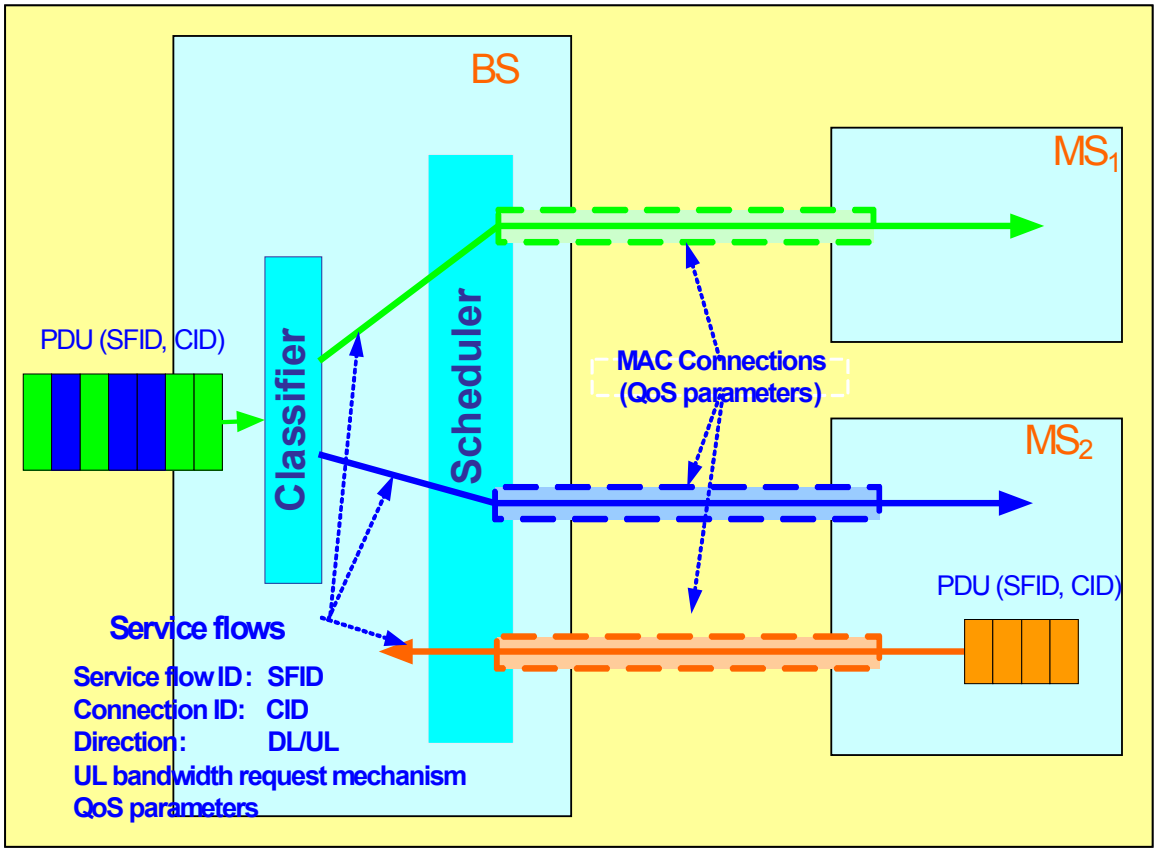

Figure 8: Mobile WiMAX QoS Support

QoS Category	Applications	QoS Specifications
UGS Unsolicited Grant Service	VoIP	• Maximum Sustained Rate • Maximum Latency Tolerance • Jitter Tolerance
rtPS Real-Time Packet Service	Streaming Audio or Video	• Minimum Reserved Rate • Maximum Sustained Rate • Maximum Latency Tolerance • Traffic Priority
ErtPS Extended Real-Time Packet Service	Voice with Activity Detection (VoIP)	• Minimum Reserved Rate • Maximum Sustained Rate • Maximum Latency Tolerance • Jitter Tolerance • Traffic Priority
nrtPS Non-Real-Time Packet Service	File Transfer Protocol (FTP)	• Minimum Reserved Rate • Maximum Sustained Rate • Traffic Priority
BE Best-Effort Service	Data Transfer, Web Browsing, etc.	• Maximum Sustained Rate • Traffic Priority

Table 4: Mobile WiMAX Applications and Quality of Service

1.3.2 MAC Scheduling Service

The Mobile WiMAX MAC scheduling service is designed to efficiently deliver broadband data services including voice, data, and video over time varying broadband wireless channel. The MAC scheduling service has the following properties that enable the broadband data service:

- **Fast Data Scheduler:** The MAC scheduler must efficiently allocate available resources in response to bursty data traffic and time-varying channel conditions. The scheduler is located at each base station to enable rapid response to traffic requirements and channel conditions. The data packets are associated to service flows with well defined QoS parameters in the MAC layer so that the scheduler can correctly determine the packet transmission ordering over the air interface. The CQICH channel provides fast channel information feedback to enable the scheduler to choose the appropriate coding and modulation for each allocation. The adaptive modulation/coding combined with HARQ provides robust transmission over the time-varying channel.
- **Scheduling for both DL and UL:** The scheduling service is provided for both DL and UL traffic. In order for the MAC scheduler to make an efficient resource allocation and provide the desired QoS in the UL, the UL must feedback accurate and timely information as to the traffic conditions and QoS requirements. Multiple uplink bandwidth request mechanisms, such as bandwidth request through ranging channel, piggyback request and polling are designed to support UL bandwidth requests. The UL service flow defines the feedback mechanism for each uplink connection to ensure predictable UL scheduler behavior. Furthermore, with orthogonal UL subchannels, there is no intra-cell interference. UL scheduling can allocate resource more efficiently and better enforce QoS.
- **Dynamic Resource Allocation**: The MAC supports frequency-time resource allocation in both DL and UL on a per-frame basis. The resource allocation is delivered in MAP messages at the beginning of each frame. Therefore, the resource allocation can be changed on frame-by-frame in response to traffic and channel conditions.

Additionally, the amount of resource in each allocation can range from one slot to the entire frame. The fast and fine granular resource allocation allows superior QoS for data traffic.

- **QoS Oriented:** The MAC scheduler handles data transport on a connection-by-connection basis. Each connection is associated with a single data service with a set of QoS parameters that quantify the aspects of its behavior. With the ability to dynamically allocate resources in both DL and UL, the scheduler can provide superior QoS for both DL and UL traffic. Particularly with uplink scheduling - *the uplink resource is more efficiently allocated, performance is more predictable, and QoS is better enforced.*
- **Frequency Selective Scheduling:** The scheduler can operate on different types of sub-channels. For frequency-diverse sub-channels such as PUSC permutation, where sub-carriers in the sub-channels are pseudo-randomly distributed across the bandwidth, sub-channels are of similar quality. Frequency-diversity scheduling can support a QoS with fine granularity and flexible time-frequency resource scheduling. With contiguous permutation such as AMC permutation, the sub-channels may experience different attenuation. The frequency-selective scheduling can allocate mobile users to their corresponding strongest sub-channels. The frequency-selective scheduling can enhance system capacity with a moderate increase in CQI overhead in the UL[x].

2. System Modeling architecture

[19 cell, discrete event simulation, review 3GPP evaluation document, overall framework]

2.1 System Modeling Assumptions

2.1.1 Antenna Pattern

The antenna pattern used for each sector of 3-sector BS, is defined as :

$$A(\theta) = -\min\left[12\left(\frac{\theta}{\theta_{3\,dB}}\right)^2, A_m\right],$$

where θ is the angle between the direction of the main lobe of the antenna and direction of interest, and its range is $-180 \le \theta \le 180$. The min[ ] is the minimum function, θ_{3dB} is the 3dB beamwidth (corresponding to $\theta_{3dB} = 70$ degrees) , and A_m= 20 dB is the maximum attenuation. The antenna gain for presented model is 14dBi.

2.1.2 Antenna Orientation

The antenna bearing is defined as the angle between a line directed due east and the main antenna lobe center given in degrees. The bearing angle increases in a clockwise direction. Figure 2.1.1 shows an example of the 3-sector 120-degree center cell site, with Sector 1 bearing angle of 330 degrees. Figure 2.1.2 shows the orientation of the center cell (target cell) hexagon and its three sectors corresponding to the antenna bearing orientation proposed for the simulations. The main antenna lobe center directions each point to the sides of the hexagon. The main antenna lobe center directions of the 18 surrounding cells shall be parallel to those of the center cell. Figure 2.1.2 also shows the orientation of the cells and sectors in the two tiers of cells surrounding the central cell.

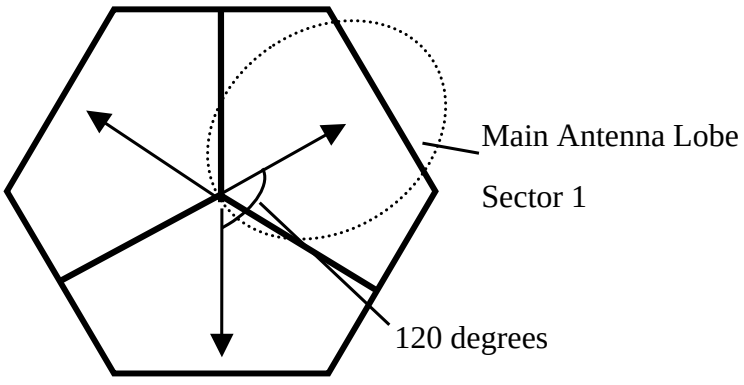

FIGURE 2.1.1: CENTRE CELL ANTENNA BEARING ORIENTATION DIAGRAM

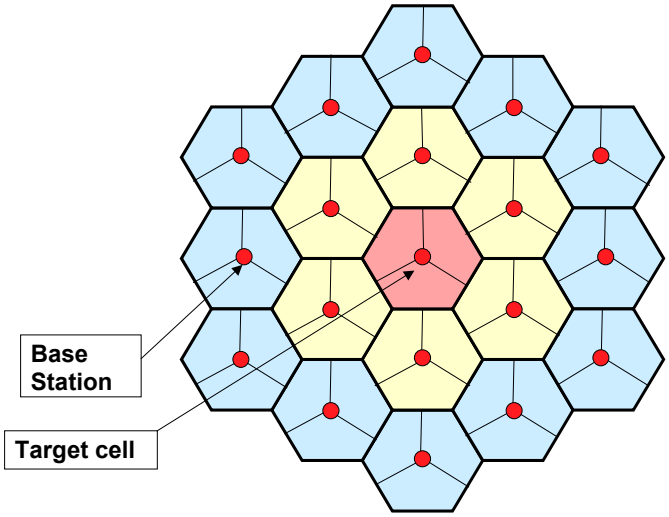

Figure 2.1.2: Configuration of adjacent tiers of neighbouring cells, sectors, and Base Stations

2.1.3 OFDM performance analysis

2.1.3.1 Reference System Scenario for High Speed Data Services Capacity Evaluation

This section describes equivalent reference scenarios for comparing the throughput of WCDMA and OFDM radio interfaces in the context of high speed data services. While such a comparison forms an essential part of the Study Item, it is recognized that the Study Item will not be concluded based on the performance of the radio interface alone. The remaining issues include the drawbacks associated with the additional HSDPA carrier, frequency availability and planning, carrier access and handover issues. Such issues are addressed in section 6.

2.1.3.1.1 OFDM Downlink

In the Section, an initial reference system configuration is proposed to evaluate an OFDM downlink. The reference architecture is generic, and is compatible with the current 3GPP Rel 5 configuration. In the proposed configuration, new data services are provided through the use of a separate 5 MHz downlink carrier, supporting the OFDM HS-DSCH transmission. The reference architecture is shown in Figure 12.

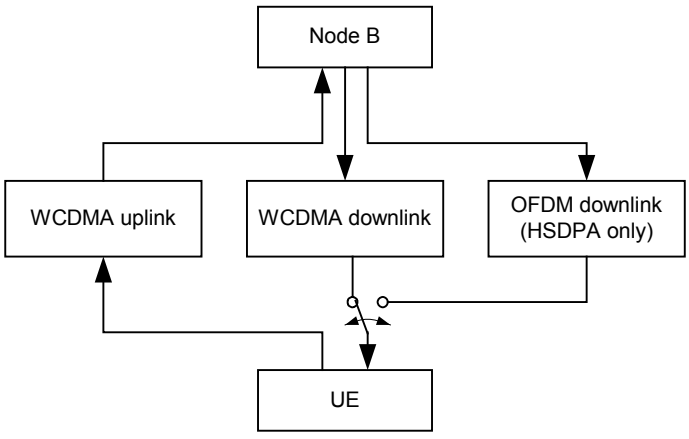

Figure 12: Network deployment for the OFDM HS-DSCH transmission

The separate OFDM DL carrier is operated using HSDPA features, such as link adaptation and HARQ. At this stage, it is assumed that network access is performed through the WCDMA architecture, and handover to the OFDM carrier occurs, when needed, for interactive background and streaming data services. In this case, a UE with OFDM HS-DSCH

receiving capabilities would also have WCDMA receiving capabilities. In the first stage, the WCDMA link would be used to achieve the initial network access. However, when there is a requirement for high bit rate traffic, the HS-DSCH mode may be initiated, using either the WCDMA DL carrier (Rel 5 HSDPA) or the separate OFDM DL carrier.

Based on this initial reference scenario, a UE with OFDM HS-DSCH receiving capabilities is not required to receive the WCDMA and OFDM carriers simultaneously. This implies that, if there is a need for real time services, such as voice communications supported only on the WCDMA carrier, the UE would use the WCDMA mode. Note however that if OFDM proves to be useful in the HS-DSCH scenario, other services could also be mapped to the OFDM downlink in future work. In the proposed configuration, the current UMTS uplink carrier is reused and is considered to have sufficient capacity to support either a Rel 5 WCDMA DL carrier, or the separate OFDM DL carrier. There is no special assumption about the separate carrier frequency.

2.1.3.1.2 Equivalent WCDMA Scenario

Since the objective of the study item is to evaluate the potential benefits of OFDM as a radio interface for UTRAN, the evaluation should be decoupled from the impact of other factors. To achieve this, the proposed OFDM HSDPA-only carrier is compared to an equivalent HSDPA-only carrier, which employs the existing UTRAN radio interface. This is shown in Figure 13, where a speculative WCDMA HSDPA-only carrier was added to the Release-5 system, ensuring a 'like-with-like' comparison of the two radio interfaces. It should be recognised that the introduction of the standalone WCDMA HS-DSCH carrier within the OFDM study item is speculative and serves purely to aid the evaluation process.

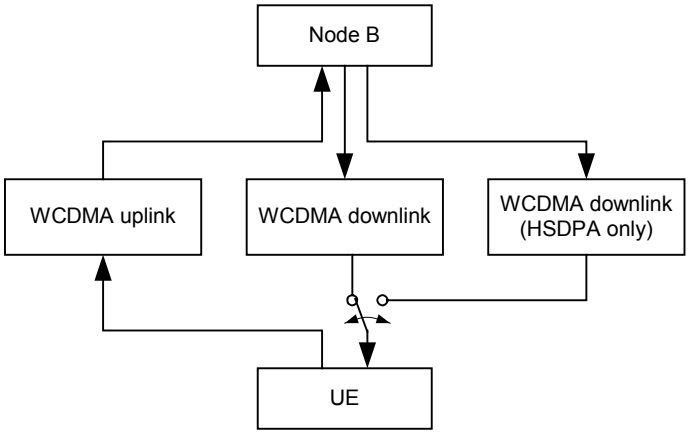

Figure 13: Release-5 system with an 'HSDPA only' WCDMA downlink

It is assumed that the UE is not required to receive the Release-5 downlink and the additional HSDPA-only downlink (whether WCDMA or OFDM) simultaneously. The network access is performed through the Release-5 architecture, and handover to the HSDPA-only carrier occurs when needed.

The second downlink is also assumed to be entirely available for HS-DSCH transfers, i.e. 15 out of 16 codes (with SF = 16) are available for data services.

2.1.3.2 Reference OFDM configuration for the evaluation

Two sets of reference OFDM configuration parameters are listed in Table1.

Table 1: Reference OFDM configuration parameter sets

Parameters	Set 1	Set 2
TTI duration (msec)	2	2
FFT size (points)	512	1024
OFDM sampling rate (Msamples/sec)	7.68	6.528
Ratio of OFDM sampling rate to UMTS chip rate	2	17/10
Guard time interval (cyclic prefix) (samples/μsec)	56 / 7.29 57 / 7.42(NOTE1)	64/9.803
Subcarrier separation (kHz)	15	6.375
# of OFDM symbols per TTI	27	12
OFDM symbol duration (μsec)	73.96/74.09(NOTE2)	166.67
# of useful subcarriers per OFDM symbol	299	705
OFDM bandwidth (MHz)	4.485	4.495
NOTE1: Requires one extra prefix sample for 8 out of 9 OFDM symbols NOTE2: Depending on guard interval duration		

The parameter set 1 consists of nine OFDM symbols that fit into a 0.667 us timeslot. The useful symbol duration is equal to 512 samples. The guard interval is equal to 56 samples for the 0^{th} symbol, and 57 samples for symbols 1..8 of every timeslot, as illustrated in figure 14. The actual position of the 56-sample GI symbol is believed to be inconsequential as long as it is known by both the transmitter and receiver. Therefore, it may be revisited in future, should a different location be deemed more favourable.

It should be noted that spectral shaping of the OFDM signal is required for out-of-band emission compliance. The implications of spectral shaping on delay spread robustness are discussed in a separate section of this report.

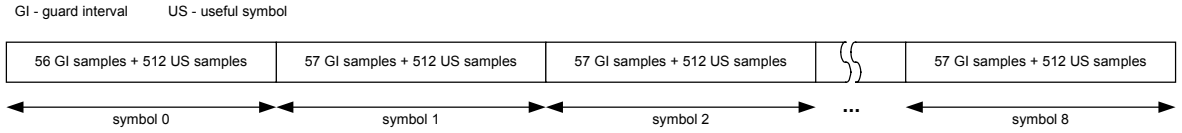

Figure 14: Temporal structure of the OFDM signal (one timeslot), parameter set 1.

2.1.3.3 Performance Analysis Results

Detailed results can be found in annex A.5.

2.2 Frequency re-use and Inter-cell Interference

2.2.1 Frequency Re-use

The assumption regarding the frequency re-use for the OFDM study has been that the same 5MHz carrier can be re-used in each cell, which is often referred to a full frequency re-use, or frequency re-use factor of 1. The main benefit of such a frequency re-use is mainly ease of deployment, given that no frequency planning is required. In the case of the introduction of OFDM in UTRAN, it would be also desirable to maintain this property, which is already available with WCDMA.

Note however that using the same 5MHz carrier in each cell does not necessarily imply that all of the OFDM sub-carriers would be re-used equally in each cell. One could consider several methods based on the orthogonality of OFDM sub-carriers (even in systems that are not time-synchronised) to improve the coverage. The feasibility, benefits and costs of such methods are FFS.

2.2.2 Inter-cell Interference

Given a frequency re-use factor of 1, the system becomes interference-limited, and the interference perceived by the UE from the different cells might not be perfectly white, as assumed for most of the simulations. First, the interfering signals undergo time dispersion, and hence, do not have a flat spectrum. Furthermore, if the OFDM units are not all being used in the interfering cells, the resulting spectrum from each of these partially-load interfering cells will contain gaps. It is therefore likely that the total interference spectrum observed by the UE would not be flat, and hence, it might not be accurately modelled using white noise.

The impact of realistic inter-cell interference on performance has therefore been evaluated using the Exponential Effective SIR Mapping (EESM). The results are presented in Annex A.2 for PedA and PedB. The following conclusions might be drawn from these results:

- As expected, the performance is improving when the number of OFDM units used in the interfering cells is reduced (as in WCDMA). Hence, the fully loaded case can be considered as a worse-case.
- The throughput obtained with the realistic interference profile is larger or equal to that obtained for interference modeled as AWGN with the same power. Hence, the AWGN assumption is conservative.

2.3 Channel Models and Interference

2.3.1 Channel Models

[*Rok: Please refer to Annex A borrowed from SCM document that describes spatial channel models and ensure that descriptions of Model 1 through 6 referenced below are described in the annex. Please also include description to items in other columns of this table such as multipath, # of path, speed, fading, etc.*]

Several channel model scenarios for wireless applications exist. For fixed wireless applications WiMAX forum has adopted Erceg model and referenced SUI model scenarios within **Error! Reference source not found.**. 3GPP has based its OFDM feasibility study for UTRAN deployment **Error! Reference source not found.**on ITU-R models **Error! Reference source not found.**, and the same approach had been adopted by 3GPP2 **Error! Reference source not found.**. While the first model accounts for stationary use case only, the later two include portable, simple mobility and fully mobility use cases also. Although the scenarios do seem distinct, the corresponding output differences may be neglected when model is used as a PHY abstraction for application performance evaluation.

Channel model scenario adopted in this work corresponds to the one used by 3GPP **Error! Reference source not found.**. It consists of six channel models that are randomly assigned to various users according probability distribution indicated in Table 20. The particular model assigned to the user remains fixed over the duration of a simulation drop.

A channel model is characterized by Erceg B propagation model, and corresponds to a specific number of paths, a power profile giving the relative powers and delays of these multiple paths, MS velocity and fading model to specify the fading rate. The multiple paths for a specific channel model are adopted from ITU-R models as specified in Table 21.

Table 20: Channel Models and associated assignment probability distribution

Channel Model	Multi-path Model	# of Paths	Speed (km/h)	Fading	Assignment Probability
Model 1	Flat fading	1	30	Jakes	0.1
Model 2	Flat fading	1	120	Jakes	0.1
Model 3	ITU Vehicular A	6	30	Jakes	0.1
Model 4	ITU Vehicular A	6	120	Jakes	0.1
Model 5	ITU Pedestrian A	4	3	Jakes	0.3
Model 6	ITU Pedestrian B	6	3	Jakes	0.3

Note that a separate link-level simulation must be performed for each specific channel model and MS velocity combination. Hence, there is a desire to minimize the number of different possible channel model combinations, while ensuring that an accurate modelling of reality is also made. The assignment probabilities in Table 20 were selected to agree with the corresponding probabilities in [1], while reducing the number of different distinct fading velocities in order to reduce the number of link level simulations that must be performed.

The normalized power profiles for the different channel models such as flat fading , ITU vehicular-A, ITU pedestrian-A, and ITU pedestrian-B are given in Table 21 together with associated relative delays for each path.

Proposed channel models consider several distinct types of signal propagation effects. These are mean path loss, slow variation about the mean path loss due shadowing and scattering, fast variation in the detected signal strength due to multipath effects, and corrections terms due Doppler effect because of moving receiver.

All the paths are considered to be affected by a shadow fading which is log-normally distributed. Although there may be subtle differences between the four used channel models, we take the standard deviation of shadow fading distribution to be 10 dB, which is reasonable according ITU **Error! Reference source not found.**.

Since we consider all channel models to be mobile, the shape of Doppler spectrum is that proposed by Jakes.

2.3.2.1 Path loss model

Path loss model is Erceg B propagation model. This model encounters for intermediate path loss condition between high path loss of hilly terrain with moderate-to-heavy tree densities (Erceg A) and low path loss in a flat terrain with light tree densities (Erceg C). The model has been chosen due solid backup of experimental data collected in an existing macrocells at 1.9 GHz. Note that proposed path loss model accounts also for frequency correction, as long as carrier frequency falls in range [1 GHz, 4 GHz].

For a given close-in distance d_0 the average path loss in dB is given by

$$PL = A + 10\gamma \log\left(\frac{d}{d_0}\right) + s,$$

Where

- d_0 is 100 m
- $A=20 \log(4\pi d_0/\lambda)$, λ is carrier wavelength
- γ is the path loss exponent with $\gamma=a-b*h_b+c/h_b$, for base station height h_b between 10 m and 80 m, and a, b, c are constants of Erceg B propagation model with corresponding values of 4, 0.0065 and 17.1
- s represents the shadowing effect which follows lognormal distribution with a standard deviation of 10 dB.

The constant values defined above have been derived from measurements at 1.9 GHz carrier frequency and receive antenna heights of around 2 m. To apply the model for 3.5 GHz carrier frequency correction term has to be added, while we ignore receiver height correction term.

$$PL_{corrected} = PL + \Delta PL_{freq}$$

The frequency correction term in dB is given by

$$\Delta PL_{freq} = 6\log(f / 2GHz)$$

Where f is the frequency of the carrier.

2.3.2.2 Multipath models

Each channel model is characterized by a tapped-delay line as presented in Table 21. For the channel models that correspond to the standard ITU channel models, the relative ratios of the path powers are the same as defined by ITU, but the absolute power values have been normalized so that they sum to 0 dB (unit energy) for each given channel model.

Table 21: Normalized power profiles for multi-path channel models

Channel Model		Path 1	Path 2	Path 3	Path 4	Path 5	Path 6

Flat fading	Average power (dB)	0	-	-	-	-	-
	Relative delay (ns)	-	-	-	-	-	-
ITU Vehicular A	Average power (dB)	-3.14	-4.14	-12.14	-13.14	-18.14	-23.14
	Relative delay (ns)	0	310	710	1090	1730	2510
ITU Pedestrian A	Average power (dB)	-0.51	-10.21	-19.71	-23.31	-	-
	Relative delay (ns)	0	110	190	410	-	-
ITU Pedestrian B	Average power (dB)	-3.92	-4.82	-8.82	-11.92	-11.72	-27.82
	Relative delay (ns)	0	200	800	1200	2300	3700

Each model is defined by number of paths (taps), the average power relative to first path, time delay relative to first path. Often each path is characterized by Doppler spectrum, but we take that all paths have the same shape of Doppler power spectral density that proposed by Jakes.

2.3.2.3 Doppler spectrum

To address Doppler fading we assume Jakes fading for all channel models. According Clarke/Jakes assumption the scattering environment is random in a sense that at the receiver (mobile) the angle of arrival of a received plane wave is uniformly distributed random variable. As a consequence the Doppler power spectrum, being a measure for fading rate of particular propagation path, does not depend neither on the path itself nor on direction of mobile's movement. It is expressed as

$$D(f) = \frac{1}{\pi} \cdot \frac{1}{\sqrt{\left(\frac{V}{c} \cdot f_{Ch}\right)^2 - f^2}}, |f| < \frac{V}{c} f_{Ch}$$

Where

f: frequency parameter of Doppler spectrum

V: the speed of mobile

C: speed of signal propagation (assumed to be speed of light)

f_{Ch} : the carrier frequency

2.4 Common System Level Modeling Assumptions

The assumptions used in the system-level modeling are listed in Table 2.2.1 and are primarily taken from **[1]**.

Table 2.3.1 Down-link system-level modeling assumptions

Parameter	Explanation/Assumption	Comments
Cellular layout	Hexagonal grid, 3-sector sites	See Figure 43
Antenna horizontal pattern	70 deg (-3 dB) with 20 dB front-to-back ratio	
Site to site distance	2800 m	Or 1000 m
Propagation model	$L = 128.1 + 37.6\ Log_{10}(R)$	R in kilometers
CPICH power	-10 dB	
Other common channels	-10 dB	
Power allocated to WiMAX transmission, including associated signalling	Max. 80 % of total cell power	
Slow fading	As modelled in UMTS 30.03, B 1.4.1.4	
Standard deviation of slow fading	8 dB	
Correlation between sectors	1.0	
Correlation between sites	0.5	
Correlation distance of slow fading	50 m	
Carrier frequency	2000 MHz	
BS antenna gain	14 dB	
UE antenna gain	0 dBi	
UE noise figure	9 dB	
Thermal noise density	-174 dBm/Hz	
Max. # of retransmissions	3	Retransmissions by fast HARQ. Does not include the initial transmission. Programmable
Fast HARQ scheme	Chase combining or incremental redundancy	
Scheduling algorithm	TBD	
BS total Tx power	Up to 44 dBm	
Specific fast fading model	Jakes spectrum	
WiMAX slot length	2 msec	
MCS feedback delay	2 TTIs	This implies that after a channel measurement is made, it requires two additional TTIs before it can be used at the Base station. For example, a channel measurement made during TTI 1 would be transmitted to the base station and processed during TTIs 2 and 3, and could be used to select the MCS level for TTI 4.
UE spatial distribution	Uniform random spatial distribution over elementary single cell hexagonal central base station	
MIMO configuration *NT:NR*	1:1	
Channel width	5 MHz	
Frequency Re-use	1	

2.5 Performance Metrics

This section describes the performance statistics that are generated as an output from the system-level simulations. In each case, a performance curve given as a function of the number of users per sector is generated.

2.5.1 Output Metrics

The following statistics related to data traffics should be generated and included in the evaluation report for each scheme. A frame as used below is also referred to as a transport block and consists of information bits, CRC, and tail bits.

1. **Average cell throughput [kbps/cell]** is used to study the network throughput performance, and is measured as

$$R = \frac{b}{k \cdot T}$$

where b is the total number of correctly received data bits in all data UEs in the simulated system over the whole simulated time, k is the number of cells in the simulation and T is the simulated time. In the case of only evaluating the center cell site, k is the number of sectors.

2. **Average packet call throughput [kbps]** for user i is defined as

$$R_{pktcall}(i) = \frac{\sum_{k} \text{good bits in packet call } k \text{ of user } i}{\sum_{k} \left(t_{end\_k} - t_{arrival\_k} \right)}$$

where k = denotes the k^{th} packet call from a group of K packet calls where the K packet calls can be for a given user i , $t_{arrival\_k}$ = first packet of packet call k arrives in queue, and t_{end_k} = last packet of packet k is received by the UE. Note for uncompleted packet calls, t_{end_k} is set to simulation end time. The mean, standard deviation, and distribution of this statistic are to be provided.

3. **The packet service session FER** is calculated for all the packet service sessions. A packet service session FER is defined as the ratio

$$FER_{session} = \frac{n_{erroneous\_frames}}{n_{frames}},$$

where $n_{erroneous\_frames}$ is the total number of erroneous frames in the packet service session and n_{frames} is the total number of frames in the packet service session. These individual packet service session FERs from all packet service sessions form the distribution for this statistic. The mean, standard deviation, and the distribution of this statistic are to be provided.

A Definition of a Packet Service Session: A Packet Service Session contains one or several packet calls depending on the application. Packet service session starts when the transmission of the first packet of the first packet call of a given service begins and ends when the last packet of the last packet call of that service has been transmitted. (One packet call contains one or several packets.) Note, that FER statistics are only collected from those frames during which UE is receiving data.

4. **The residual FER** is calculated for each user for each packet service session. A packet service session residual FER is defined by the ratio

$$FER_{residual} = \frac{n_{dropped\_frames}}{n_{frames}},$$

where $n_{dropped\_frames}$ is the total number of dropped frames in the packet service session and n_{frames} is the total number of frames in the packet service session. A dropped frame is one in which the maximum ARQ or HARQ re-transmissions have been exhausted without the frame being successfully decoded. It does not include the RLC initiated re-transmissions. The mean, standard deviation, and distribution of this statistic over all the packet service sessions in the simulation are to be provided.

5. **The averaged packet delay per sector** is defined as the ratio of the accumulated delay for all packets for all UEs received by the sector and the total number of packets. The delay for an individual packet is defined as the time between when the packet enters the queue at transmitter and the time when the packet is received

successively by the UE. If a packet is not successfully delivered by the end of a run, its ending time is the end of the run.

6. **System Outage**

   A user is in outage if more than a given percentage of packets (blocks) experience a delay of greater than a certain time. The system is considered to be in outage if any individual users are in outage.

3 Application Traffic Models

[Describe full buffer and real traffic model. Refer to existing AWG work. More description, More figures, cost implications]

Following traffic types are suggested for evaluation purposes.

3.1 HTTP Traffic Model Characteristics

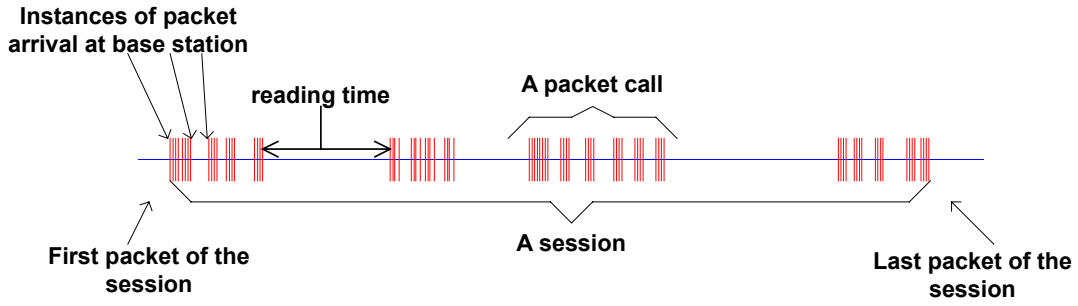

Figure 3.1.1: Packet Trace of a Typical Web Browsing Session

Figure 3.1.1 shows the packet trace of a typical web browsing session. The session is divided into ON/OFF periods representing web-page downloads and the intermediate reading times, where the web-page downloads are referred to as packet calls. These ON and OFF periods are a result of human interaction where the packet call represents a user's request for information and the reading time identifies the time required to digest the web-page.

As is well known, web-browsing traffic is self-similar. In other words, the traffic exhibits similar statistics on different timescales. Therefore, a packet call, like a packet session, is divided into ON/OFF periods as in Figure 3.1.1. Unlike a packet session, the ON/OFF periods within a packet call are attributed to machine interaction rather than human interaction. A web-browser will begin serving a user's request by fetching the initial HTML page using an HTTP GET request. The retrieval of the initial page and each of the constituent *objects* is represented by ON period within the packet call while the parsing time and protocol overhead are represented by the OFF periods within a packet call. For simplicity, the term "page" will be used in this paper to refer to each packet call ON period.

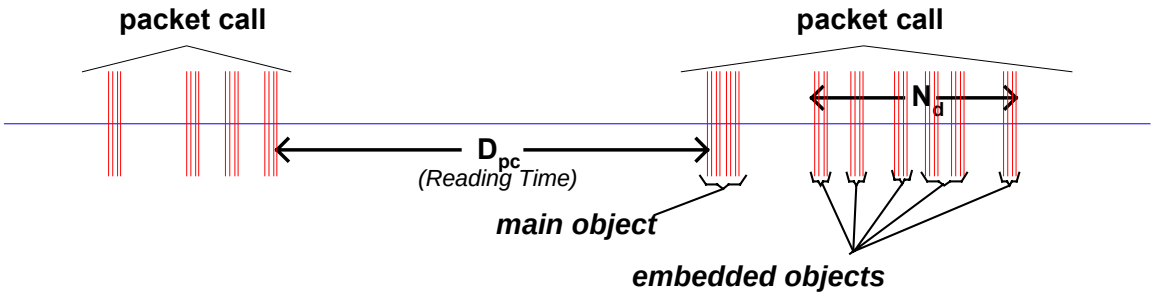

Figure 3.1.2: Contents in a Packet Call

The parameters for the web browsing traffic are as follows:

- S_M: Size of the main object in a page
- S_E: Size of an embedded object in a page
- N_d: Number of embedded objects in a page
- D_{pc}: Reading time
- T_p: Parsing time for the main page

HTTP/1.1 persistent mode transfer is used to download the objects, which are located at the same server and the objects are transferred serially over a single TCP connection as modelled in[5]. The distributions of the parameters for the web browsing traffic model are described in Table 3.1.1. Based on observed packet size distributions, 76% of the HTTP packet calls should use an MTU of 1500 bytes, with the remaining 24% of the HTTP packet calls using an MTU of 576 bytes. These two potential packet sizes also include a 40 byte IP packet header (thereby resulting in useful data payloads of 1460 and 536 bytes, respectively), and this header overhead for the appropriate number of packets must be added to the object data sizes calculated from the probabilistic distributions in Table 3.1.1.

Table 3.1.1: HTTP Traffic Model Parameters

Component	Distribution	Parameters	PDF
Main object size (S_M)	Truncated Lognormal	Mean = 10710 bytes Std. dev. = 25032 bytes Minimum = 100 bytes Maximum = 2 Mbytes	$f_x = \frac{1}{\sqrt{2\pi}\sigma x}\exp\left[\frac{-(\ln x-\mu)^2}{2\sigma^2}\right], x \geq 0$ $\sigma = 1.37, \mu = 8.35$
Embedded object size (S_E)	Truncated Lognormal	Mean = 7758 bytes Std. dev. = 126168 bytes Minimum = 50 bytes Maximum = 2 Mbytes	$f_x = \frac{1}{\sqrt{2\pi}\sigma x}\exp\left[\frac{-(\ln x-\mu)^2}{2\sigma^2}\right], x \geq 0$ $\sigma = 2.36, \mu = 6.17$
Number of embedded objects per page (N_d)	Truncated Pareto	Mean = 5.64 Max. = 53	$f_x = \frac{\alpha k^{\alpha}}{x^{\alpha+1}}, k \leq x < m$ $f_x = \left(\frac{k}{m}\right)^{\alpha}, x = m$ (NOTE) $\alpha = 1.1, k = 2, m = 55$
Reading time (D_{pc})	Exponential	Mean = 30 sec	$f_x = \lambda e^{-\lambda x}, x \geq 0$ $\lambda = 0.033$
Parsing time (T_p)	Exponential	Mean = 0.13 sec	$f_x = \lambda e^{-\lambda x}, x \geq 0$ $\lambda = 7.69$
Note: Subtract k from the generated random value to obtain N_d			

3.2 FTP Traffic Model Characteristics

In FTP applications, a session consists of a sequence of file transfers, separated by *reading times*. The two main parameters of an FTP session are:

1. S : the size of a file to be transferred
2. D_{pc}: reading time, i.e., the time interval between end of download of the previous file and the user request for the next file.

The underlying transport protocol for FTP is TCP. The model of TCP connection described in [5]will be used to model the FTP traffic. The packet trace of an FTP session is shown in Figure 3.1.3.

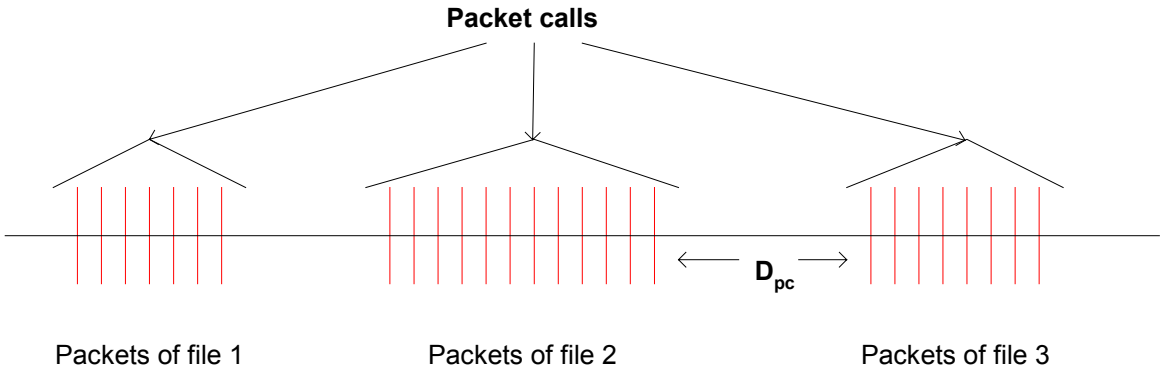

Figure 3.1.3: Packet Trace in a Typical FTP Session

The parameters for the FTP application sessions are described in Table 3.2.1.

Table 3.2.1: FTP Traffic Model Parameters

Component	Distribution	Parameters	PDF
File size (S)	Truncated Lognormal	Mean = 2Mbytes Std. Dev. = 0.722 Mbytes Maximum = 5 Mbytes	$f_x = \frac{1}{\sqrt{2\pi}\sigma x}\exp\left[\frac{-(\ln x-\mu)^2}{2\sigma^2}\right], x \geq 0$ $\sigma = 0.35, \mu = 14.45$
Reading time (D_{pc})	Exponential	Mean = 180 sec.	$f_x = \lambda e^{-\lambda x}, x \geq 0$ $\lambda = 0.006$

Based on the results on packet size distribution, 76% of the files are transferred using and MTU of 1500 bytes and 24% of the files are transferred using an MTU of 576 bytes. Note that these two packet sizes also include a 40 byte IP packet header (thereby resulting in useful data payloads of 1460 and 536 bytes, respectively) and this header overhead for the appropriate number of packets must be added to the file sizes calculated from the probabilistic distributions in Table 3.2.1. For each file transfer a new TCP connection is used whose initial congestion window size is 1 segment (i.e. MTU).

3.3 NRTV (Near Real Time Video) Traffic Model Characteristics

This section describes a model for streaming video traffic on the forward link. Figure 3.1.4 describes the steady state of video streaming traffic from the network, as seen by the base station. Latency at call startup is not considered in this steady-state model.

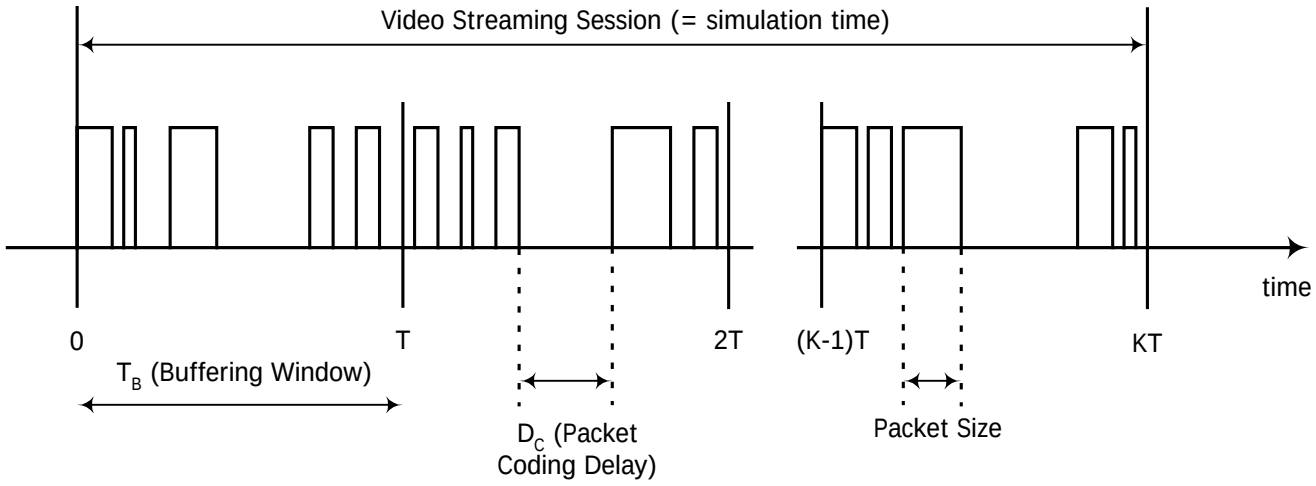

Figure 3.1.4: Video Streaming Traffic Model

A video streaming session is defined as the entire video streaming call time, which is equal to the simulation time for this model. Each frame of video data arrives at a regular interval T determined by the number of frames per second (fps). Each frame is decomposed into a fixed number of slices, each transmitted as a single packet. The size of these packets/slices is distributed as a truncated Pareto distribution. Encoding delay, Dc, at the video encoder introduces delay intervals between the packets of a frame. These intervals are modelled by a truncated Pareto distribution.

The parameter T_B is the length (in seconds) of de-jitter buffer window in the mobile station, and is used to guarantee a continuous display of video streaming data. This parameter is not relevant for generating the traffic distribution, but it is useful for identifying periods when the real-time constraint of this service is not met. At the beginning of the simulation, it is assumed that the mobile station de-jitter buffer is full with (T_B x source video data rate) bits of data. Over the simulation time, data is "leaked" out of this buffer at the source video data rate and "filled" as forward link traffic reaches the mobile station. As a performance criterion, the mobile station can record the length of time, if any, during which the de-jitter buffer runs dry. The de-jitter buffer window for the video streaming service is 5 seconds.

Using a source video rate of 64 kbps, the video traffic model parameters are defined in Table 3.3.1.

Table 3.3.1: Video Streaming Traffic Model Parameters.

Information types	Inter-arrival time between the beginning of each frame	Number of packets (slices) in a frame	Packet (slice) size	Inter-arrival time between packets (slices) in a frame
Distribution	Deterministic (Based on 10fps)	Deterministic	Truncated Pareto (Mean= 50bytes, Max= 250bytes)	Truncated Pareto (Mean= 6ms, Max= 12.5ms)
Distribution Parameters	100ms	8	K = 40 bytes α = 1.2	K = 2.5ms α = 1.2

Only system-level simulations with homogenous traffic mixes are to be conducted. That is, for a particular simulation, all users will either have all FTP traffic, all HTTP traffic, or all NRTV traffic. There is no mixing of different traffic types within a single simulation.

4. Protocol layer modules

[TCP, UDP, RTSP, anything that can be taken from NS2 contributions]

5. MAC layer abstraction

[Frame structure, Schedulers, service classes, WiMAX optional profile elements such as power control, Link layer ARQ, details in Annex-C]

6. PHY modem abstraction for system model

[Level of abstraction that is required. HARQ. reference to Annex-B]

6.1 Reference System Scenario for High Speed Data Services Capacity Evaluation

This section describes reference scenarios for evaluating the throughput of OFDM radio interfaces in the context of high speed data services. The remaining issues include the drawbacks associated with the additional carrier, frequency availability and planning, carrier access and handover issues.

6.1.1 OFDM Downlink

In the Section, an initial reference system configuration is proposed to evaluate an OFDM downlink. The OFDM DL carrier is operated using WiMAX features, such as link adaptation and HARQ.

6.2 Reference OFDM configuration for the evaluation

Two sets of reference OFDM configuration parameters are listed in Table 7.2.1.

Table 7.2.1: Reference OFDM configuration parameter sets

Parameters	Set 1	Set 2
TTI duration (msec)	2	2
FFT size (points)	512	1024
OFDM sampling rate (Msamples/sec)	7.68	6.528
Ratio of OFDM sampling rate to UMTS chip rate	2	17/10
Guard time interval (cyclic prefix) (samples/μsec)	56 / 7.29 57 / 7.42(NOTE1)	64/9.803
Subcarrier separation (kHz)	15	6.375
# of OFDM symbols per TTI	27	12
OFDM symbol duration (μsec)	73.96/74.09(NOTE2)	166.67
# of useful subcarriers per OFDM symbol	299	705
OFDM bandwidth (MHz)	4.485	4.495
NOTE1: Requires one extra prefix sample for 8 out of 9 OFDM symbols NOTE2: Depending on guard interval duration		

The parameter set 1 consists of nine OFDM symbols that fit into a 0.667 us timeslot. The useful symbol duration is equal to 512 samples. The guard interval is equal to 56 samples for the 0^{th} symbol, and 57 samples for symbols 1..8 of every timeslot, as illustrated in figure 7.2.1. The actual position of the 56-sample GI symbol is believed to be inconsequential as long as it is known by both the transmitter and receiver. Therefore, it may be revisited in future, should a different location be deemed more favourable.

It should be noted that spectral shaping of the OFDM signal is required for out-of-band emission compliance. The implications of spectral shaping on delay spread robustness are discussed in a separate section of this report.

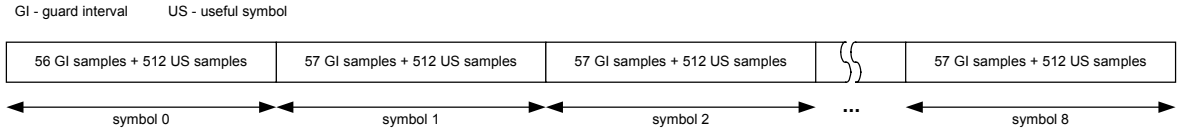

Figure 7.2.1: Temporal structure of the OFDM signal (one timeslot), parameter set 1.

6.3 Frequency re-use and Inter-cell Interference

6.3.1 Frequency Re-use

The assumption regarding the frequency re-use for the OFDM study has been that the same 5MHz carrier can be re-used in each cell, which is often referred to a full frequency re-use, or frequency re-use factor of 1. The main benefit of such a frequency re-use is mainly ease of deployment, given that no frequency planning is required.

Note however that using the same 5MHz carrier in each cell does not necessarily imply that all of the OFDM sub-carriers would be re-used equally in each cell. One could consider several methods based on the orthogonality of OFDM sub-carriers (even in systems that are not time-synchronised) to improve the coverage. The feasibility, benefits and costs of such methods are FFS.

6.3.2 Inter-cell Interference

Given a frequency re-use factor of 1, the system becomes interference-limited, and the interference perceived by the UE from the different cells might not be perfectly white, as assumed for most of the simulations. First, the interfering signals undergo time dispersion, and hence, do not have a flat spectrum. Furthermore, if the OFDM units are not all being used in the interfering cells, the resulting spectrum from each of these partially-load interfering cells will contain gaps. It is therefore likely that the total interference spectrum observed by the UE would not be flat, and hence, it might not be accurately modelled using white noise.

- The impact of realistic inter-cell interference on performance has therefore been evaluated using the Exponential Effective SIR Mapping (EESM). The results are presented in Annex.

7 Channel Models and Interference for System Model

[Propagation loss model to be applied in system simulation, provide references to Annex A]

7.1 Channel Models

In this context, a channel model corresponds to a specific number of paths, a power profile giving the relative powers of these multiple paths (ITU multi-path models), and Doppler frequencies to specify the fade rate.

The channel models (from 1 to 6) are randomly assigned to the various users according to the probability distribution listed in Table 8.1.1. The channel model assigned to a specific user remains fixed over the duration of a simulation drop.

Table 8.1.1: Channel Models and associated assignment probability distribution

Channel Model	Multi-path Model	# of Paths	Speed (km/h)	Fading	Assignment Probability
Model 1	Ch-100	1	30	Jakes	0.1
Model 2	Ch-100	1	120	Jakes	0.1
Model 3	Ch-104	6	30	Jakes	0.1
Model 4	Ch-104	6	120	Jakes	0.1
Model 5	Ch-102	4	3	Jakes	0.3
Model 6	Ch-103	6	3	Jakes	0.3

The channel models, UE speeds (for fading rates), and assignment probabilities listed in Table 8.1.1 are adapted from [1]. Note that a separate link-level simulation must be performed for each specific channel model and UE velocity combination. Hence, there is a desire to minimize the number of different possible channel model combinations, while ensuring that an accurate modelling of reality is also made. The assignment probabilities in Table 8.1.1 were selected to agree with the corresponding probabilities in [1], while reducing the number of different distinct fading velocities in order to reduce the number of link level simulations that must be performed.

The normalized power profiles for the different channel models such as flat fading: Ch-100, ITU vehicular-A: Ch-104, ITU pedestrian-A: Ch-102, and ITU pedestrian-B: Ch-103 are given in Table 8.1.2. For the channel models that correspond to the standard ITU channel models, the relative ratios of the path powers are the same, but the absolute power values have been normalized so that they sum to 0 dB (unit energy) for each given channel model.

Table 8.1.2: Normalized power profiles for multi-path channel models

Channel Model	Path 1 (dB)	Path 2 (dB)	Path 3 (dB)	Path 4 (dB)	Path 5 (dB)	Path 6 (dB)	Rake Fingers
Flat Fading Ch-100	0	–	–	–	–	–	1
ITU Vec. A Ch-104	-3.14	-4.14	-12.14	-13.14	-18.14	-23.14	1,2,3,4,5,6
ITU Ped. A Ch-102	-0.51	-10.21	-19.71	-23.31	–	–	1,2,3,4
ITU Ped. B Ch-103	-3.92	-4.82	-8.82	-11.92	-11.72	-27.82	1,2,3,4,5,6

The Rake finger column in the above table indicates the paths to which Rake fingers will be assigned. It is assumed that Rake fingers will be assigned to each multipath component within a given channel model [1]. It is also possible to assign Rake fingers only to those channel taps that contain most of the signal power eg. not assign Rake fingers to channel taps that attenuate the transmitted signal more than 10 dB.

-

Annex A: Channel Models for System Modeling

A.1 Special Channel Models Terminology

In this document the following are terms that are commonly used interchangeably and are equivalent. To promote consistency, the term on the left will be preferred in this document unless otherwise stated.

MS = Mobile Station = UE = User Equipment = Terminal = Subscriber Unit

BS = Base Station = Node-B = BTS

AS = Angle Spread = Azimuth Spread = σ_{AS}

DS = delay spread = σ_{DS}

LN = lognormal shadow fading = σ_{AS}

Path = Ray

Path Component = Sub-ray

PAS = Power Azimuth Spectrum

DoT = Direction of TravelAoA = Angle of Arrival

AoD = Angle of Departure

PDP = Power Delay Profile

A.2 Focus Areas for System level evaluation.

Within this category, a list of four focus areas are identified, however the emphasis here is on items a & b.

a. Physical parameters (e.g. power delay profiles, angle spreads, dependencies between parameters)

b. System evaluation methodology.

c. Antenna arrangements, reference cases and definition of minimum requirements.

d. Some framework (air interface) dependent parameters.

A.3 Link Level Channel Models for Calibration Purposes

The link level models are defined only for calibration purposes. This section describes physical parameters for link level modeling.

Link level simulations alone will not be used for system comparison because they reflect only one snapshot of the channel behavior. Furthermore, they do not account for system attributes such as scheduling and HARQ. For these reasons, link level simulations do not allow any conclusions about the typical behavior of the system. Only system level simulations can achieve that.

A.3.1 Link Level Channel Model Parameter Summary

The table below summarizes the physical parameters to be used for link level modeling.

Table 0-1. Summary of Suggested SCM Link Level Parameters for Calibration Purposes

Model		Case I		Case II		Case III		Case IV	
Corresponding 3GPP Designator*		Case B		Case C		Case D		Case A	
Corresponding 3GPP2 Designator*		Model A, D, E		Model C		Model B		Model F	
PDP		Modified Pedestrian A		Vehicular A		Pedestrian B		Single Path	
# of Paths		1) 4+1 (LOS on, K = 6dB) 2) 4 (LOS off)		6		6		1	
Relative Path Power (dB)	Delay (ns)	1) 0.0 2) -Inf	0	0,0	0	0.0	0	0	0
		1) -6.51 2) 0.0	0	-1.0	310	-0.9	200		
		1) -16.21 2) -9.7	110	-9.0	710	-4.9	800		
		1) -25.71 2) –19.2	190	-10.0	1090	-8.0	1200		
		1) -29.31 2) -22.8	410	-15.0	1730	-7.8	2300		
				-20.0	2510	-23.9	3700		
Speed (km/h)		1) 3 2) 30, 120		3, 30, 120		3, 30, 120		3	
UE/Mobile Station	Topology	Reference 0.5λ		Reference 0.5λ		Reference 0.5λ		N/A	
	PAS	1) LOS on: Fixed AoA for LOS component, remaining power has 360 degree uniform PAS. 2) LOS off: PAS with a Lapacian distribution, RMS angle spread of 35 degrees per path		RMS angle spread of 35 degrees per path with a Lapacian distribution Or 360 degree uniform PAS.		RMS angle spread of 35 degrees per path with a Lapacian distribution		N/A	
	DoT (degrees)	0		22.5		-22.5		N/A	
	AoA (degrees)	22.5 (LOS component) 67.5 (all other paths)		67.5 (all paths)		22.5 (odd numbered paths), -67.5 (even numbered paths)		N/A	
Node B/	Topology	Reference: ULA with 0.5λ-spacing or 4λ-spacing or 10λ-spacing						N/A	

Model		Case I	Case II	Case III	Case IV
	PAS	Lapacian distribution with RMS angle spread of 2 degrees or 5 degrees, per path depending on AoA/AoD			N/A
	AoD/AoA (degrees)	50^o for 2^o RMS angle spread per path 20^o for 5^o RMS angle spread per path			N/A

*Designators correspond to channel models previously proposed in 3GPP and 3GPP2 ad-hoc groups.

A.3.2 Spatial Parameters per Path

Each resolvable path is characterized by its own spatial channel parameters (angle spread, angle of arrival, power azimuth spectrum). All paths are assumed independent. These assumptions apply to both the BS and the MS specific spatial parameters. The above assumptions are in effect only for the Link Level channel model.

A.3.3 BS and MS Array Topologies

The spatial channel model should allow any type of antenna configuration to be selected, although details of a given configuration must be shared to allow others to reproduce the model and verify the results.

Calibrating simulators at the link level requires a common set of assumptions including a specific set of antenna topologies to define a baseline case. At the MS, the reference element spacing is 0.5λ. At the BS, three values for reference element spacing are defined: 0.5λ, 4λ, and 10λ.

A.3.4 Spatial Parameters for the BS

A.3.4.1 BS Antenna Pattern

The 3-sector antenna pattern used for each sector, Reverse Link and Forward Link, is plotted in Figure 0-1 and is specified by

$$A(\theta) = -\min\left[12\left(\frac{\theta}{\theta_{3dB}}\right)^2, \ A_m\right] \quad \text{where} \quad -180 \le \theta \le 180$$

θ is defined as the angle between the direction of interest and the boresight of the antenna, θ_{3dB} is the 3dB beamwidth in degrees, and A_m is the maximum attenuation. For a 3 sector scenario θ_{3dB} is 70^o, $A_m = 20dB$, and the antenna boresight pointing direction is given by Figure 0-2. For a 6 sector scenario θ_{3dB} is 35^o, $A_m = 23dB$, which results in the pattern shown in Figure 0-3, and the boresight pointing direction defined by Figure 0-4. The boresight is defined to be the direction to which the antenna shows the maximum gain. The gain specified by previous 3GPP documents[xi] for the 3-sector 70^o antenna is 14dBi. By reducing the beamwidth by half to 35^o, the corresponding gain will be 3dB higher resulting in 17dBi. The antenna pattern shown is targeted for diversity oriented implementations (i.e. large inter-element spacings). For beamforming applications that require small spacings, alternative antenna designs may have to be considered leading to a different antenna pattern.

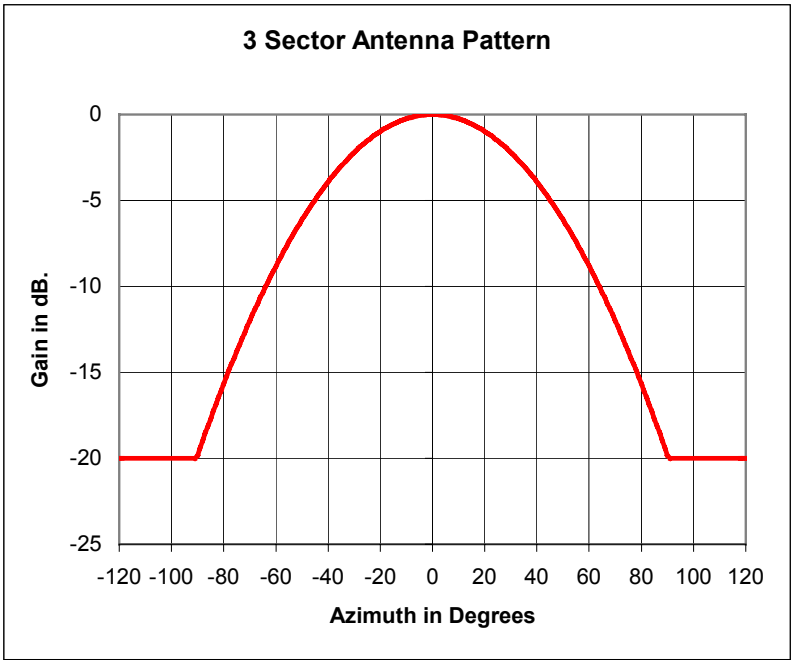

Figure 0-1 Antenna Pattern for 3-Sector Cells

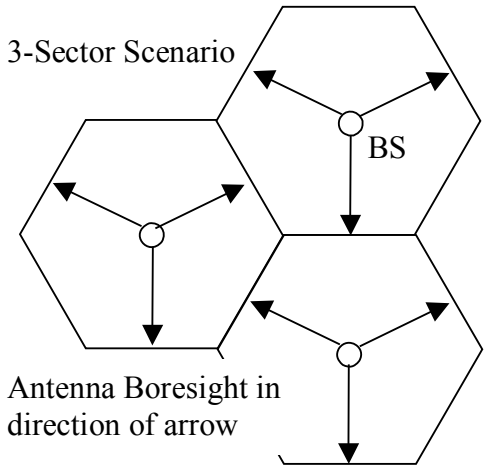

Figure 0-2 Boresight pointing direction for 3-sector cells

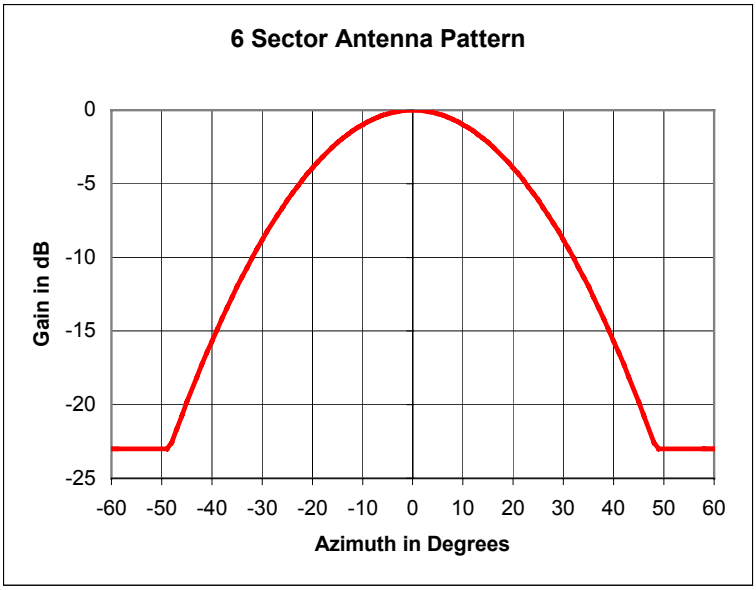

Figure 0-3 Antenna Pattern for 6-Sector Cells

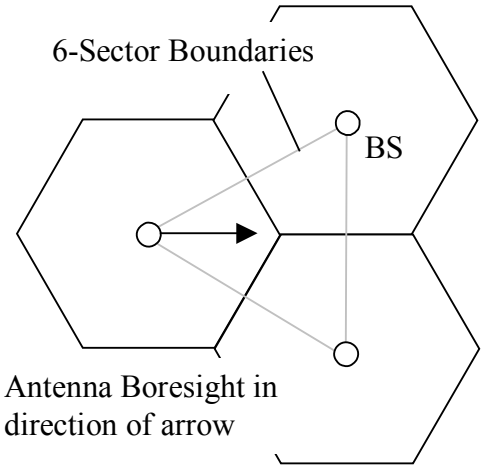

Figure 0-4 Boresight Pointing direction for 6-Sector Cells

A.3.4.2 Per Path BS Angle Spread (AS)

The base station per path angle spread is defined as the root mean square (RMS) of angles with which an arriving path's power is received by the base station array. The individual path powers are defined in the temporal channel model described in Table 0-1. Two values of BS angle spread (each associated with a corresponding mean angle of arrival, AoA) are considered:

- AS: 2 degrees at AoA 50 degrees
- AS: 5 degrees at AoA 20 degrees

It should be noted that attention should be paid when comparing the link level performance between the two angle spread values since the BS antenna gain for the two corresponding AoAs will be different. The BS antenna gain is applied to the path powers specified in Table 0-1.

A.3.4.3 Per Path BS Angle of Arrival

The Angle of Arrival (AoA) or Angle of Departure (AoD) is defined to be the mean angle with which an arriving or departing path's power is received or transmitted by the BS array with respect to the boresite. The two values considered are:

- AoA: 50 degrees (associated with the RMS Angle Spread of 2 degrees)
- AoA: 20 degrees (associated with the RMS Angle Spread of 5 degrees)

A.3.4.4 Per Path BS Power Azimuth Spectrum

The Power Azimuth Spectrum (PAS) of a path arriving at the base station is assumed to have a Laplacian distribution. For an incoming AOA $\bar{\theta}$ and RMS angle-spread σ, the BS per path PAS value at an angle θ is given by:

$$P(\theta,\sigma,\bar{\theta}) = N_o \exp\left[\frac{-\sqrt{2}\left|\theta-\bar{\theta}\right|}{\sigma}\right] G(\theta)$$

where both angles $\bar{\theta}$ and θ are given with respect to the boresight of the antenna elements. It is assumed that all antenna elements' orientations are aligned. Also, P is the average received power and G is the numeric base station antenna gain described in Section 0 by

$$G(\theta) = 10^{0.1A(\theta)}$$

Finally, N_o is the normalization constant:

$$N_o^{-1} = \int_{-\pi+\bar{\theta}}^{\pi+\bar{\theta}} \exp\left[\frac{-\sqrt{2}\left|\theta-\bar{\theta}\right|}{\sigma}\right] \cdot G(\theta) d\theta$$

In the above equation, θ represents path components (sub-rays) of the path power arriving at an incoming AoA $\bar{\theta}$. The distribution of these path components is TBD.

A.3.5 Spatial Parameters for the MS

A.3.5.1 MS Antenna Pattern

For each and every antenna element at the MS, the antenna pattern will be assumed omni directional with an antenna gain of -1 dBi.

A.3.5.2 Per Path MS Angle Spread (AS)

The MS per path AS is defined as the root mean square (RMS) of angles of an incident path's power at the MS array. Two values of the path's angle spread are considered:

- AS: 104 degrees (results from a uniform over 360 degree PAS),
- AS: 35 degrees for a Laplacian PAS with a certain path specific Angle of Arrival (AoA).

A.3.5.3 Per Path MS Angle of Arrival

The per path Angle of Arrival (AOA) is defined as the mean of angles of an incident path's power at the UE/Mobile Station array with respect to the broadside as shown Figure 0-5.

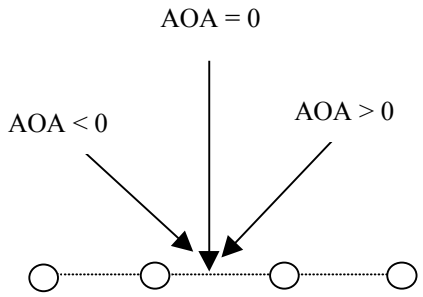

Figure 0-5. Angle of Arrival orientation at the MS.

Three different per path AoA values at the MS are suggested for the cases of a non-uniform PAS, see Table 0-1 for details:

- AoA: -67.5 degrees (associated with an RMS Angle Spread of 35 degrees)
- AoA: +67.5 degrees (associated with an RMS Angle Spread of 35 degrees)
- AoA: +22.5 degrees (associated with an RMS Angle Spread of 35 degrees or with an LOS component)

A.3.5.4 Per Path MS Power Azimuth Spectrum

The Laplacian distribution and the Uniform distribution are used to model the per path Power Azimuth Spectrum (PAS) at the MS.

The Power Azimuth Spectrum (PAS) of a path arriving at the MS is modeled as either a Laplacian distribution or a uniform over 360 degree distribution. Since an omni directional MS antenna gain is assumed, the received per path PAS will remain either Laplacian or uniform. For an incoming AOA $\bar{\theta}$ and RMS angle-spread σ, the MS per path Laplacian PAS value at an angle θ is given by:

$$P(\theta, \sigma, \bar{\theta}) = N_o \exp\left[\frac{-\sqrt{2}\left|\theta - \bar{\theta}\right|}{\sigma}\right],$$

where both angles $\bar{\theta}$ and θ are given with respect to the boresight of the antenna elements. It is assumed that all antenna elements' orientations are aligned. Also, P is the average received power and N_o is the normalization constant:

$$N_o^{-1} = \int_{-\pi+\bar{\theta}}^{\pi+\bar{\theta}} \exp\left[\frac{-\sqrt{2}\left|\theta - \bar{\theta}\right|}{\sigma}\right] d\theta .$$

In the above equation, θ represents path components (sub-rays) of the path power arriving at an incoming AoA $\bar{\theta}$. The distribution of these path components is TBD.

A.3.5.5 MS Direction of Travel

The mobile station direction of travel is defined with respect to the broadside of the mobile antenna array as shown in Figure 0-5.

A.3.5.6 Per Path Doppler Spectrum

The per path Doppler Spectrum is defined as a function of the direction of travel and the per path PAS and AoA at the MS. This should correspond to the per path fading behavior for either the correlation-based or ray-based method.

A.3.6 Calibration and Reference Values

For the purpose of link level simulations, reference values of the average correlation are given below in Table 0-2. The reference values are provided for the calibration of the simulation software and to assist in the resolution of possible errors in the simulation methods implemented. Specifically, the average complex correlation and magnitude of the complex correlation is reported between BS antennas and between MS antennas. The spatial parameter values used are those defined already throughout Section 0.

Table 0-2. Reference Correlation Values.

	Antenna Spacing	AS (degrees)	AOA (degrees)	Correlation (magnitude)	Complex Correlation
BS	0.5 λ	5	20	0.9688	0.4743+0.8448i
	0.5 λ	2	50	0.9975	-0.7367+0.6725i
	4 λ	5	20	0.3224	-0.2144+0.2408i
	4 λ	2	50	0.8624	0.8025+0.3158i
	10 λ	5	20	0.0704	-0.0617+i0.034
	10 λ	2	50	0.5018	-0.2762-i0.4190
MS	λ /2	104	0	0.3042	-0.3042
	λ /2	35	-67.5	0.7744	-0.6948-i0.342
	λ /2	35	22.5	0.4399	0.0861+0.431i
	λ /2	35	67.5	0.7744	-0.6948+i0.342

A.4 System Level Spatial Channel Model

The spatial channel model for use in the system-level simulations is described in this section.

As opposed to link simulations which simply consider a single BS transmitting to a single MS, the system simulations typically consist of multiple cells, BSs, and MSs. Performance metrics such as throughput and delay are collected over D drops, where a "drop" is defined as a simulation run for a given number of cells, BSs, and MSs, over a specified number of frames. During a drop, the channel undergoes fast fading according to the motion of the MSs. Channel state information is fed back from the MSs to the BSs, and the BSs use schedulers to determine which user(s) to transmit to. Typically, over a series of D drops, the cell layout and locations of the BSs are fixed, but the locations of the MSs are randomly varied at the beginning of each drop. To simplify the simulation, only a subset of BSs will actually be simulated while the remaining BSs are assumed to transmit with full power. (Questions remain about how to model interfering BS powers.)

The goal of this section is to define the methodology and parameters for generating the spatial and temporal channel coefficients between a given base and mobile for use in system level simulations. For an S element BS array and a U element MS array, the channel coefficients for one of N multipath components (note that these components are not necessarily time resolvable, meaning that the time difference between successive paths may be less than a chip period) are given by an S -by- U matrix of complex amplitudes. We denote the channel matrix for the nth multipath component ($n = 1,\ldots,N$) as $\mathbf{H}_n(t)$. It is a function of time t because the complex amplitudes are undergoing fast fading governed by the movement of the MS. The overall procedure for generating the channel matrices consists of three basic steps:

1. Specify an environment, either suburban macro, urban macro, or urban micro (Section 3.2).

2. Obtain the parameters to be used in simulations, associated with that environment (Section 3.3).
3. Generate the channel coefficients based on the parameters (Section 3.4).

Sections 3.2, 3.3, and 3.4 give the details for the general procedure. Figure 0-6below provides a roadmap for generating the channel coefficients. (This diagram should be greatly expanded and should show which section numbers each of the items is discussed.) Section 3.5 considers options for modifying the general procedure. Section 3.6 describes the procedure for generating correlated log normal user parameters used in Section 3.3. Section 3.7 describes the method for accounting for intercell interference. Section 3.8 presents calibration results.

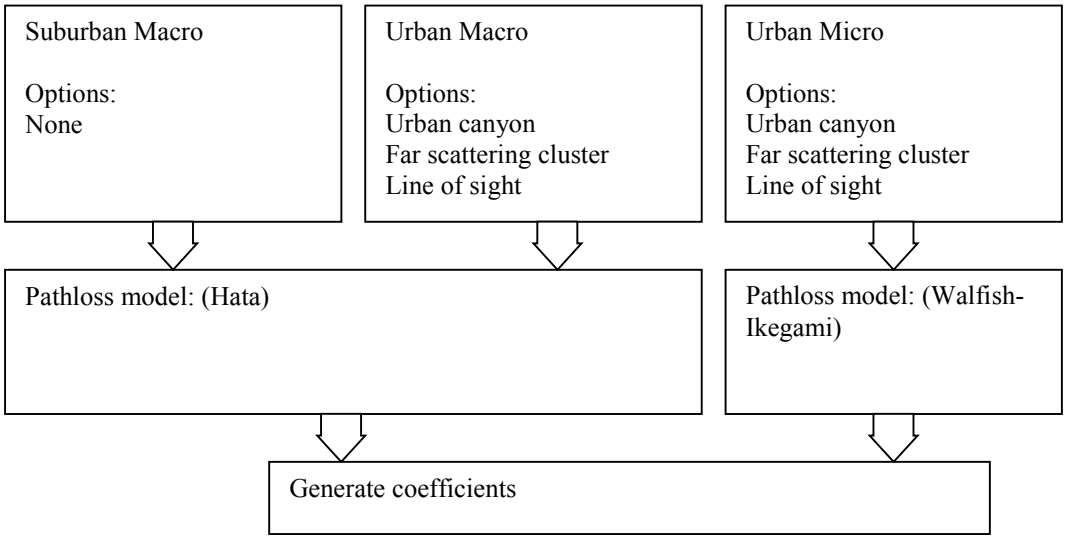

Figure 0-6, Model Structure

A.4.1 General definitions , parameters, and assumptions

The received signal at the MS consists of *N* time-delayed multipath replicas of the transmitted signal. These *N* paths are defined by powers and delays and are chosen randomly according to the channel generation procedure. Each path consists of *M* subpaths.

Figure 0-7 shows the angular parameters used in the model. The following definitions are used:

Ω_{BS} BS antenna array orientation, defined as the difference between the broadside of the BS array and the absolute North (N) reference direction.

θ_{BS} LOS AoD direction between the BS and MS, with respect to the broadside of the BS array.

$\delta_{n,AoD}$ AoD for the *n*th ($n = 1 \ldots N$) path with respect to the LOS AoD θ_0.

$\Delta_{n,m,AoD}$ Offset for the *m*th ($m = 1 \ldots M$) subpath of the *n*th path with respect to $\delta_{n,AoD}$.

$\theta_{n,m,AoD}$ Absolute AoD for the *m*th ($m = 1 \ldots M$) subpath of the *n*th path at the BS with respect to the BS broadside.

Ω_{MS} MS antenna array orientation, defined as the difference between the broadside of the MS array and the absolute North reference direction.

θ_{MS} Angle between the BS-MS LOS and the MS broadside.

$\delta_{n,AoA}$ AoA for the *n*th ($n = 1 \ldots N$) path with respect to the LOS AoA $\theta_{0,MS}$.

$\Delta_{n,m,AoA}$ Offset for the *m*th ($m = 1 \ldots M$) subpath of the *n*th path with respect to $\delta_{n,AoA}$.

$\theta_{n,m,AoA}$ Absolute AoA for the *m*th ($m = 1 \ldots M$) subpath of the *n*th path at the BS with respect to the BS broadside.

v MS velocity vector.

θ_v Angle of the velocity vector with respect to the MS broadside: $\theta_v = \arg(\mathbf{v})$.

The angles shown in Figure 1 that are measured in a clockwise direction are assumed to be negative in value.

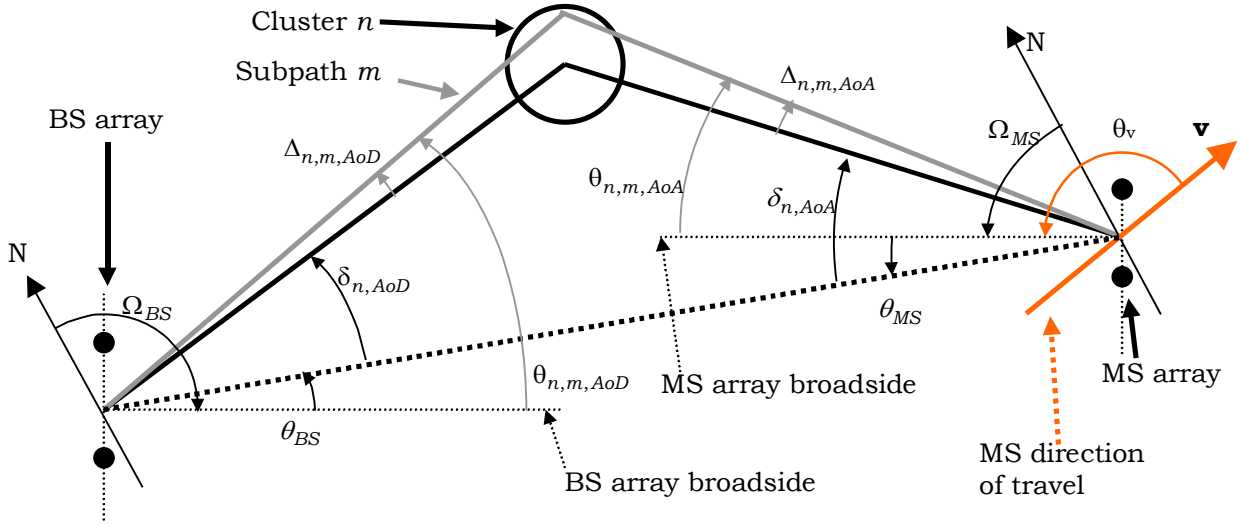

Figure 0-7 BS and MS angle parameters

For system level simulation purposes, the fast fading per-path will be evolved in time, although bulk parameters including angle spread, delay spread, log normal shadowing, and MS location will remain fixed during the evaluation of the given MS.

The following are general assumptions made for all simulations, independent of environment:

1. Mapping of paths to resolvable paths. TBD
2. Fractional Unrecovered Power (FURP) is TBD.
3. Uplink-Downlink Reciprocity: The AoD/AoA values are identical between the uplink and downlink.
4. Random path phases between UL, DL are uncorrelated.
5. Mobile-to-mobile shadowing is uncorrelated.
6. The spatial channel model should allow any type of antenna configuration to be selected, although details of a given configuration must be shared to allow others to reproduce the model and verify the results. It is intended that the spatial channel model be capable of operating on any given antenna array configuration. In order to compare algorithms, reference antenna configurations based on uniform linear array configurations with 0.5, 4, and 10 wavelength inter-element spacing will be used.

A.4.2 Environments

We consider the following three environments.

1. Suburban macrocell (approximately 3Km distance BS to BS)
2. Urban macrocell (approximately 3Km distance BS to BS)

3. Urban microcell (less than 1Km distance BS to BS)

The characteristics of the macro cell environments assume that BS antennas are above rooftop height. For the urban microcell scenario, we assume the BS antenna is at rooftop height. Table 0-3 describes the parameters used in each of the environments.

Table 0-3 Scenario parameters

Channel Scenario	**Suburban Macro**	**Urban Macro**	**Urban Micro**
Number of paths (*N*)	6	6	6
Number of sub-paths (*M*) per path	20	20	20
Mean composite AS at BS	$E(\sigma_{AS})=5^0$	$E(\sigma_{AS})=8^0, 15^0$	NLOS: $E(\sigma_{AS})=19^0$
r_{DS} ($\sigma_{delays}/\sigma_{DS}$)	1.4	1.7	N/A
r_{AS} ($\sigma_{AoD}/\sigma_{PAS}$)	1.2	1.3	N/A
Composite AS at BS as a lognormal RV when simulating with 6 paths $\sigma_{AS} = 10 \wedge (\varepsilon_{AS} x + \mu_{AS})$, $x \sim \eta(0,1)$	$\mu_{AS}= 0.69$ $\varepsilon_{AS}= 0.13$	8^0 $\mu_{AS}= 0.810$ $\varepsilon_{AS}= 0.3295$ 15^0 $\mu_{AS}= 1.18$ $\varepsilon_{AS}= 0.210$	N/A
Per path AS at BS (Fixed)	2 deg	2 deg	5 deg (LOS and NLOS)
BS Per path AoD Distribution st dev	$N(0, \sigma^2_{AoD})$, where $\sigma_{AoD} = r_{AS}*\sigma_{AS}$	$N(0, \sigma^2_{AoD})$, where $\sigma_{AoD} = r_{AS}*\sigma_{AS}$	U(-40deg, 40deg)
Mean of RMS composite AS at MS	$E(\sigma_{AS, comp,UE})=72^0$	$E(\sigma_{AS, comp, UE})=72^0$	$E(\sigma_{AS, comp, UE})=72^0$
Per path AS at MS (fixed)	35^0	35^0	35^0
MS Per path AoA Distribution	$N(0, \sigma^2_{AoA}(P_r))$	$N(0, \sigma^2_{AoA}(P_r))$	$N(0, \sigma^2_{AoA}(P_r))$
Mean total RMS Delay Spread	$E(\sigma_{DS})=0.17$ μs	$E(\sigma_{DS})=0.65$ μs	N/A
Distribution for path delays			U(0, 1.2μs)
Narrowband composite delay spread as a lognormal RV when simulating with 6 paths $\sigma_{DS} = 10 \wedge (\varepsilon_{DS} x + \mu_{DS})$, $x \sim \eta(0,1)$	$\mu_{DS}= - 6.80$ $\varepsilon_{DS}= 0.288$	$\mu_{DS}= -6.18$ $\varepsilon_{DS}= 0.18$	N/A
Lognormal shadowing standard deviation	8dB	8dB	10dB

The following are assumptions made for the macrocell environments.

1. The macrocell pathloss from 3GPP2 evaluation methodology will be used, as shown below.

Propagation Model (BTS Ant Ht=32m, MS=1.5m)	28.6+ 35log10(d) dB, d in meters	Modified Hata Urban Prop. Model @1.9GHz (COST 231). Minimum of 35 meters separation between MS and BS.[3]

2. Antenna patterns at the BS are the same as those used in the link simulations given in Section 2.5.1.

3. Site-to-site LN correlation is $\eta = 0.5$. This parameter is used in Section 3.6.2.

The following are assumptions made for the microcell environments.

The pathloss model: for NLOS, use Walfish-Ikegami modelwith the following parameters for all orientations, (so that the intercept is a constant for all positions in the cell.) Once the slope and intercept are defined, the building information is no longer used.

For NLOS:

Building = 12m, Building to building distance = 50m,

Antenna height = 12.5m, Street width = 25m,

Mobile height = 1.5m, Orientation = 30 deg for all paths,

Frequency = 2 GHz.

These parameters produce the following path loss equations.

Resulting Slope = 38dB/dec Resulting 1Km intercept = 150 dB

This equation reduces to: 36 + 38*log10(d), d in meters.

For LOS, use Walfish-Ikegami street canyon equation: L=42.6 + 26log10(d) + 20log(fc) where d is in Km, fc in MHz. At 2.0 GHz, this reduces to: 30.6 + 26*log10(d), d in meters.

1. Antenna patterns at the BS are the same as those used in the link simulations given in Section 2.5.1. Question about backlobes remain since micro-cells typically have poor backlobes.

2. Site-to-site LN correlation. Shadowing between different paths (delay) are iid. Site-to-site correlation for the same delay follows the macrocell model ($\eta = 0.5$). Some questions remain on this method.

3. A separate bulk log normal shadowing is needed for the path loss is 10dB for NLOS. The value for LOS is TBD.

4. The hexagonal cell repeats will be the assumed layout.

A.4.3 Generating User Parameters

For a given scenario and set of parameters given by a column of Table 3-1, realizations of each user's parameters such as the path delays, powers, and subpath angles of departure and arrival can be derived using the procedure described here in Section 3.3. In particular, Section 3.3.1 gives the steps for the urban macrocell and suburban macrocell environments, and Section 3.3.2 gives the steps for the urban microcell environments.

A.4.3.1 Generating user parameters for urban macrocell and suburban macrocell environments

Step 1: *Choose either an urban macrocell or suburban macrocell environment.*

Step 2: *Determine various distance and orientation parameters.* The placement of the MS with respect to each BS is to be determined according to the cell layout. From this placement, the distance between the MS and the BS (*d*) and the

LOS directions with respect to the BS and MS (θ_{BS} and θ_{MS} , respectively) can be determined. The MS antenna array orientations (Ω_{MS}), are i.i.d., drawn from a uniform 0 to 360 degree distribution. The MS velocity vector **v** has a magnitude $\|\mathbf{v}\|$ drawn according to a velocity distribution (to be determined) and direction θ_v drawn from a uniform 0 to 360 degree distribution.

Step 3: *Determine the DS, AS, and LN.* These variables, given respectively by σ_{DS} , σ_{AS} , and σ_{LN} , are generated as described in Section 0 below. Note that $10\text{^}(\mu_{DS})$ is in units of seconds so that the narrowband composite delay spread σ_{DS} is in units of seconds. Note also that we have dropped the BS indicies used in Section 3.6.1 to simplify notation.

Step 4: *Determine random delays for each of the N multipath components.* For macrocell environments, $N = 6$ as given in Table 3.1. Generate random variables $\tau'_1,\ldots,\tau'_N$ according to

$$\tau'_n = -r_{DS}\sigma_{DS}\log z_n \qquad n = 1,\ldots,N$$

where z_n ***(n = 1,…,N) are i.i.d. random variables with uniform distributionU(0,1),*** r_{DS} ***is given in Table 0-3, and*** σ_{DS} ***is derived in Step 2 above. These variables are ordered so that*** $\tau'_{(N)} > \tau'_{(5)} > \ldots > \tau'_{(1)}$ ***and the minimum of these is subtracted from all so that the first delay is always zero. The delays are quantized in time to the nearest 1/16th chip interval. Then the 6 delays are given by:***

$$\tau_n = \frac{T_c}{16}\cdot\text{floor}\left(\frac{\tau'_{(n)}-\tau'_{(1)}}{T_c/16}+0.5\right), \quad n = 1,\ldots,N,$$

where floor(x) is the integer part of x, and T_c ***is the chip interval (*** $T_c = 1/3.84\text{x}10^6$ ***sec for 3GPP and*** $T_c = 1/1.2288\text{x}10^6$ ***sec for 3GPP2). Then the 6 delays are given by:***

$$\tau_n = \tau'_{(n)} - \tau'_{(1)}, \quad n = 1,\ldots,N.$$

Note that these delays are ordered so that $\tau_N > \tau_5 > \ldots > \tau_1 = 0$. (See notes 1 and 2 at the end of Section 3.3.1.)

Step 5: *Determine random average powers for each of the N multipath components*. Let the unnormalized powers be given by

$$P'_n = e^{\frac{(1-r_{DS})\cdot(\tau'_{(n)}-\tau'_{(1)})}{r_{DS}\cdot\sigma_{DS}}}\cdot 10^{-\xi_n}, n = 1,\ldots,6$$

where ξ_n (n = 1,…,6) are i.i.d. Gaussian random variables with variance σ^2_{RND} = 3 dB, which is a shadowing randomization effect on the per-path powers. Note that the powers are determined using the unquantized channel delays. Average powers are normalized so that total average power for all six paths is equal to one:

$$P_n = \frac{P'_n}{\sum_{n=1}^{6} P'_n}.$$

(See note 3 at the end of Section 3.3.1.)

Step 6: *Determine AoDs for each of the N multipath components*. First generate i.i.d. zero-mean Gaussian random variables:

$$\delta'_n \sim \eta(0,\sigma^2_{AoD}), \qquad n = 1,\ldots,N,$$

where $\sigma_{AoD} = r_{AS}*\sigma_{AS}$. The value r_{AS} is given in Table 3-1 and depends on whether the urban or suburban macrocell environment is chosen. The angle spread σ_{AS} is generated in Step 3. These variables are given in degrees. They are ordered in increasing absolute value so that $|\delta'_{(1)}| < |\delta'_{(2)}| < \ldots < |\delta'_{(N)}|$. The AoDs $\delta_{n,AoD}$, $n = 1,\ldots,N$ are assigned to the ordered variables so that $\delta_{n,AoD} = \delta'_{(n)}$, $n = 1,\ldots,N$. (See note 4 at the end of Section 3.3.1.)

Step 7: *Associate the multipath delays with AoDs.* The *n*th delay τ_n generated in Step 3 is associated with the *n*th AoD $\delta_{n,AoD}$ generated in Step 6.

Step 8: *Determine the powers, phases, and offset AoDs of the M = 20 sub-paths for each of the N paths at the BS.* All 20 sub-path associated with the *n*th path have identical powers (P_n/20 where P_n is from Step 5) and i.i.d phases $\Phi_{n,m}$ drawn from a uniform 0 to 360 degree distribution. The relative offset of the *m*th subpath (*m* = 1,…, *M*) $\Delta_{n,m,AoD}$ is a fixed value given in **Table 0-4**. For example, for the urban and suburban macrocell cases, the offsets for the first and second sub-paths are respectively $\Delta_{n,1,AoD}$ = 0.0894 and $\Delta_{n,2,AoD}$ = -0.0894 degrees. These offsets are chosen to result in the desired per path angle spread (2 degrees for the macrocell environments, and 5 degrees for the microcell environment).

Step 9: *Determine the AoAs for each of the multipath components.* The AoAs are i.i.d Gaussian random variables

$$\delta_{n,AoA} \sim \eta(0, \sigma^2_{n,AoA}), \qquad \textbf{n = 1,..., N,}$$

where $\sigma_{n,AoA} = 104.12\left(1\text{-}\exp\left(\text{-}0.2175\left|10\log_{10}(P_n)\right|\right)\right)$ and P_n is the relative power of the *n*th path from Step 5.

Step 10: *Determine the offset AoAs at the UE of the M = 20 sub-paths for each of the N paths at the MS.* As in Step 8 for the AoD offsets, the relative offset of the *m*th subpath (*m* = 1,…, *M*) $\Delta_{n,m,AoA}$ is a fixed value given in **Table 0-4**. These offsets are chosen to result in the desired per path angle spread of 35 degrees.

Step 11: *Associate the BS and MS paths and sub-paths.* The *n*th BS path (defined by its delay τ_n, power P_n, and AoD $\delta_{n,AoD}$) is associated with the *n*th MS path (defined by its AoA $\delta_{n,AoA}$). For the *n*th path pair, randomly pair each of the *M* BS sub-paths (defined by its offset $\Delta_{n,m,AoD}$ and phase $\Phi_{n,m}$) with a MS sub-path (defined by its offset $\Delta_{n,m,AoA}$). To simplify the notation, we renumber the *M* MS sub-path offsets with their newly associated BS sub-path. In other words, if the first (*m* = 1) BS sub-path is randomly paired with the 10th (*m* = 10) MS sub-path, we re-associate $\Delta_{n,1,AoA}$ (after pairing) with $\Delta_{n,10,AoA}$ (before pairing).

Step 12: *Determine the antenna gains of the BS and MS sub-paths as a function of their respective sub-path AoDs and AoAs.* For the *n*th path, the AoD of the *m*th sub-path (with respect to the BS antenna array broadside) is

$$\theta_{n,m,AoD} = \theta_{BS} + \delta_{n,AoD} + \Delta_{n,m,AoD}.$$

Similarly, the AoA of the *m*th sub-path for the *n*th path (with respect to the MS antenna array broadside) is

$$\theta_{n,m,AoA} = \theta_{MS} + \delta_{n,AoA} + \Delta_{n,m,AoA}.$$

The antenna gains are dependent on these sub-path AoDs and AoAs. For the BS and MS, these are given respectively as $G_{BS}(\theta_{n,m,AoD})$ and $G_{MS}(\theta_{n,m,AoA})$.

Notes:

Note 1: In the development of the Spatial Channel Model, care was taken to include the statistical relationships between Angles and Powers, as well as Delays and Powers. This was done using the proportionality factors $r_{DS} = \sigma_{delays}/\sigma_{DS}$ and $r_{AS} = \sigma_{AoD}/\sigma_{PAS}$ that were based on measurements.)

Note 2: While there is some evidence that delay spread may depend on distance between the transmitter and receiver, the effect is considered to be minor (compared to other dependencies: DS-AS, DS-LN.). Various inputs based on multiple data sets indicate that the trend of DS can be either slightly positive or negative, and may sometimes be relatively flat with distance. For these reasons and also for simplicity, a distance dependence on DS is not modeled.

Note 3: The equations presented here for the power of the nth path are based on an power-delay envelope which is the average behavior of the power-delay profile. Defining the powers to reproduce the average behavior limits the dynamic range of the result and does not reproduce the expected randomness from trial to trial. The randomizing noise ξ_n is used to vary the powers with respect to the average envelope to reproduce the variations experienced in the actual channel. This parameter is also necessary to produce a dynamic range comparable to measurements.

Note 4: The quantity r_{AS} describes the distribution of powers in angle and $r_{AS} = \sigma_{AoD}/\sigma_{AS}$, i.e. the spread of angles to the power weighted angle spread. Higher values of r_{AS} correspond to more power being concentrated in a small AoD or a small number of paths that are closely spaced in angle.

A.4.3.2 Generating user parameters for urban microcell environments

Urban microcell environments differ from the macrocell environments in that the individual multipaths are independently shadowed. Also, only $N = 3$ (instead of 6) paths are modeled because of the reduced delay spread in microcells. We list the entire procedure but only describe the details of the steps that differ from the corresponding step of the macrocell procedure.

Step 1: *Choose the urban microcell environment.*

Step 2: *Determine various distance and orientation parameters.*

Step 3: *Determine the DS, AS, and LN.*

Step 4: *Determine the random delays for each of the N multipath components*. For the microcell environment, $N = 6$. The delays τ_n, $n = 1, \ldots, N$ are i.i.d. random variables drawn from a uniform distribution from 0 to 1.2 μs.

Step 5: *Determine random average powers for each of the N multipath components*. The PDP consists of N=6 distinct paths that are uniformly distributed between 0 and 1.2μs. The powers for each path are exponentially decaying in time with the addition of a lognormal randomness, which is independent of the path delay:

$$P_n = 10^{-(\tau_n + z_n)}$$

where τ_n is given in units of microseconds, and z_n (n = 1,…,N) are i.i.d. zero mean Gaussian random variables with variance of (3dB)^2. The lognormal variation of each path produces the variation seen in the path powers, and a separate log normal shadowing value is applied in common to all paths.

Step 6: *Determine AoDs for each of the N multipath components*. The AoDs (with respect to the LOS direction) are i.i.d. random variables drawn from a uniform distribution over –40 to +40 degrees:

$$\delta_{n,AoD} \sim U(-40, +40), \qquad n = 1, \ldots, N,$$

Associate the AoD of the nth path $\delta_{n,AoD}$ with the power of the nth path P_n. Note unlike the macrocell environment, the AoDs do not need to be sorted before being assigned to a path power.

Step 7: *Associate the multipath delays with AoDs.*

Step 8: *Determine the powers, phases, and offset AoDs of the M = 20 sub-paths for each of the N paths at the BS.* The offsets are given in Table 3-2, and the resulting per path AS is 5 degrees instead of 2 degrees for the macrocell case.

Step 9: *Determine the AoAs for each of the multipath components.* The AoAs are i.i.d Gaussian random variables

$$\delta_{n,AoA} \sim \eta(0, \sigma^2_{n,AoA}), \qquad \textbf{n = 1,…, N,}$$

where $\sigma_{n,AoA} = 104.12\left(1\text{-}\exp\left(\text{-}0.265\left|10\log_{10}(P_n)\right|\right)\right)$ and P_n is the relative power of the nth path from Step 5.

Step 10: *Determine the offset AoAs of the M = 20 sub-paths for each of the N paths at the MS.*

Step 11: *Associate the BS and MS paths and sub-paths.*

Step 12: *Determine the antenna gains of the BS and MS sub-paths as a function of their respective sub-path AoDs and AoAs.*

-

Table 0-4. Sub-path AoD and AoA offsets

Sub-path # (m)	Offset for a 2 deg AS at BS (Macrocell)	Offset for a 5 deg AS at BS (Microcell)	Offset for a 35 deg AS at MS

	$\Delta_{n,m,AoD}$ (degrees)	$\Delta_{n,m,AoD}$ (degrees)	$\Delta_{n,m,AoA}$ (degrees)
1, 2	± 0.0894	± 0.2236	± 1.5649
3, 4	± 0.2826	± 0.7064	± 4.9447
5, 6	± 0.4984	± 1.2461	± 8.7224
7, 8	± 0.7431	± 1.8578	± 13.0045
9, 10	± 1.0257	± 2.5642	± 17.9492
11, 12	± 1.3594	± 3.3986	± 23.7899
13, 14	± 1.7688	± 4.4220	± 30.9538
15, 16	± 2.2961	± 5.7403	± 40.1824
17, 18	± 3.0389	± 7.5974	± 53.1816
19, 20	± 4.3101	± 10.7753	± 75.4274

The values in Table 0-4 are selected to produce a biased standard deviation equal to 2, 5, and 35 degrees, which is equivalent to the per-path power weighted azimuth spread for equal power sub-paths.

A.4.4 Generating channel coefficients

Given the user parameters generated in Section 3.3, we use them to generate the channel coefficients. For an *S* element BS array and a *U* element MS array, the channel coefficients for one of *N* multipath components are given by an *S* -by-*U* matrix of complex amplitudes. We denote the channel matrix for the *n*th multipath component (*n* = 1,…,*N*) as $\mathbf{H}_n(t)$. The (*s,u*)th component (*s* = 1,…,*S*; *u* = 1,…,*U*) of $\mathbf{H}_n(t)$ is given by

$$h_{s,u,n}(t) = \sqrt{\frac{P_n}{M}}\left(\sum_{m=1}^{M} \sqrt{G_{BS}(\theta_{n,m,AoD})}\exp\left(jkd_s\sin(\theta_{n,m,AoD})\right)\times \sqrt{G_{MS}(\theta_{n,m,AoA})}\exp\left(j\left[kd_u\sin(\theta_{n,m,AoA})+\Phi_{n,m}\right]\right)\right)\cdot\exp\left(jk\|\mathbf{v}\|\cos(\theta_{m,n,AoA}-\theta_v)\,t\right)$$

where

P_n is the power of the *n*th path (Step 5).

M is the number of subpaths per path.

$\theta_{n,m,AoD}$ is the the AoD for the *m*th subpath of the *n*th path (Step 12).

$\theta_{n,m,AoA}$ is the the AoA for the *m*th subpath of the *n*th path (Step 12).

$G_{BS}(\theta_{n,m,AoD})$ is the BS antenna array gain (Step 12).

$G_{MS}(\theta_{n,m,AoA})$ is the MS antenna array gain (Step 12).

j is the square root of -1.

k is the wave number $2\pi/\lambda$ where λ is the carrier wavelength in meters.

d_s is the distance in meters from BS antenna element *s* from the reference (*s* = 1) antenna. For the reference antenna *s* = 1, d_1=0.

d_u is the distance in meters from MS antenna element *u* from the reference (*u* = 1) antenna. For the reference antenna *u* = 1, d_1=0.

$\Phi_{n,m}$ is the phase of the *m*th subpath of the *n*th path (Step 8).

$\|\mathbf{v}\|$ is the magnitude of the MS velocity vector (Step 2).

θ_v is the angle of the MS velocity vector (Step 2).

A.4.5 Optional system simulation features

A.4.5.1 Polarized arrays

Practical antennas on handheld devices require spacings much less than λ/2. Polarized antennas are likely to be the primary way to implement multiple antennas. A cross-polarized model is therefore included here.

A method of describing polarized antennas is presented, which is compatible with the 12 step procedure given in section 0. The following steps extend the original 12 to account for the additional polarized components. Each element of the *S* element BS array and *U* element MS array consists of cross-polarized elements.

- **Step 13:** *Generate additional quadrature subpaths.* For each of the 6 paths of Step 4, generate an addition *M* subpaths at the MS and *M* subpaths at the BS to represent the portion of each signal that leaks into the quadrature antenna orientation due to scattering.

- **Step 14:**. *Set subpath AoDs and AoAs.* Set the AoD and AoA of each subpath in Step 13 equal to that of the corresponding subpath of the inline antenna orientation. (Orthogonal sub-rays arrive/depart at common angles.)

- **Step 15:** *Generate phase offsets for the cross-polarized elements.* We define $\Phi_{n,m}^{(x,y)}$ to be the phase offset of the *m*th subpath of the *n*th path between the *x* component (either the horizontal *h* or vertical *v*) of the BS element and the *y* component (either the horizontal *h* or vertical *v*) of the MS element. Set $\Phi_{n,m}^{(h,h)}$ to be $\Phi_{n,m}$ generated in Step 8 of Section 3.3. Generate $\Phi_{n,m}^{(h,v)}$, $\Phi_{n,m}^{(v,h)}$, and $\Phi_{n,m}^{(v,v)}$ as i.i.d random variables drawn from a uniform 0 to 360 degree distribution.

- **Step 16:** The power P2 of each ray in the quadrature orientation is set relative to the power P1 of each ray in the inline orientation according to an XPD ratio, defined as XPD= P1/P2. For urban macrocells: P2 = P1 - A - B*N(0,1), where A=0.34*(mean relative path power)+7.2 dB, and B=5.5dB is the standard deviation of the XPD variation.

  For urban microcells: P2 = P1 - A - B*N(0,1), where A=8 dB, and B=8dB is the standard deviation of the XPD variation.

- **Step 17:** Decompose each of the inline and quadrature sub-rays into vertical and horizontal components based on the in-line and quadrature orientations.

- **Step 18:** At the receive antennas, decompose each of the vertical and horizontal components into components that are in-line and quadrature with the receive antennas and sum the in-line components.

The fading behavior between the cross pol elements will be a function of the per-ray spreads and the Doppler. The fading between orthogonal polarizations has been observed to be independent and therefore the sub-rays phases are chosen randomly. The propagation characteristics of V-to-V paths are assumed to be equivalent to the propagation characteristics of H-to-H paths.

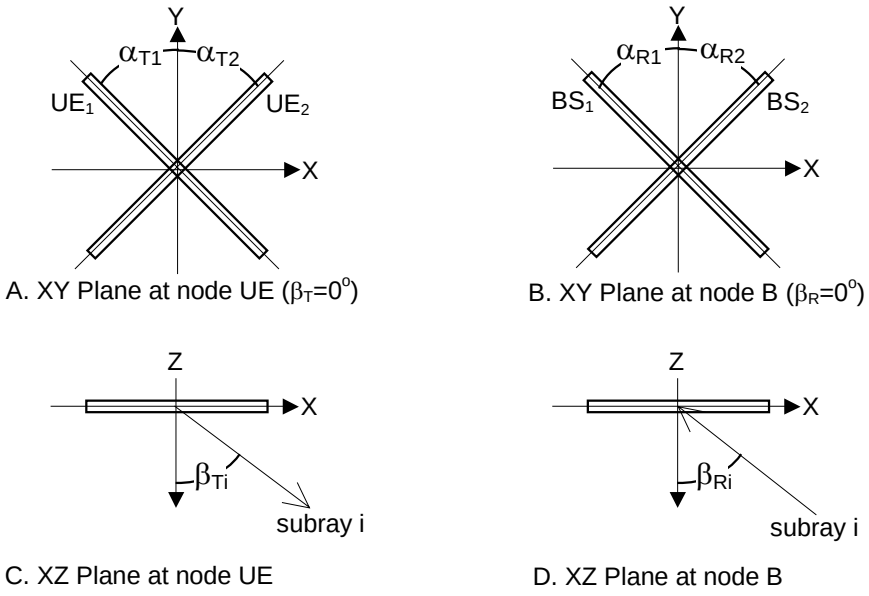

Figure 0-8 Dual Polarization Example

The polarization model can be illustrated by a matrix describing the propagation of and mixing between horizontal and vertical amplitude of each sub-path. The resulting channel realization is:

$$h_{s,u,n}(t) = \sqrt{\frac{P_n}{M}}\left(\sum_{m=1}^{M} \begin{bmatrix} \sqrt{G_{BS}^{(v)}(\theta_{n,m,AoD})} \\ \sqrt{G_{BS}^{(h)}(\theta_{n,m,AoD})} \end{bmatrix}^T \begin{bmatrix} \exp\left(\Phi_{n,m}^{(v,v)}\right) & \sqrt{r_n}\exp\left(\Phi_{n,m}^{(h,v)}\right) \\ \sqrt{r_n}\exp\left(\Phi_{n,m}^{(v,h)}\right) & \exp\left(\Phi_{n,m}^{(h,h)}\right) \end{bmatrix} \begin{bmatrix} \sqrt{G_{MS}^{(v)}(\theta_{n,m,AoD})} \\ \sqrt{G_{MS}^{(h)}(\theta_{n,m,AoD})} \end{bmatrix} \times \right.$$
$$\left. \exp\left(jkd_s \sin(\theta_{n,m,AoD})\right) \times \exp\left(jkd_u \sin(\theta_{n,m,AoA})\right) \times \exp\left(jk\|\mathbf{v}\|\cos(\theta_{n,m,AoA} - \theta_v)\, t\right) \right)$$

where:

$G_{BS}^{(v)}(\theta_{n,m,AoD})$ is the BS antenna array gain for the vertically polarized component.

$G_{BS}^{(h)}(\theta_{n,m,AoD})$ is the BS antenna array gain for the horizontally polarized component.

$G_{MS}^{(v)}(\theta_{n,m,AoD})$ is the MS antenna array gain for the vertically polarized component.

$G_{MS}^{(h)}(\theta_{n,m,AoD})$ is the MS antenna array gain for the horizontally polarized component.

r_n is the average power ratio of waves of the *n*th path leaving the BS in the vertical direction and arriving at the MS in the horizontal direction (v-h) to those leaving in the vertical direction and arriving in the vertical direction (v-v). By symmetry, the power ratio of the opposite process (h-v over vv) is the same.

$\Phi_{n,m}^{(h,h)}$ phase offset of the *m*th subpath of the *n*th path between the *x* component (either the horizontal *h* or vertical *v*) of the BS element and the *y* component (either the horizontal *h* or vertical *v*) of the MS element.

The other variables are described in Section 3.4.

The 2x2 matrix represents the scattering phases and amplitudes of a plane wave leaving the UE with a given angle and polarization and arriving Node B with another direction and polarization. r_n is the average power ratio of waves leaving the UE in the vertical direction and arriving at Node B in the horizontal direction (v-h) to those arriving at Node B in the vertical direction (v-v). By symmetry the power ratio of the opposite process (h-v over v-v) is chosen to be the same. Note that: r_n =1/XPD; for the macrocell model, the XPD is dependent on the path index; for the microcell model, the XPD is independent of path index.

Expression (2) assumes a random pairing of the of the sub-paths from the MS and BS. The random orientation of the MS (UE) array affects the value of the angle $\theta_{n,m,AoA}$ of each sub-path.

If for example, vertically polarized antennas are used only at both NodeB and UE then the antenna responses become $\begin{bmatrix}1\\0\end{bmatrix}$ and expression (2) becomes identical to (1). For an ideal dipole antenna at the NodeB tilted with respect to the z-axis at α degrees the above vector becomes $\begin{bmatrix}\cos(\alpha)\\ \sin(\alpha)\cdot\cos(\theta_{n,m,AoA})\end{bmatrix}$.

The elevation spectrum is not modeled.

A.4.5.2 Far scatterer clusters

The Far scatterer cluster model is switch selectable. It represents the bad-urban case where additional clusters are seen in the environment. This model is limited to use with the urban macro-cell where the first cluster will be the primary cluster and the second will be the far scattering cluster (FSC). When the model is active, it will have the following characteristics:

1. There is a reduction in the number of paths in the primary cluster from N = 6 to N = 4, with the far scattering cluster then having N = 2. Thus the total number of paths will stay the same, now N = 4 + 2. This is a modification to the SCM channel generation procedure in section 0.
2. FSCs will lie only outside a 500m radius from the BS/NodeB.
3. The FSCs will only be modeled for BSs that are modeled spatially and/or temporally. (Modeling only the serving cell FSC is under study.)
4. The model statistics of the two clusters are identical (cluster DS, AS, PDP) but independently drawn. The FSC also has independent shadowing.
5. The FCS is attenuated by 1dB/microsec delay with respect to the 1st cluster with a 10dB maximum. The excess delay will be defined as the difference in propagation time between the BS-MS LOS distance, and the BS-FSC-MS distance. The delay of the FSCs of the other cells (Ioc components) remains an open issue.
6. The FSC is modeled within the serving cell only and dropped following a uniform distribution.

The following method will be used to set the path powers: Draw the N=4 path powers from the channel generation procedure in section 0, then draw a separate set of N=2 path powers from the same procedure. The two groups are kept separate and un-normalized. Now the delay based attenuation is applied to the group of N=2 paths, and the N=6 total paths are normalized to unity power.

A.4.5.3 Line of sight

The Line-of-sight (LOS) model an option that is switch selectable. It can be selected for the urban macro and micro cases. LOS modeling will not be defined for the suburban case. It uses the following description when this function is selected.

For the NLOS case, the Rice factor is set to 0, thus the fading is determined by the combination of sub-rays as described in section 0 of the model.

For the LOS case, the Rice factor K is based on a simplified version of [Foster 1994] : K = 13-0.03*d (dB) where d is the distance between MS and BS in meters.

The probability for LOS or NLOS depends on various environmental factors, including clutter, street canyons, and distance. For simplicity, the probability of LOS is defined to be unity at zero distance, and decreases linearly until a cutoff point at d=300m, where the LOS probability is zero.

$$P(LOS) = \begin{cases} (300 - d)/300, & 0 < d < 300m \\ 0, & d > 300m \end{cases}$$

The K-factor, propagation slope, and shadow fading standard deviation will all be chosen based on the results of selecting the path to be LOS or NLOS.

The K-factor will be formed by adding a direct component (sine wave) at the average AoD and AoA of the path such that the ratio of the power assigned to the direct component to the power assigned to the 6 paths is equal to the K-factor measured in dB. After the power of the direct component is added, the total power in the channel is normalized to unity power. The K-factor is defined as the ratio of power in the LOS component to the total power in the diffused-NLOS component. The LOS path will coincide in time with the first (earliest) diffused path. When pairing sub-rays between transmitter and receiver, the direct components are paired representing the LOS path.

A.4.5.4 Urban canyon

The urban canyon model is switch selectable. When switched on, the model modifies the AoAs of the paths arriving at the subscriber unit. It is for use in both the urban macro and urban micro scenarios.

Urban-canyons exist in dense urban areas served by macro-cells, and for at-rooftop micro-cells. When this model is used, the spatial channel for all subscribers in the simulated universe will be defined by the statistical model given below. Thus for the SCM channel generation steps given in Section 0, Step 9 is replaced with steps 9a-d given below, which describe the AoAs of the paths arriving at the subscriber in the urban canyon scenario.

The following procedure is used to determine the subscriber mean AoAs of the six paths. This model does not use a building grid, but assigns angles based on statistical data presented in the figures below. The procedures is defined in terms of the subscriber terminal:

9a. Select a random street orientation from: U(0, 360˚) which also equals the direction of travel for the UE.

9b. Select a random orientation for the subscriber antenna array from U(0, 360).

9c. Given $\alpha = 0.9$, the predefined fraction of UEs to experience the urban canyon effect, Select a uniform random draw for the parameter β.

9d. If $\beta <= \alpha$, select the UE AoAs for all arriving paths to be equal, with 50% probability of being from the direction of the street orientation obtained in step 9a, and 50% the street orientation plus an offset of 180°. If $\beta > \alpha$, select the directions of arrival for all paths using the standard SCM UE AoA model given in Section 0, Step 9.

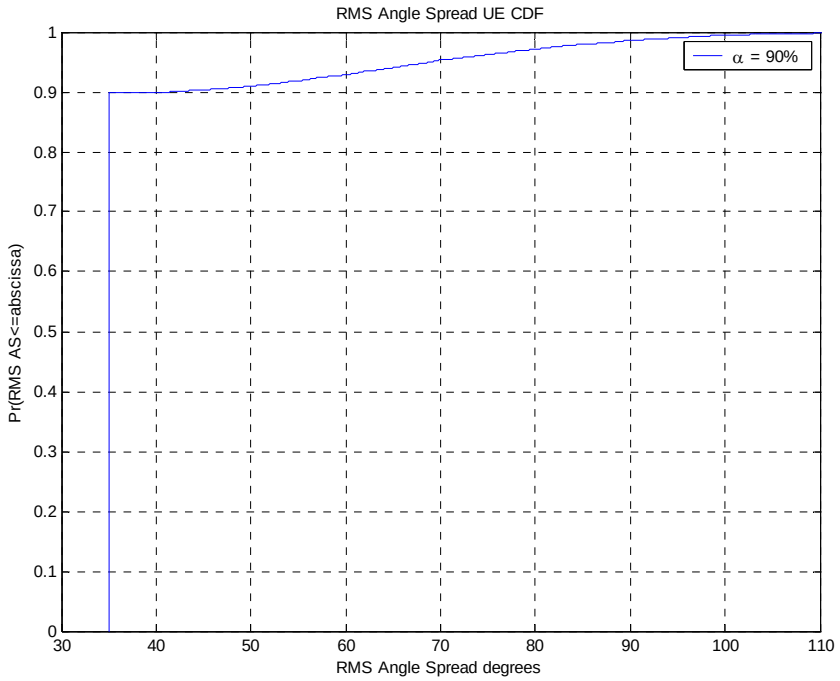

Figure 0-9, Simulated results of Urban Canyon Algorithm

In Figure 0-9, the urban canyon procedure is simulated to show the effects of the model on the composite UE angle spread. The parameter $\alpha = 0.9$, which describes the percentage of mobiles that will experience the urban canyon effects. The figure illustrates the result of selecting the AoAs, where each of the paths has a fixed 35˚ angle spread.

The parameter $\alpha = 0.9$, is set to a relatively high percentage of occurrence to emphasize the urban canyon effects, while the remaining occurrences assume some mixed arrivals to model various other conditions such as cross streets or where signals arrive from between buildings or from unknown paths at various angles.

A.5 Correlation Between Channel Parameters

In [xii], Greenstein presents a model for correlating delay spread (DS) with log normal shadow fading (LN). Since both are shown to be log-normal distributed, the correlation between the DS and LN are correlated by the coefficient ρ. The best value for suburban and urban data was shown to be $\rho = -0.75$, presented in [xii] from data measured by [xiii].

The result of the correlation between log normal shadowing and delay spread is significant because it indicates that for a strong signal (positive LN), the DS is reduced, and for a weak signal condition (negative LN), the DS is increased.

Cost 259[xiv] presents the azimuth spread (AS) as also being log-normal distributed, and likewise being correlated to the DS and LN. Since the correlation of these parameters is quite high, a spatial channel model needs to be specified that can reproduce this correlation behavior along with the expected probability and range of each parameter. For a macro-cell environment, the following values are given in [xiv]:

$\rho_{\alpha\beta}$ = Correlation between DS & AS = +0.5
$\rho_{\gamma\beta}$ = Correlation between LN & AS = -0.75
$\rho_{\gamma\alpha}$ = Correlation between LN & DS = -0.75

Suppose we wish to generate the values for DS, AS, and LN for the *n*th base station ($n = 1 \ldots N$) with respect to a given mobile user. These values are given as $\sigma_{DS,n}$, $\sigma_{AS,n}$, and $\sigma_{LN,n}$, respectively. These valuesare a function of the

respective correlated Gaussian random variables α_n, β_n, and γ_n. These correlated Gasussian random variables are in turn respectively generated from independent Gaussian random variables w_{n1}, w_{n2}, and w_{n3}. Note however, that because of correlated shadow fading from base to base, the variables w_{13} through w_{N3} are correlated and are given by:

$$w_{n3} = \xi_c \sqrt{\frac{\eta}{c_{33}^2}} + \xi_n \sqrt{1 - \frac{\eta}{c_{33}^2}}, \quad n = 1 \ldots N$$

where $\xi_c, \xi_1, \xi_2, \ldots, \xi_N$ are i.i.d. Gaussian random variables with zero mean and unit variance, η is the site-to-site correlation (assumed to be $\eta = 0.5$), and c_{33} is defined as the lower right component of the matrix square root of the correlation matrix:

$$\begin{bmatrix} c_{11} & c_{12} & c_{13} \\ c_{21} & c_{22} & c_{23} \\ c_{31} & c_{32} & c_{33} \end{bmatrix} = \begin{bmatrix} \rho_{\alpha\alpha} & \rho_{\alpha\beta} & \rho_{\alpha\gamma} \\ \rho_{\beta\alpha} & \rho_{\beta\beta} & \rho_{\beta\gamma} \\ \rho_{\gamma\alpha} & \rho_{\gamma\beta} & \rho_{\gamma\gamma} \end{bmatrix}^{1/2}.$$

Given w_{n3}, generate i.i.d. Gaussian random variables w_{n1} and w_{n2} with zero mean and unit variance. The variables α_n, β_n, and γ_n are given by:

$$\begin{bmatrix} \alpha_n \\ \beta_n \\ \gamma_n \end{bmatrix} = \begin{bmatrix} c_{11} & c_{12} & c_{13} \\ c_{21} & c_{22} & c_{23} \\ c_{31} & c_{32} & c_{33} \end{bmatrix} \begin{bmatrix} w_{n1} \\ w_{n2} \\ w_{n3} \end{bmatrix}.$$

Using nomenclature from[**Error! Bookmark not defined.**] the distribution of DS for the *n*th BS is given by:

$$\sigma_{DS,n} = 10 \wedge \left(\varepsilon_{DS} \alpha_n + \mu_{DS} \right)$$

where α_n is generated above, $\mu_{DS} = E\left(\log_{10}(\sigma_{DS})\right)$ is the logarithmic mean of the distribution of DS, and $\varepsilon_{DS} = \sqrt{E\left[\log_{10}(\sigma_{DS,n}^2)\right] - \mu_{DS}^2}$ = is the logarithmic standard deviation of the distribution of DS.

Similarly the distribution of AS is given by:

$$\sigma_{AS,n} = 10 \wedge \left(\varepsilon_{AS} \beta_n + \mu_{AS} \right)$$

where β_n is generated above, $\mu_{AS} = E\left(\log_{10}(\sigma_{AS})\right)$ is the logarithmic mean of the distribution of AS, and $\varepsilon_{AS} = \sqrt{E\left[\log_{10}(\sigma_{AS,n}^2)\right] - \mu_{AS}^2}$ is the logarithmic standard deviation of the distribution of AS. The v

Finally, the distribution for the LN is given by:

$$\sigma_{LN,n} = 10 \wedge \left(\sigma_{SF} \gamma_n / 10 \right)$$

where γ_n is given above, and σ_{SF} is the LN standard deviation given in dB. The value of σ_{SF} is obtained from analysis of the standard deviation from the regression line of the path loss versus distance. As shown in Table 3-1, these values are 8dB and 10dB for the macro and microcell cases, respectively.. Note that the linear scale value for LN is simply $\sigma_{SF} \gamma_n$.

A.6 Modeling intercell interference

Sophisticated MIMO receivers, such as those based on minimum mean-squared error spatial processing, account for the spatial characteristics of the signals from the desired base as well as from the interfering bases. The spatial characteristics of these signals can be modeled according to the channel matrix generated according to Sections 3.3, 3.4, and 3.5. However, it may be prohibitively complex to explicitly model the spatial characteristics of all interfering bases, especially those whose received powers are relatively weak. It has been shown that by modeling the signals of relatively weak interferers as spatially white (and thereby ignoring their spatial characteristics), the resulting performance

difference is negligible. The following text describes the procedure for determining which interferers to model explicitly and which to model as spatially white.

A.6.1 System Level Calibration

The following examples are given for calibration purposes. A resolvable path at the receiver is assumed to be the energy from one (or more) paths falling within one chip interval. The Chip rate in UMTS is 3.84Mcps. The PDF of the number of resulting resolvable paths is recorded.

The following table is for interim calibration purposes. "Ideal" signifies the value taken from measurements, "Input" signifies the value used in generating a random variable, "Output" signifies the resulting measured statistic.

Table 0-5, SCM Parameter Summary with Simulated Outputs

Parameter	Suburban 5° $\square_{RND}$ = 3dB		Urban 8° $\square_{RND}$ = 3dB		Urban 15° $\square_{RND}$ = 3dB		Urban Micro	
r_{DS}	Input	Output	Input	Output		Output		
	1.4	1.29	1.7	1.54	1.7	1.54		
μ_{DS}	Input	Ideal	Input	Ideal	Input	Ideal		
	-6.80	-6.92	-6.18	-6.26	-6.195	-6.26		
ξ_{DS}	Input	Ideal	Input	Ideal	Input	Ideal		
	0.288	0.363	0.18	0.25	0.18	0.25		
r_{AS}	Input	Output	Input	Output	Input	Output		
	1.2	1.22	1.3	1.37	1.3	1.37		
μ_{AS}	Input	Ideal	Input	Ideal	Input	Ideal		
	0.69	0.66	0.810	0.75	1.18	1.0938		
ξ_{AS}	Input	Ideal	Input	Ideal	Input	Ideal		
	0.13	0.18	0.34	0.37	0.21	0.2669		
$E[\sigma_{DS}]$	Ideal	Output	Ideal	Output	Ideal	Output		Output
	0.17μs	0.172μs	0.65μs	0.63μs	0.65μs	0.63μs		0.251 μs
$E[\sigma_{AS\ Node\ B}]$	Ideal	Output	Ideal	Output	Ideal	Output	Ideal	Output
	5°	5.01°	8°	7.97°	15°	14.9°	19˚	19.2˚
$E[\sigma_{AS\ UE}]$	Ideal	Output	Ideal	Output	Ideal	Output	Ideal	Output
	72°	72.59°	72°	71.49°	72°	71.35°	72°	NLOS: 71.8°

The following figures: Figure 0-10, Figure 0-11, Figure 0-12, Figure 0-13, Figure 0-14, represent calibration cases for the current SCM model. These curves correspond to the parameters presented in Table 0-5, and include the 3dB randomizing factor for the generation of path powers.

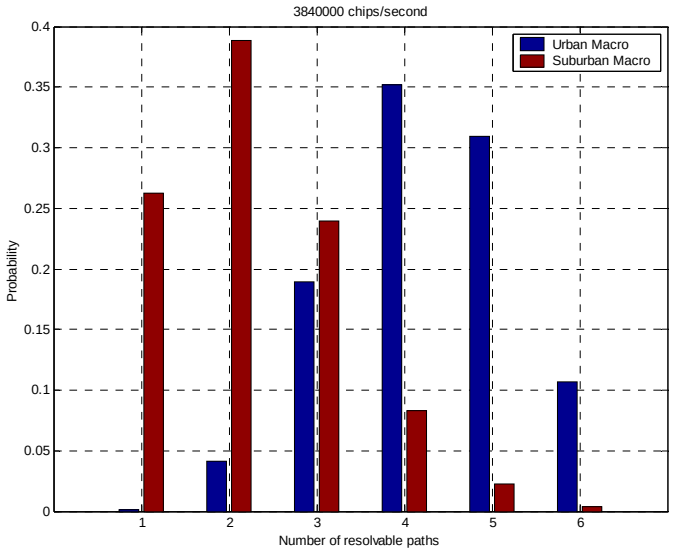

Figure 0-10, Probability of Urban and Suburban Time Resolvable Paths

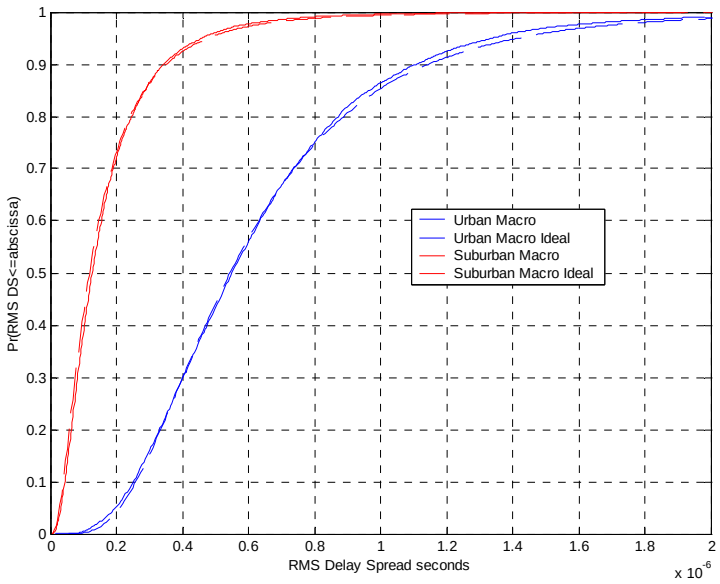

Figure 0-11, RMS Delay Spread, Simulated versus Ideal

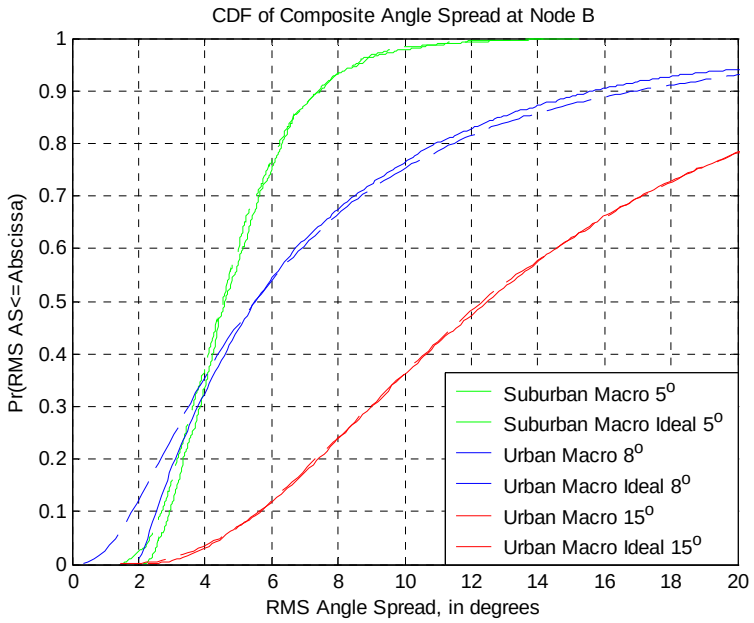

Figure 0-12, Node-B Composite Angle Spread, Simulated versus Ideal

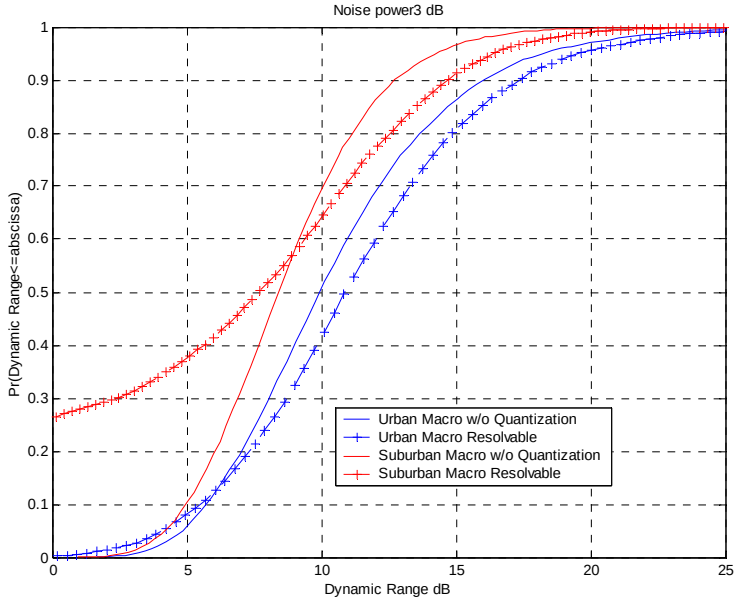

Figure 0-13, Dynamic Range (dB) for each channel model

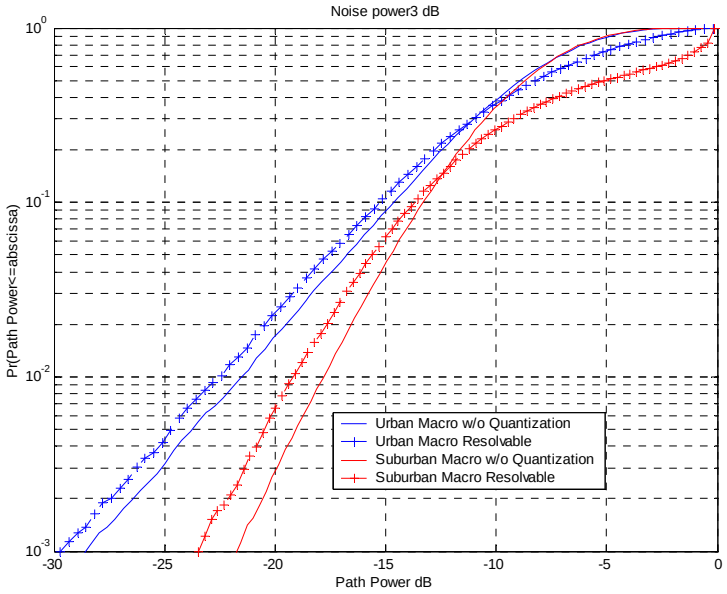

Figure 0-14, CDF of all Path Powers

Channel Scenario: Urban Microcellular

A number of parameters are shown in the following plots which are the result of simulations. Figure 0-15 illustrates the dynamic range of each channel realization, plotted as a complementary cdf. The difference between the 1x and 3x channel bandwidths are shown in the resolvable dynamic range curves. (Powers are combined within a chip time as a simple way to estimate the resolvable powers.) The 1% highest value is approximately the same for both bandwidths. The dynamic range D is calculated from D = 10*log10(max pwr / min pwr) for each channel realization.

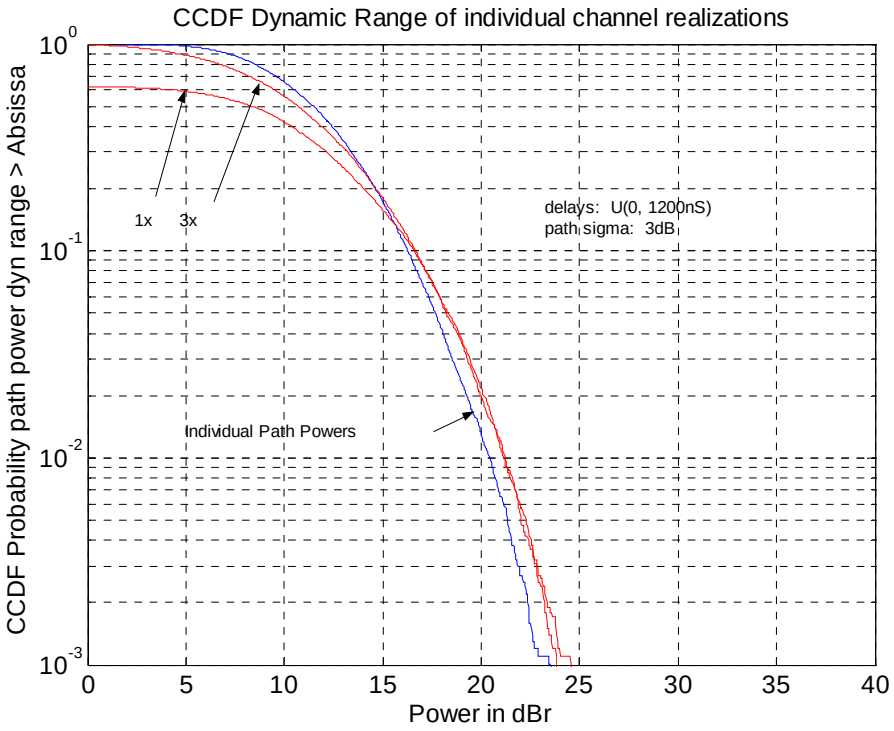

Figure 0-15, Dynamic Range of Path Powers per channel realization, (NLOS)

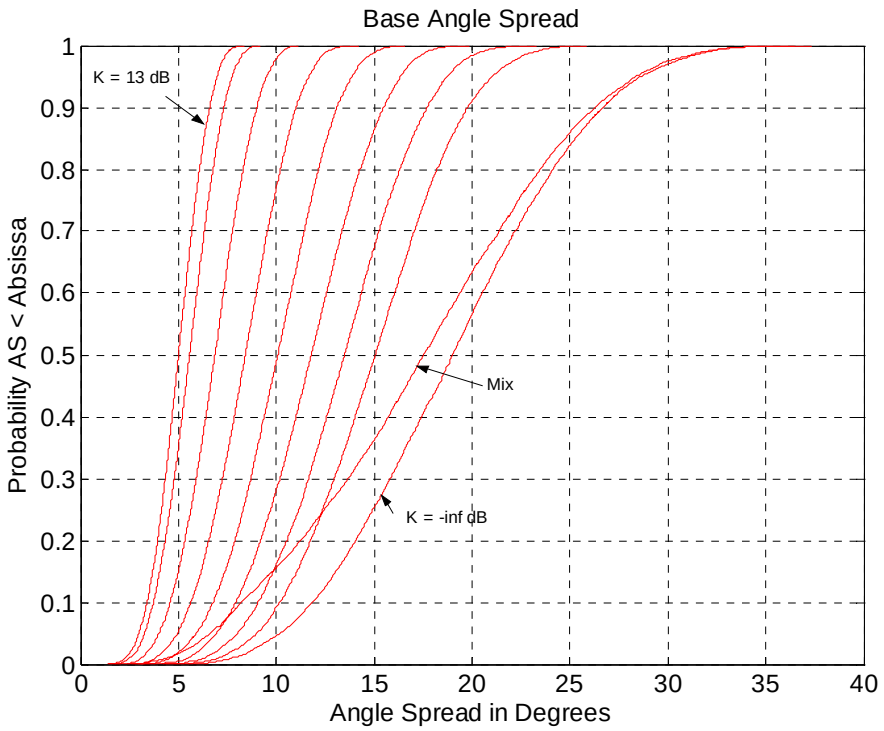

Figure 0-16, Composite Base Angle Spread

The composite angle spread at the base is described in Figure 0-16 for the various K-factors that are seen in the micro-cell model, along with the LOS/NLOS mix expected when the cell radius is 500m. For the NLOS case, the average composite Base AS = 19°. When experiencing LOS paths with increased K-factors, the angle spreads are observed to decreased accordingly. The simulated average composite Base AS for the NLOS model is: 19.2˚, and the simulated average composite Base AS for the mixed propagation model is: 17.6˚.

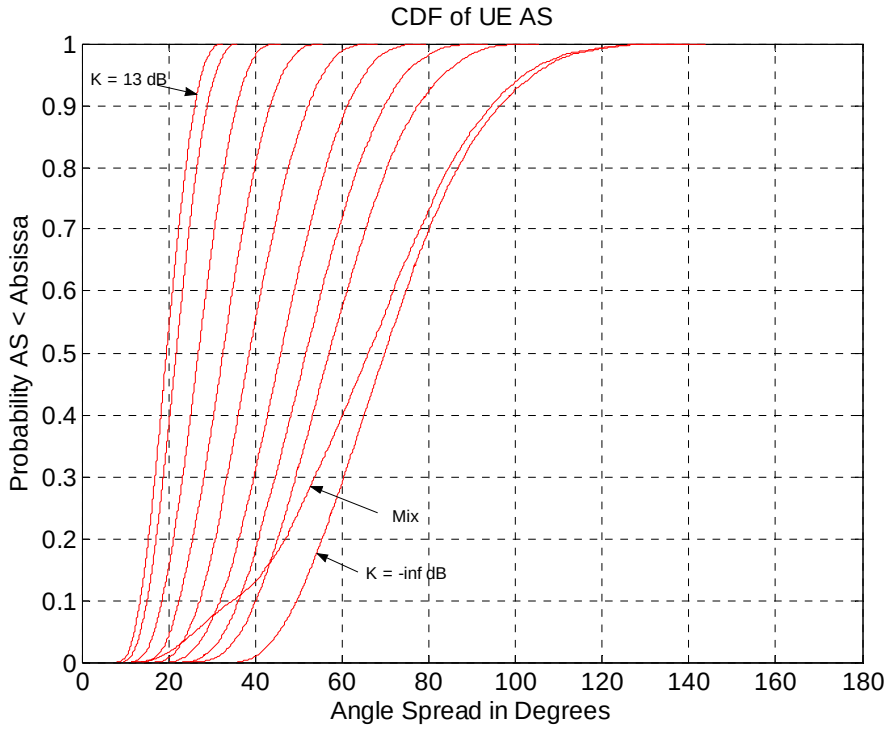

Figure 0-17, Composite UE angle Spread

The composite UE angle spread is described in Figure 0-17 for the various K-factors that are present in the micro-cell model. Increased K-factor from a LOS path, causes the composite AS to be decreased since more power is present in a single direct component. The mixed case is shown which has a slight decrease in the statistics due to the 15% of the locations experiencing the LOS condition. The simulated composite UE AS for the NLOS model is: 71.8˚, and the simulated composite UE AS for the mixed propagation model is: 65.8˚.

The delay spread is illustrated in Figure 0-18, which is also affected by the presence of a direct path. The mix is produced by the combination of LOS and NLOS paths. The simulated average delay spread for the NLOS condition is: 251 nS, and the simulated average delay spread for the mixed case is: 231 nS

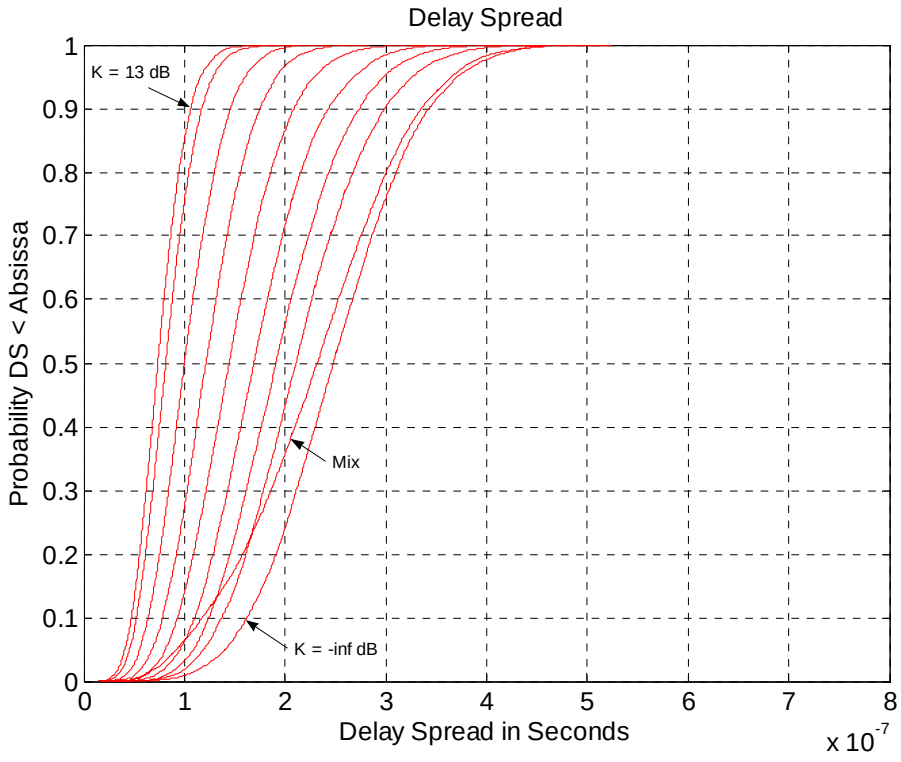

Figure 0-18, Micro-cell Delay Spread

Figure 0-19 illustrates the propagation path loss model of the Urban Micro-cell which is characterized by the mixed mode between LOS and NLOS.

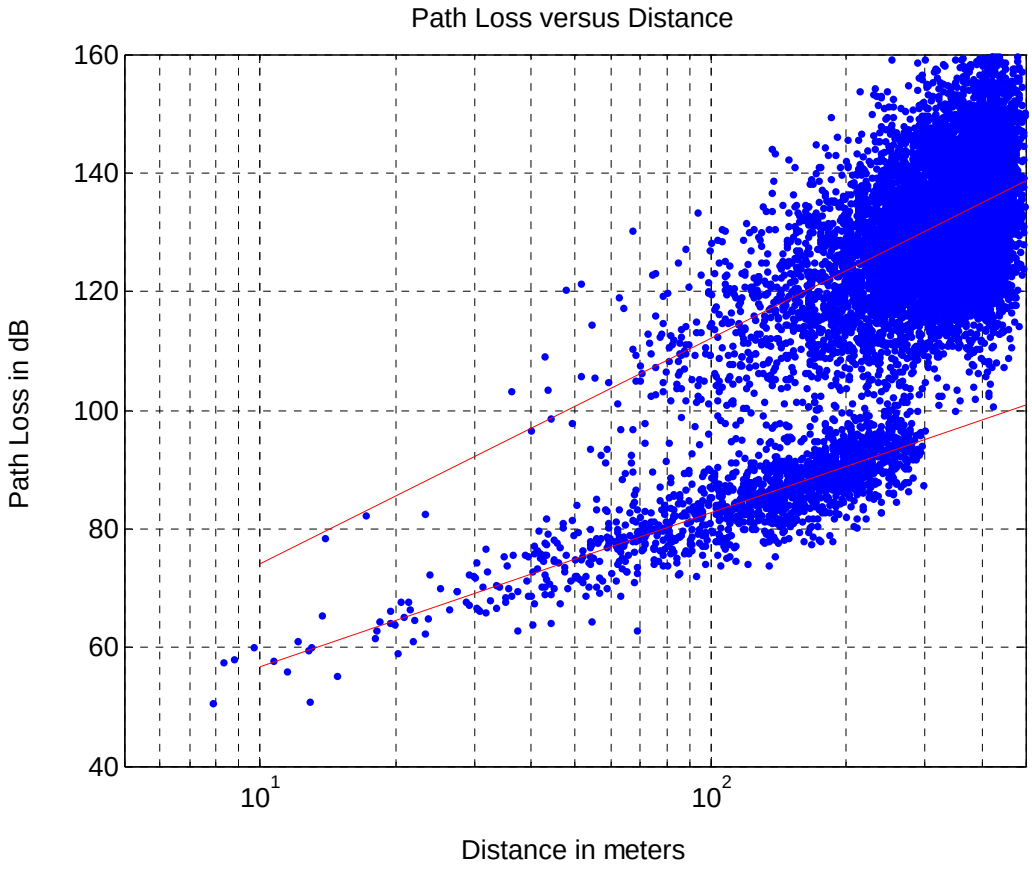

Figure 0-19, Micro-cell Path Loss Model

A.6.2 MMSE receiver description

The following text is a preliminary description of the MMSE receiver. The receiver designs described here are example receiver structures. They do not imply their use for minimum performance requirements. Their use in calibration or system level simulations is not mandatory.

This procedure generates SINR values at the output of a linear MMSE receiver for a single instant in time.

Step 1: Given the space-time propagation model and transmitter state, form a channel (expressed here as one or more convolution matrices) relating all transmitting sources and receive antennas from every sector in the system.

At the UE, the received samples are represented as a column vector,

$$\begin{aligned}\mathbf{r} &= [\mathbf{r}_1^T, \mathbf{r}_2^T, \cdots, \mathbf{r}_M^T]^T \\ &= [r_1(1), r_1(2), \cdots, r_1(N), r_2(1), r_2(2), \cdots, r_2(N), \cdots, r_M(1), r_M(2), \cdots, r_M(N)]^T,\end{aligned}$$

where M is the number of receive antennas at the UE, and N is the number of received symbols per antenna[4]. This received time-space vector is related to the transmitted symbols as follows:

[4] Actually, this is the number of received samples per antenna, if more than one sample per symbol is collected.

$$\mathbf{r} = \mathbf{G}^{(1)}\mathbf{x}^{(1)} + \sum_{j=2}^{J}\mathbf{G}^{(j)}\mathbf{x}^{(j)} + \mathbf{n} = \begin{bmatrix}\mathbf{G}_1^{(1)}\\ \mathbf{G}_2^{(1)}\\ \vdots\\ \mathbf{G}_M^{(1)}\end{bmatrix}\cdot\mathbf{x}^{(1)} + \sum_{j=2}^{J}\begin{bmatrix}\mathbf{G}_1^{(j)}\\ \mathbf{G}_2^{(j)}\\ \vdots\\ \mathbf{G}_M^{(j)}\end{bmatrix}\cdot\mathbf{x}^{(j)} + \begin{bmatrix}\mathbf{n}_1\\ \mathbf{n}_2\\ \vdots\\ \mathbf{n}_M\end{bmatrix}$$

where $\mathbf{G}_i^{(j)}$, $1 \le i, j \le M$ are Toeplitz convolution matrices defining the channel between the *i*-th receive antenna and the *j*-th transmitted data stream, $\mathbf{x}^{(j)}$ is the *j*-th transmitted data stream, *J* is the total number of data streams in the system, and **n** is the vector of noise samples. The *j* = 1 data stream is the primary data stream intended for the user. The *j*-th data stream can be a transmission from an interfering base station, another sector of the desired base station, or another data stream intended for the desired user (which is considered interference to the primary data stream). If the composite channel response is limited to *K* samples, then each of the convolution matrices has *N* rows by (*N*+*K*-*1*) columns,

$$\mathbf{G}_i^{(j)} = \begin{bmatrix} g_i^{(j)}(K) & g_i^{(j)}(K-1) & \cdots & g_i^{(j)}(1) & 0 & 0 & \cdots & 0 \\ 0 & g_i^{(j)}(K) & g_i^{(j)}(K-1) & \cdots & g_i^{(j)}(1) & 0 & \cdots & 0 \\ \vdots & \vdots & \ddots & \ddots & \cdots & \ddots & \cdots & 0 \\ 0 & 0 & \cdots & 0 & g_i^{(j)}(K) & g_i^{(j)}(K-1) & \cdots & g_i^{(j)}(1) \end{bmatrix},$$

and $\mathbf{g}_i^{(j)}$ is the vector of discrete channel samples of length *K*.

Note that in the above formulation, the vector $\mathbf{x}$ has *M*(*N*+*K*-1) rows, and thus, it is longer than the received vector, **r**. Also, the vector $\mathbf{x}$ will be interleaved with zero values if a fractionally-spaced approach with more than one received sample per symbol is used.

Step 2: Using the above channel, produce an estimate of the channel.

$$\hat{\mathbf{g}}_i^{(j)} = \mathbf{g}_i^{(j)} + \Delta\mathbf{g}_i^{(j)},$$

where $\Delta\mathbf{g}_i^{(j)}$ is a vector representing the channel estimation error for the *i*-th receive antenna and the *j*-th transmitted data stream. The estimation error is due to noise and interference in the pilot channel and can also be due to the channel estimator's inability to track a fast fading channel.

Step 3: Using the estimated channel, compute the SINR per data stream at the output of the MMSE filters.

$$SINR_j = \frac{\left|\mathbf{f}_j^H\hat{\mathbf{\Omega}}_j^{-1}\hat{\mathbf{f}}_j\right|^2}{\hat{\mathbf{f}}_j^H\hat{\mathbf{\Omega}}_j^{-1}\mathbf{\Omega}_j\hat{\mathbf{\Omega}}_j^{-1}\hat{\mathbf{f}}_j},$$

where

$$\mathbf{\Omega}_j = \mathbf{G}^{(j)}E\left[\mathbf{x}^{(j)}\mathbf{x}^{(j)H}\right]\mathbf{G}^{(j)H} - \mathbf{f}^{(j)}E\left[x^{(j)}(d)x^{(j)}(d)^*\right]\mathbf{f}^{(j)H} + \sum_{\substack{m=1\\ m\neq j}}^{J}\mathbf{G}^{(m)}E\left[\mathbf{x}^{(m)}\mathbf{x}^{(m)H}\right]\mathbf{G}^{(m)H} + E\left[\mathbf{n}\mathbf{n}^H\right],$$

$\hat{\mathbf{\Omega}}_j$ is an estimate of $\mathbf{\Omega}_j$, $d = \max\left(\lceil (N-K)/2\rceil + K, K\right)$, $\mathbf{f}_j$ is the *d*-th column of $\mathbf{G}^{(j)}$, $x^{(j)}(d)$ is the *d*-th element (desired symbol) of the $\mathbf{x}^{(j)}$ data stream vector, and $SINR_j$ represents the SINR for the *j*-th transmitted data stream in the system. In this example, the primary data stream sent to a user will be *j* = 1. In a MIMO system where multiple data streams are sent to a single user, the second stream could be *j* = 2, etc.

A.7 WiMAX System-Level Evaluation Methodology

This section of the Annex defines one possible methodology for the system-level evaluation methodology of HSDPA channels. This methodology may be used and referenced in submitting evaluations. If this methodology is not used then a description of the methodology employed should be provided.

Figure A.1.1 illustrates a methodology for the system-level evaluation of WiMAX performance. This methodology is especially applicable to the case of low/medium Doppler, i.e. when the channel can be assumed to be constant during a TTI.

On system level, a UE exists within the simulated deployment. Based on the UE position, a short-time-average geometry $\overline{G}$, including the effect of distance-dependent path-loss, shadowing, and thermal noise, is determined for each UE. For each UE and each TTI, an instantaneous channel-impulse response $h(t)$ is generated according to the average channel-delay profile (Pedestrian B, Vehicular A, etc.). In practice, the impulse response $h(t)$ will be a sampled impulse response, e.g. with a sampling time equal to the chip time.

In a time-dispersive environment, the channel will cause intra-cell interference due to loss of downlink orthogonality. Thus, the MCS selection and the corresponding block-error probability depend on both the geometry $\overline{G}$ and the instantaneous channel $h(t)$. To directly map $\overline{G}$ and $h(t)$ to an accurate estimate of the block-error probability would require an overwhelming effort on link level and is not a feasible path. Instead, a well-defined mapping function $SIR_{eff}(\overline{G}; h)$ is introduced, that maps $\overline{G}$ and $h(t)$ to an *effective SIR* (a scalar value). The basic idea is that the interference part of the effective SIR should include not only the inter-cell interference and noise but also the non-orthogonal part of the intra-cell interference. Once the effective SIR is calculated, it can be used to find the block-error probability for different MCS from basic AWGN link-level-performance curves.

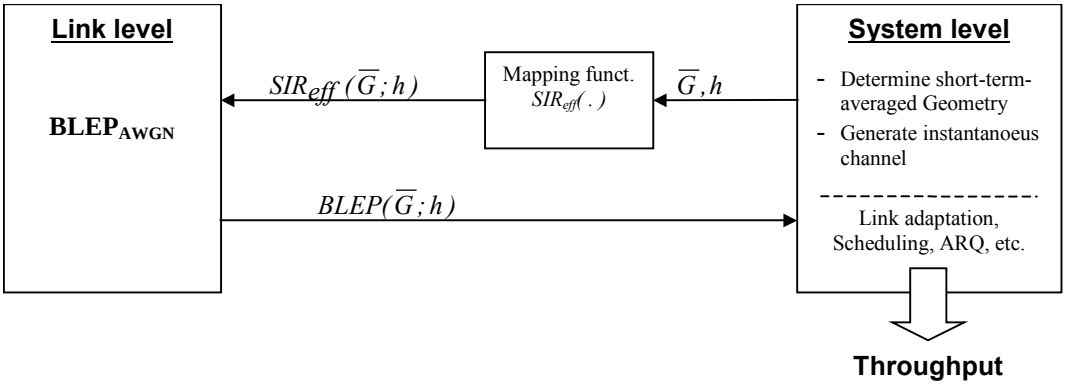

Figure A.1.1: System-level methodology for HSDPA release 5

In case of low/medium Doppler, when the channel can be assumed to be constant over a TTI, it is straightforward to derive the mapping function $SIR_{eff}(\overline{G}; h)$ for different linear receiver structures, such as a simple RAKE, a G-RAKE, or a chip-level equalizer using e.g. the MMSE criteria.

In the case of high Doppler, i.e. when the channel cannot be assumed to be constant over the TTI, the above methodology cannot be applied as straightforwardly as for the case of low/medium Doppler. The reason is that, in this case, the effective SIR cannot be assumed to be constant during the TTI. Thus, a more complex mapping function may be needed for accurate performance estimation.

A.8 OFDM modulation

For OFDM with a sufficiently large cyclic prefix, there is no intra-cell interference even in case of a time-dispersive channel. However, this does not imply that OFDM performance will not suffer from a frequency-selective (time-dispersive) channel. The reason is that, in case of OFDM and a frequency-selective channel, different coded bits will be subject to different instantaneous channel quality (different SIR). Channel coding and frequency-domain interleaving

will reduce the negative effect of a frequency-selective channel on OFDM performance but will not eliminate it completely (the negative effect will be much higher at higher-rate coding, i.e. higher data rates, though).

For a correct system-level comparison, the negative effect of a frequency-selective channel on OFDM performance obviously needs to be taken into account in a sufficiently accurate way. It is also preferred that the methodology used to evaluate the system performance of WiMAX using OFDM modulation is aligned as much as possible with the system methodology used for WiMAX. In this way, irrelevant performance deviations that are due to differences in the methodology are minimized and one can focus on the inherent differences of the different techniques.

Thus, this methodology for evaluating the system-level performance of OFDM modulation consists of the following steps:

-. On system level, a UE exists within the simulated deployment and a short-term averaged geometry $\overline{G}$ is calculated for each UE.

-. For each UE and each TTI, an instantaneous channel is derived. In the OFDM case, the channel is preferable expressed in the frequency domain, i.e. as a frequency response $H(f)$ (in practice $H(f)$ is sampled in the frequency domain).

-. A mapping function $SIR_{eff}(\overline{G};H)$ is introduced that maps the geometry $\overline{G}$ and the frequency response $H(f)$ to an effective SIR value (a scalar value).

-. The effective SIR is used to find the block-error probability from AWGN link-level-performance curves.

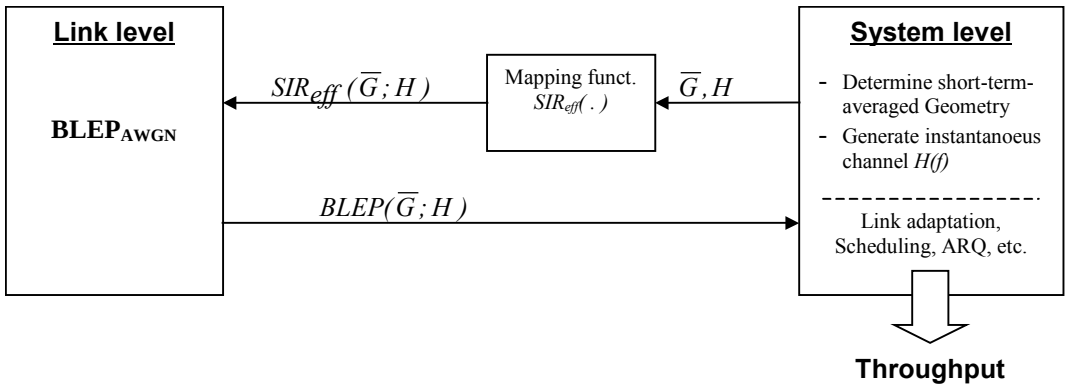

Figure A.2.1: System-level methodology for WiMAX using OFDM modulation

A.9 Effective SIR Mapping Functions

A.9.1 Effective SIR Mapping Functions for OFDM

This section contains proposed mapping functions for mapping the current channel conditions in an OFDM system-level simulator to an effective SIR that can then be used to determine the expected BLER from AWGN curves.

A.9.1.1 OFDM Exponential Effective SIR Mapping

The OFDM subcarrier SIR for an OFDM receiver may be calculated at the system-level as a function of the subcarrier power (which is a function of the channel's current frequency response), the current geometry ($\overline{G}$), the FFT size (N), and the cyclic prefix length (N_p), the percentage of maximum total available transmission power allocated to the data subcarriers (R_D), the number of data subcarriers per TTI (N_{SD}), and the number of total useful subcarriers per TTI (N_{ST}):

$$\gamma_k = P(k) \times \overline{G} \times \left(\frac{N}{N + N_p} \right) \times \frac{R_D}{N_{SD} / N_{ST}}$$

Assuming that the multi-path fading magnitudes $M_p(t)$ and phases $\theta_p(t)$ are constant over the observation interval, the frequency-selective fading power profile value for the k^{th} subcarrier can be calculated as:

$$P(k) = \left| \sum_{p=1}^{\text{paths}} M_p A_p e^{j[\theta_p - 2\pi f_k T_p]} \right|^2 = \left| \sum_{p=1}^{\text{paths}} M_p A_p e^{j\theta_p} e^{-j2\pi f_k T_p} \right|^2$$

where p represents the multi-path path index, A_p is the amplitude value corresponding to the long-term average power for the p^{th} path (assuming that the sum of the long-term path powers in the channel model has been normalized), f_k is the relative frequency offset of the k^{th} subcarrier within the spectrum, and T_p is the relative time delay of the p^{th} path. It is assumed here that the fading profile is normalised such that $E[P(k)] = 1$.

The effective SIR mapping for these channel conditions can then be computed as

$$SIR_{eff} = -\beta \ln \left(\frac{1}{N_u} \sum_{k=1}^{N_u} e^{-\frac{\gamma_k}{\beta}} \right),$$

where β is a parameter that must be optimized from link-level simulation results for every modulation and coding rate combination. Note that a subset of the N_u useful subcarriers could also be used to evaluate the effective SIR for reasons of computational efficiency.

A.9.1.2 Effective SIR Mapping Function for OFDM with Base station Impairments

The effective SIR for OFDM when including the effect of the Tx EVM is determined by computing the SIR for each sub-carrier m with the expression

$$\gamma_m = \frac{1}{\frac{1}{\gamma_{\text{m,no EVM}}} + \frac{1}{\gamma_{\text{m,EVM}}}}$$

where $\gamma_{m,\text{no EVM}}$ is the SIR of sub-carrier m without the EVM as specified in section A.4.3.2.1 and $\gamma_{m,\text{EVM}}$ the constant value specified by,

$$\gamma_{m,\text{EVM}} = \frac{T_u}{EVM^2 N_D \left(\frac{P_x}{P_{traff}} \right)}.$$

where, EVM is the error vector magnitude value (assumed to be 12.5% as specified as the maximum permitted for 16-QAM transmission), , N_D is the number of data symbols per OFDM symbol, T_u is the useful OFDM symbol duration, and $\frac{P_x}{P_{traff}}$ is the ratio of total transmitted power to traffic power.

Therefore, for parameter set 2 and with EVM=12.5%, N_D= 7200/12 = 600, and $\frac{P_{traff}}{P_x} = 0.8$, then $\gamma_{m,EVM} = 17.1\,\text{dB}$. Once the SIR is determined for all of the sub-carriers, the effective SIR can be computed with, for instance, the exponential mapping,

$$SIR_{eff} = -\beta \ln\left(\frac{1}{N_u} \sum_{k=1}^{N_u} e^{-\frac{\gamma_k}{\beta}} \right).$$

A.10 System-Level HARQ Modelling

A.10.1 Chase-Combining HARQ Modelling for OFDM

The effects of chase-combining HARQ for OFDM can be modelled at the system-level using the following steps.

1. For each TTI, calculate the signal strength for each OFDM subcarrier (QAM symbol) from the channel frequency response for the corresponding OFDM symbol.
2. Calculate the interference-plus-noise power for each OFDM subcarrier (QAM symbol) in the TTI.
3. Permute the signal strength and interference-plus-noise power values according to the physical channel mapping and user multiplexing that is in effect for the current TTI in order to place the QAM symbols in the correct order for QAM demapping.
4. Perform HARQ combining by adding the signal magnitudes for the just received TTI to those present from any previous HARQ combining for that particular data block, and then calculate the power of the combined signal for each QAM symbol.
5. Sum the interference-plus-noise powers for multiple transmission attempts of the same data block.
6. The individual SIR values on the HARQ-combined QAM symbols may then be used to perform the effective SIR mapping mapping.

For greater computational efficiency, the following simplifying assumptions may be made if appropriate.

- For slowly varying channels (e.g. 3 km/h pedestrian channels), the channel frequency response can be assumed to be the same for all OFDM symbols in a given TTI. For a higher velocity channel, it may be necessary to recalculate the current channel frequency response for each OFDM symbol.
- A subset of equally-spaced representative subcarriers (or corresponding QAM symbols) may be used in place of all of the subcarriers (or QAM symbols) within a TTI.
    - The interference-plus-noise power will be the same for all subcarriers (or QAM symbols) within a TTI if flat fading is assumed from the interfering cells and all cells (both the target cell and interfering cells) are assumed to be fully loaded. Otherwise, it will be necessary to calculate the interference-plus-noise power individually for each subcarrier (or QAM symbol).

Annex-B : PHY abstractions for WiMAX System Modeling

B.1 Objective

For a network system-level simulator, to simulate the physical layer links between multiple BSs and SSs can be computationally prohibitive. Therefore, a PHY abstraction model is used to predict link layer performance in a computationally simply way.

B.2 Definition of PHY Abstraction

PHY abstraction is defined as a mapping function *L=F(C, MCS)* between *link layer performance indicator (L)* and *channel quality indicator (C)* for different modulation and coding schemes (MCS), which was obtained from PHY/Link Layer Simulation (LLS).

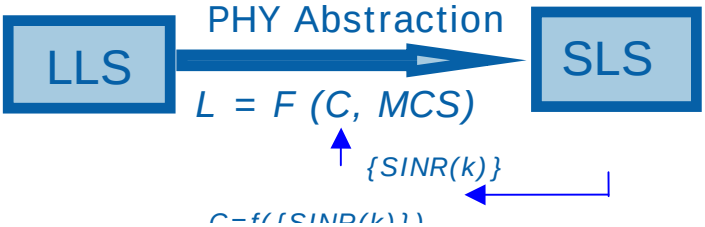

Choices of the indicators can be multiple. Especially for MIMO-OFDM wireless system which operates in frequency selective channel, the right choice is important and actually a matter of numerous researches.

Channel quality indicator *(C)* are derived from instantaneous channel state, such as the instantaneous SINR for each sub-carrier in OFDM as {SINR(k)}, (k=0,1,2…). The alternative metrics of *C* can be:

- Average SNR
- Mean instantaneous capacity (MIC)
- Effective SINR
- Exponential effective SINR and etc.

Link layer performance indicator (*L*) can be chosen according to the need of system level simulator:

- Packet (burst) error rate (PER)
- Block-error probability (BLEP)
- Bit error rate (BER)
- Symbol error rate (SER)
- Slot error rate (SLER) and etc.

B.3 Implementation of PHY Abstraction

There are several types of PHY abstraction models which are commonly used, depending on the indicators a model chooses:

- Average SNR:

- MIC
- Effective SINR Mapping (ESM)
- Exponential Effective SINR Mapping (EESM) etc.

Average SNR is known to be problematic for OFDM in broadband channels, because averaging the SINR on different tones which undergo different amounts of fading does not give a true picture of the channel.

In this document, EESM is used as the default abstraction. Other possibilities are also described.

B.3.1 Effective Exponential SINR Model (EESM)

1) **Calculate instantaneous per subcarrier SINR {SINR(k)} for each subcarrier**.

2) **Calculate the instantaneous effective SINR ($SINR_{eff}$):**

   a. Compute effective SINR:

$$SINR_{eff} = 2^{MIC} - 1$$

3) **Compute BLER** from a table or a curve function calculated in advance (from LLS) for basic AWGN channel associated with given $SINR_{eff}$ from step two and the current used MCS:

$$PER = F_{AWGN}(SINR_{eff}, MCS)$$

   The methodology is based on the assumption that the actual BLER for the instantaneous OFDM channel state {SINR(k)} can be approximated from the BLER for a basic AWGN channel with the effective SINR for the specific MCS.

$PER(\{SINR(k)\}, MCS) \approx F_{AWGN}(SINR_{eff}, MCS)$.

B.3.2: Mean Instantaneous Capacity (MIC)

1) **Calculate instantaneous per subcarrier SINR {SINR(k)}:**

   In OFDM based WiMax SLS simulation, per subcarrier SINR is computed according to the location of BS and MSS, the channel gain, and per subcarrier interferes from neighboring cells.

2) **Calculate the MIC:**

   a. Compute the capacity of the *kth* subcarrier

$$c(k) = \log_2(1 + SINR(k))$$

   b. Compute the MIC by averaging per subcarrier capacities across the subcarriers,

$$MIC = \frac{1}{N}\sum_{k=1}^{N} c(k)$$, where N is the number of used subcarriers.

3) **Compute PER** from a table or a curve function calculated in advance (from LLS) for basic AWGN channel associated with given ***MIC*** from step two and the current used MCS:

$$PER = F_{AWGN}(MIC, MCS)$$

   The methodology is based on the assumption that the actual PER for the instantaneous OFDM channel state {SINR(k)} can be approximated from the PER for a basic AWGN channel with the MIC for the specific MCS:

$$PER(\{SINR(k)\}, MCS) \approx F_{AWGN}(MIC, MCS)$$

B.3.3 Effective SINR Method (ESM)

1) **Calculate instantaneous per subcarrier SINR {SINR(k)}:** same as above.

2) **Calculate the instantaneous effective SINR ($SINR_{eff}$):**

   a. Compute MIC: $MIC = \frac{1}{N}\sum_{k=1}^{N} c(k)$, same as above.

   b. Compute effective SINR:

$$SINR_{eff} = 2^{MIC} - 1$$

3) **Compute PER** from a table or a curve function calculated in advance (from LLS) for basic AWGN channel associated with given $SINR_{eff}$ from step two and the current used MCS:

$$PER = F_{AWGN}(SINR_{eff}, MCS)$$

The methodology is based on the assumption that the actual PER for the instantaneous OFDM channel state {SINR(k)} can be approximated from the PER for a basic AWGN channel with the effective SINR for the specific MCS.

$$PER(\{SINR(k)\}, MCS) \approx F_{AWGN}(SINR_{eff}, MCS).$$

B.3.4: Shannon Capacity Model

B.3.5: Effective Code Rate Method (ECRM)

Instead of computing effective SINR, compute effective code rate

ECRM-1:

Reff=R0 (1/N S SINRk2)/(1/N S SINRk)2

ECRM-2:

Reff = R0 [1/N S log2(1+b SINRk)]/[1/N S log(1+b SINRk]2

R0 is the transmitted code rate, and
Reff is the effective code rate

Annex C : MAC abstraction details

Annex D : Enhanced MAC abstraction requirement

D.1: Reference AWGN TTI BLER Curves for System-Level Models

Figure D.1.1 and Figure D.1.2 contain reference AWGN TTI BLER curves for use when modelling link-level performance within a system-level simulator. These curves are for a payload size corresponding to 15 data units (7200 QAM symbols per TTI) , and are valid for **OFDM**. For greater accuracy, the specific points on the TTI BLER curves are also listed in Table D.1.1 and Table D.1.2. Note that the columns labeled SIR in the tables refer to post-receiver SIR (as measured at the output of the receiver or, equivalently, at the input to the CCTrCH decoder). The turbo decoder used for these link-level simulations used a log-MAP decoding algorithm. A maximum of eight iterations were used, although an early stopping criterion was also in effect if the turbo decoder converged prior to the maximum number of decoding iterations being performed.

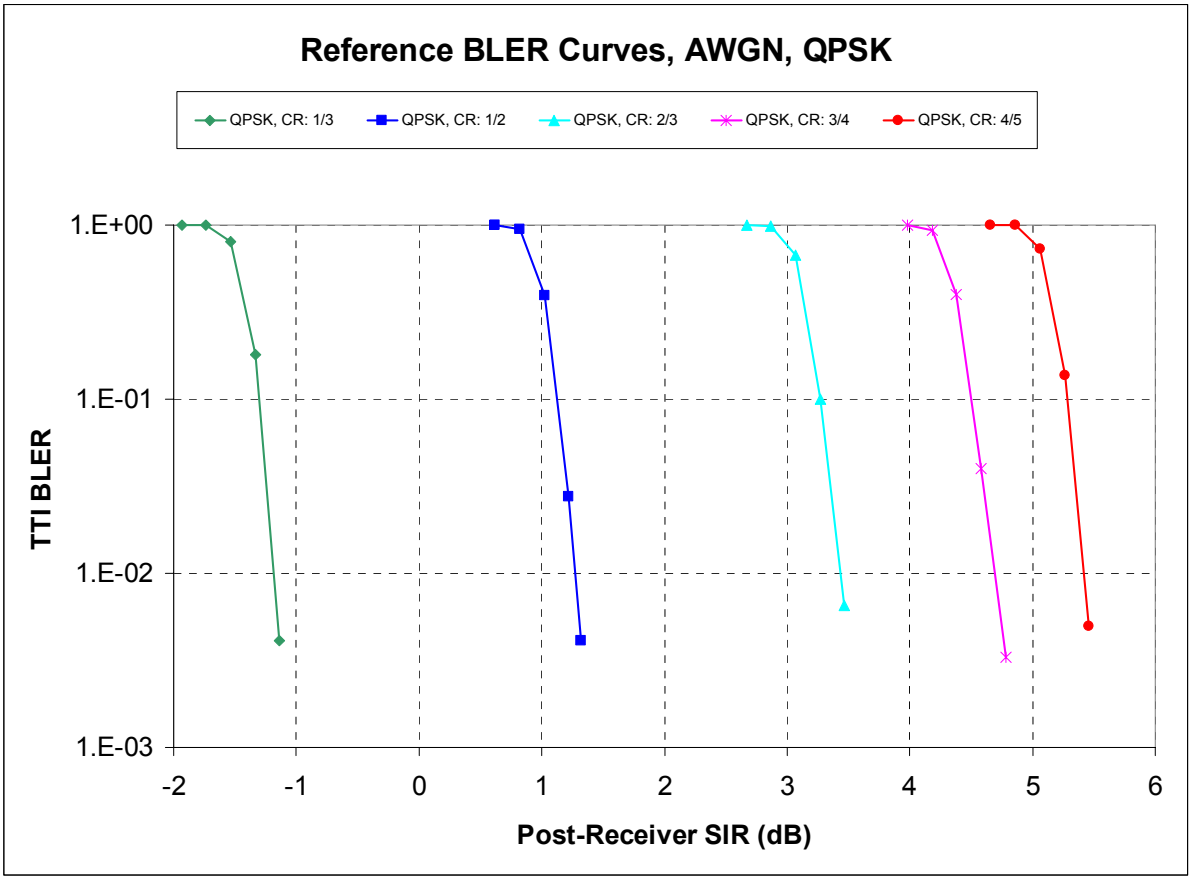

Figure D.1.1: Reference TTI BLER curves in an AWGN channel (QPSK link modes)

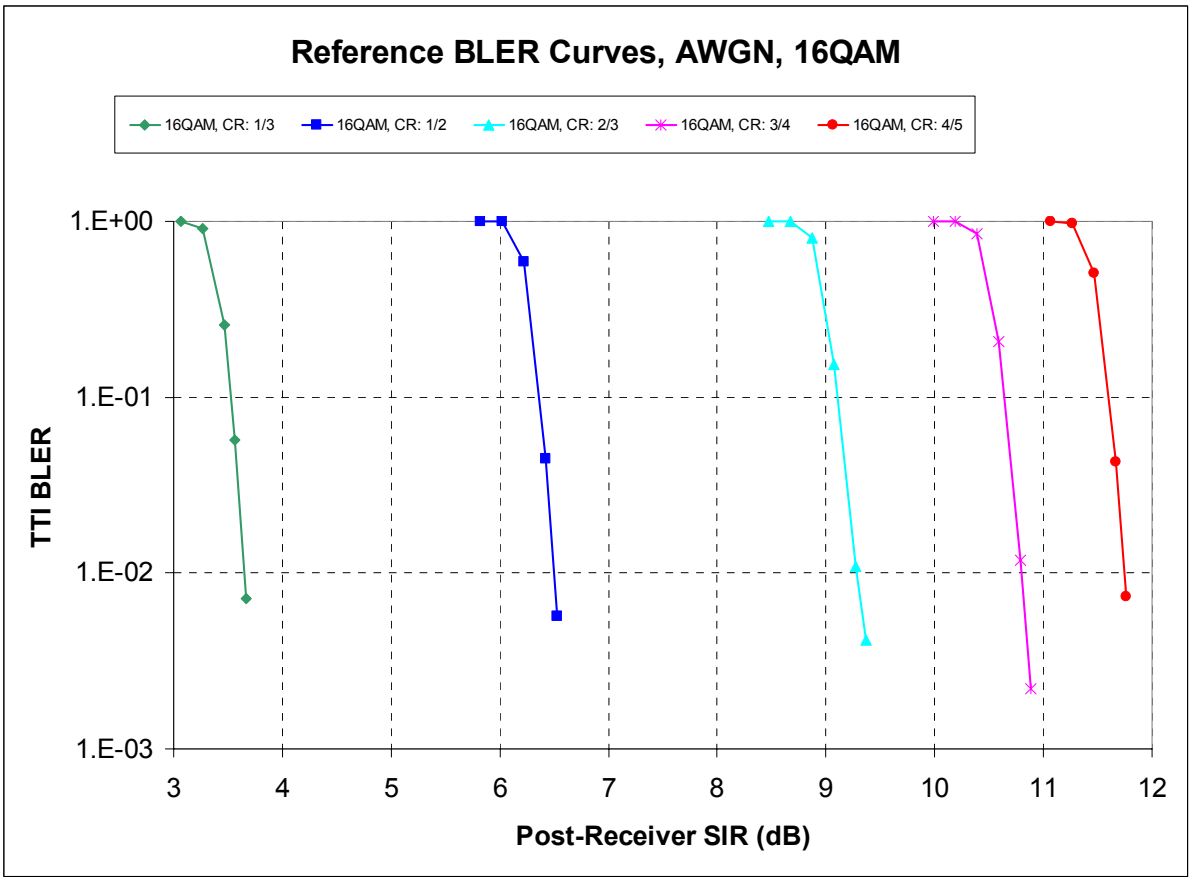

Figure D.1.2: Reference TTI BLER curves in an AWGN channel (16QAM link modes)

Table D.1.1: Reference TTI BLER curve points for an AWGN channel (QPSK link modes)

QPSK, Rate 1/3		QPSK, Rate 1/2		QPSK, Rate 2/3		QPSK, Rate 3/4		QPSK, Rate 4/5	
SIR (dB)	BLER	SIR (dB)	BLER	SIR (dB)	BLER	SIR (dB)	BLER	SIR (dB)	BLER
-1.94	1.00E+0	0.62	1.00E+0	2.67	1.00E+0	3.98	1.00E+0	4.66	1.00E+0
-1.74	9.95E-1	0.82	9.45E-1	2.87	9.90E-1	4.18	9.40E-1	4.86	9.94E-1
-1.54	8.03E-1	1.02	3.95E-1	3.07	6.76E-1	4.38	3.98E-1	5.06	7.28E-1
-1.34	1.79E-1	1.22	2.76E-2	3.27	9.97E-2	4.58	3.97E-2	5.26	1.38E-1
-1.14	4.10E-3	1.32	4.13E-3	3.47	6.50E-3	4.78	3.30E-3	5.46	4.97E-3

Table D.1.2: Reference TTI BLER curve points for an AWGN channel (16QAM link modes)

16QAM, Rate 1/3		16QAM, Rate 1/2		16QAM, Rate 2/3		16QAM, Rate 3/4		16QAM, Rate 4/5	
SIR (dB)	BLER	SIR (dB)	BLER	SIR (dB)	BLER	SIR (dB)	BLER	SIR (dB)	BLER
3.06	1.00E+0	5.82	1.00E+0	8.47	1.00E+0	10.18	1.00E+0	11.07	1.00E+0
3.26	9.14E-1	6.02	9.94E-1	8.67	9.92E-1	10.38	8.95E-1	11.27	9.51E-1
3.46	2.58E-1	6.22	5.89E-1	8.87	6.67E-1	10.58	2.79E-1	11.47	3.60E-1
3.56	5.72E-2	6.42	4.49E-2	9.07	1.08E-1	10.78	2.00E-2	11.67	2.42E-2
3.66	7.15E-3	6.52	5.70E-3	9.27	1.11E-2	10.98	1.57E-3	11.77	3.30E-3
				9.37	3.80E-3				

D.2 Reference β Values for the OFDM EESM Approach in System-Level Models

D.2.1 Reference β Values Using a Random OFDM Subcarrier Interleaver

Table D.2.1 contains a reference set of β values that may be used with the OFDM Exponential Effective SIR Mapping (EESM) technique described in Section A.4.3.2.1 for performing OFDM system-level simulations with the reference AWGN BLER curves from Section A.4.4. Note that these β values were estimated from link-level simulations using a random OFDM subcarrier interleaver.

Table D.2.1: Estimated values for the β parameter in the Exponential Effective SIR Mapping (EESM) for each link mode using a random OFDM subcarrier interleaver

Modulation	Code Rate	β
QPSK	1/3	1.49
	1/2	1.57
	2/3	1.69
	3/4	1.69
	4/5	1.65
16QAM	1/3	3.36
	1/2	4.56
	2/3	6.42
	3/4	7.33
	4/5	7.68

Annex E. NS2 framework common modules

[Describe NS2 eco-system and modules that are available readily]

Annex F: System Modeling Results

Appendix G: Simulation Design Decisions and Issues Living List

1. Packet sizes will be quantized
2. Packet = MAC PDU
3. PER vs BLER: Methodology will address only BLER and not PER unless Mutu comes up with a contribution explaining benefits of PER
4. Arvind will send out slides showing how packets are broken into blocks

History:

7/10/06

Added EESM, MIC, ECRM

Added intro from performance white paper

Appendix H: List of Acronyms

3GPP	3G Partnership Project
3GPP2	3G Partnership Project 2
AAS	Adaptive Antenna System also Advanced Antenna System
ACK	Acknowledge
AES	Advanced Encryption Standard
AG	Absolute Grant
AMC	Adaptive Modulation and Coding
A-MIMO	Adaptive Multiple Input Multiple Output (Antenna)
ASM	Adaptive MIMO Switching
ARQ	Automatic Repeat reQuest
ASN	Access Service Network
ASP	Application Service Provider
BE	Best Effort
CC	Chase Combining (also Convolutional Code)
CCI	Co-Channel Interference
CCM	Counter with Cipher-block chaining Message authentication code
CDF	Cumulative Distribution Function
CINR	Carrier to Interference + Noise Ratio
CMAC	block Cipher-based Message Authentication Code
CP	Cyclic Prefix
CQI	Channel Quality Indicator
CSN	Connectivity Service Network
CSTD	Cyclic Shift Transmit Diversity
CTC	Convolutional Turbo Code
DL	Downlink
DOCSIS	Data Over Cable Service Interface Specification
DSL	Digital Subscriber Line
DVB	Digital Video Broadcast
EAP	Extensible Authentication Protocol
EESM	Exponential Effective SIR Mapping
EIRP	Effective Isotropic Radiated Power
ErtVR	Extended Real-Time Variable Rate
FBSS	Fast Base Station Switch

FCH	Frame Control Header
FDD	Frequency Division Duplex
FFT	Fast Fourier Transform
FTP	File Transfer Protocol
FUSC	Fully Used Sub-Channel
HARQ	Hybrid Automatic Repeat reQuest
HHO	Hard Hand-Off
HMAC	keyed Hash Message Authentication Code
HO	Hand-Off
HTTP	Hyper Text Transfer Protocol
IE	Information Element
IEFT	Internet Engineering Task Force
IFFT	Inverse Fast Fourier Transform
IR	Incremental Redundancy
ISI	Inter-Symbol Interference
LDPC	Low-Density-Parity-Check
LOS	Line of Sight
MAC	Media Access Control
MAI	Multiple Access Interference
MAN	Metropolitan Area Network
MAP	Media Access Protocol
MBS	Multicast and Broadcast Service
MDHO	Macro Diversity Hand Over
MIMO	Multiple Input Multiple Output (Antenna)
MMS	Multimedia Message Service
MPLS	Multi-Protocol Label Switching
MS	Mobile Station
MSO	Multi-Services Operator
NACK	Not Acknowledge
NAP	Network Access Provider
NLOS	Non Line-of-Sight
NRM	Network Reference Model
nrtPS	Non-Real-Time Packet Service
NSP	Network Service Provider

OFDM	Orthogonal Frequency Division Multiplex
OFDMA	Orthogonal Frequency Division Multiple Access
PER	Packet Error Rate
PF	Proportional Fair (Scheduler)
PKM	Public Key Management
PUSC	Partially Used Sub-Channel
QAM	Quadrature Amplitude Modulation
QPSK	Quadrature Phase Shift Keying
RG	Relative Grant
RR	Round Robin (Scheduler)
RRI	Reverse Rate Indicator
RTG	Receive/transmit Transition Gap
rtPS	Real-Time Packet Service
RUIM	Removable User Identify Module
SDMA	Space (or Spatial) Division (or Diversity) Multiple Access
SF	Spreading Factor
SFN	Single Frequency Network
SGSN	Serving GPRS Support Node
SHO	Soft Hand-Off
SIM	Subscriber Identify Module
SINR	Signal to Interference + Noise Ratio
SISO	Single Input Single Output (Antenna)
SLA	Service Level Agreement
SM	Spatial Multiplexing
SMS	Short Message Service
SNIR	Signal to Noise + Interference Ratio
SNR	Signal to Noise Ratio
S-OFDMA	Scalable Orthogonal Frequency Division Multiple Access
SS	Subscriber Station
STC	Space Time Coding
TDD	Time Division Duplex
TEK	Traffic Encryption Key
TTG	Transmit/receive Transition Gap
TTI	Transmission Time Interval

TU	Typical Urban (as in channel model)
UE	User Equipment
UGS	Unsolicited Grant Service
UL	Uplink
UMTS	Universal Mobile Telephone System
USIM	Universal Subscriber Identify Module
VoIP	Voice over Internet Protocol
VPN	Virtual Private Network
VSF	Variable Spreading Factor
WiFi	Wireless Fidelity
WAP	Wireless Application Protocol
WiBro	Wireless Broadband (Service)
WiMAX	Worldwide Interoperability for Microwave Access

References

[0] **Hassan Yaghoobi, "Scalable OFDMA Physical Layer in IEEE 802.16 WirelessMAN," Intel Technology Journal, Volume 8, Issue 3, 2004**

[1]. *IEEE P802.16-2004*, standard for local and metropolitan area networks Part 16: Air Interface for Fixed Broadband Wireless Access Systems Name (To be published).

[2]. *ETS 300 744 rev 1.2.1*, *(1999-01),* "digital broadcasting systems for television, sound and data services (DVB-T); framing structure, channel coding and modulation for digital terrestrial."

[3]. *IEEE Std 802.11a-1999, Part 11*, "Wireless LAN Medium Access Control (MAC) and Physical Layer (PHY) specifications; high-speed physical layer in the 5 GHz band."

[4]. *IEEE 802.11g-2003*, "IEEE Standard for Information technology, telecommunications and information exchange between systems, local and metropolitan area networks, specific requirements, Part 11: Wireless LAN Medium Access Control (MAC) and Physical Layer (PHY) specifications, Amendment 4: further higher-speed physical layer extension in the 2.4 GHz band."

[5]. *IEEE P802.16e*, "draft amendment to IEEE standard for local and metropolitan area networks, Part 16: air interface for fixed and mobile broadband wireless access systems, amendment for physical and medium access control layers for combined fixed and mobile operation in licensed bands."

[6]. *IEEE C802.16d-04_47*, "applying scalability for the OFDMA PHY layer."

[7]. *IEEE C802.16REVd-04/50r1*, "OFDMA PHY enhancements for better mobility performance."

[8]. *IEEE C802.16d-04/72*, "additional optional symbol structure."

[9]. *IEEE C802_16e-04/88-r3*, "128 FFT sizes for OFDMA PHY."

[10]. *C802.16REVd-04_50r3*, "OFDMA PHY enhancements for better mobility performance."

[11]. *IEEE C802.16d-04/90*, "AAS enhancements for OFDMA PHY."

[12]. *IEEE 802.16d-04/65*, "Enhancing MIMO features for OFDMA PHY layer."

[13]. *IEEE C802.16e-04_72r2*, "STC Enhancements for optional FUSC and AMC zones for OFDMA PHY layer."

[14]. *IEEE C802.16e-04/208r2*, "space-time codes for 3 transmit antennas for the OFDMA PHY."

[15]. Rappaport, T.S., *Wireless Communications Principles and Practice,* Second Edition 2002, Prentice Hall PTR, Upper Saddle River, NJ.

[16]. Li, Y., Cimini, L.J., "Bounds on the Interchannel Interference of OFDM in Time-Varying Impairments," *IEEE Transactions ON Communications, Vol. 49, No. 3*, March 2001, pp. 401-404.

[17]. *IEEE 802.16.3c-01/29r4*, "channel models for fixed wireless applications."

[18]. *Recommendation ITU-R M.1225*, "Guidelines for evaluation of Radio transmission technologies for IMT-2000, 1997."

[19]. Alamouti, S. A., "Simple Transmit Diversity Technique for Wireless Communications," *IEEE Journal on Select Areas in Communications*, *Vol. 16, No. 8*, October 1998.

[20]. *IEEE P802.16REVd/D5-2004*, standard for local and metropolitan area networks Part 16: Air Interface for Fixed Broadband Wireless Access Systems Name.

[0] **3GPP, "TR 25.892: Feasibility Study for Orthogonal Frequency Division Multiplexing (OFDM) for UTRAN enhancement (Release 6)," Version 6.0.0, June 2004.**

[1] 3GPP, "TR 25.848: Physical layer aspects of UTRA High Speed Downlink Packet Access", Version 4.0.0, March/2001.

[2] 3GPP, "TR 25.855: High Speed Downlink Packet Access: Overall UTRAN Description", Version 5.0.0, September/2001.

[3] 3GPP, "TR 25.858: High Speed Downlink Packet Access: Physical Layer Aspects", Version 5.0.0, March/2002.

[4] 3GPP, "TS 25.212: Multiplexing and channel coding (FDD)", Version 5.0.0, March/2002.

[5] 3GPP2, "1xEV-DV Evaluation Methodology – Addendum (V6)", July 2001.

[6] 3GPP, "TS 25.141: Base station conformance testing (FDD)", Version 5.4.0, September/2002.

[7] Huawei, "Time-frequency mappings of OFDM units for full frequency reuse without resource planning", Tdoc R1-030799, New York, NY, USA, August 25-29, 2003.

[8] Huawei, "Link-level OFDM performances under realistic inter-cell interference", Tdoc R1-031171, Lisbon, Portugal, November 17-21, 2003.

[9] 3GPP, TSG-RAN1, Nortel Networks, "Effective SIR Computation for WCDMA System-Level Simulations", Document R1-03-1299, Meeting #35, Lisbon, Portugal, November 17-21, 2003.

[10] R4-021406, "Problem on PN9 seed setting in Test Model 5", Lucent, RAN4#25, Nov 2002.

[11] 3GPP, "TS25.104: Base Station (BS) radio transmission and reception (FDD)", v6.5.0, Mar 2004.

[0] **3GPP, "Spatial Channel Models," V2.3, January 30, 2003**

[1] WG5 Evaluation Methodology – Addendum (V6), WG5 Evaluation AHG, July 25, 2001

[2] Nokia, Ericsson, Motorola. Common HSDPA system simulation assumptions. TSG-R1 document, TSGR#15(00)1094, 22-25th, August, 2000, Berlin, Germany, 12 pp.

[3] L. Greenstein, V. Erceg, Y. S. Yeh, M. V. Clark, "A New Path-Gain/Delay-Spread Propagation Model for Digital Cellular Channels," IEEE Transactions on Vehicular Technology, VOL. 46, NO.2, May 1997, pp.477-485.

[4] E. Sousa, V. Jovanovic, C. Daigneault, "Delay Spread Measurements for the Digital Cellular Channel in Toronto," IEEE Transactions on Vehicular Technology, VOL. 43, NO.4, Nov 1994, pp.837-847.

[5] L. M. Correia, Wireless Flexible Personalized Communications, COST 259: European Co-operation in Mobile Radio Research, Chichester: John Wiley & Sons, 2001.

---

i "Air Interface for Fixed Broadband Wireless Access Systems," IEEE Std 802.16 – 2004, October 2004.

ii "Air Interface for Fixed and Mobile Broadband Wireless Access Systems," IEEE P802.16e/D12, February, 2005.

iii Hassan Yagoobi, "Scalable OFDMA Physical Layer in IEEE 802.16 WirelessMAN", Intel Technology Journal, Vol 08, August 2004.

iv "WiMAX End-to-End Network Systems Architecture - Stage 2: Architecture Tenets, Reference Model and Reference Points," WiMAX Forum, December, 2005.

v "Mobile WiMAX – Part II: Competitive Analysis", WiMAX Forum, February, 2006

vi L.J. Cimini, "Analysis and Simulation of a Digital Mobile Channel Using Orthogonal Frequency Division Multiplexing," IEEE Trans. Comm., vol. COM-33, no. 7, pp 665-675, June 1985.

vii Richard Van Nee and Ramjee Prasad, "OFDM for Wireless Multimedia Communications," Artech House, 2000.

viii W. Xiao and R. Ratasuk, "Analysis of Hybrid ARQ with Link Adaptation", *Proceedings of the Annual Allerton Conference on Communications, Control, and Computing*, pp. 1618-1619, Oct 2002.

ix G. Nair, J. Chou, T. Madejski, K. Perycz, P. Putzolu and J. Sydir "IEEE 802.16 Medium Access Control and Service Provisioning", Intel Technology Journal, vol 08, August 2004.

x F. Wang, A. Ghosh, R. Love, K. Stewart et.al., *"IEEE 802.16e System Performance – Analysis and Simulation Results"*, Proc. of PIMRC, Berlin, Germany, Sept. 2005.

[xi] Nokia, Ericsson, Motorola. Common HSDPA system simulation assumptions. TSG-R1 document, TSGR#15(00)1094, 22-25th, August, 2000, Berlin, Germany, 12 pp.

[xii] L. Greenstein, V. Erceg, Y. S. Yeh, M. V. Clark, "A New Path-Gain/Delay-Spread Propagation Model for Digital Cellular Channels," IEEE Transactions on Vehicular Technology, VOL. 46, NO.2, May 1997, pp.477-485.

[xiii] E. Sousa, V. Jovanovic, C. Daigneault, "Delay Spread Measurements for the Digital Cellular Channel in Toronto," IEEE Transactions on Vehicular Technology, VOL. 43, NO.4, Nov 1994, pp.837-847.

[xiv] L. M. Correia, Wireless Flexible Personalized Communications, COST 259: European Co-operation in Mobile Radio Research, Chichester: John Wiley & Sons, 2001.

[Rok Preseren's References]

Literature:

[1] V. Erceg et al, "Channel Models for Fixed Wireless Applications", IEEE 802.16.3 task group contribution, July 2001, IEEE 802.16.3c-01/29r4

[2] 3GPP TR 25.892 v6.0.0. (2004-06), 3rd Generation Partnership Project; Technical specification Group Radio Access Network; Feasibility Study for Orthogonal Frequency Division Multiplexing (OFDM) for UTRAN enhancement (Release 6)

[3] 3GPP2 C.R1002-0 Version 1.0, CDMA2000 Evaluation Methodology, Version 0, December 2004

[4] ITU-R M.1225, Guidelines for evaluation of radio transmission technologies for IMT-2000

[References for MIC Annex]

[1] Shilpa Talwar, "System Level Simulations for 802.16e", Jan 2006.

[2] Alexander Maltserv, et al "802.16e System Level Simulations", Rev0.3, Mar 2005.

[3] Muthu Venkatachalam, "Some BKMs for AWG simlations", Jun 2006.

[4] Mustafa Demirhan, Ali Koc, Song Liu and Chunmei Liu, "Mobility Extensions for OPNET WiMax Model", Apr 2006.